ผลกระทบของสภาพวงจรการไหลต่อเสถียรภาพของการไหลเวียนโดยธรรมชาติแบบสองเฟสเนื่องจากการเดือด

นาย ชัยวัฒน์ มั่นเจริญ

สถาบันวิทยบริการ
จุฬาลงกรณ์มหาวิทยาลัย

วิทยานิพนธ์นี้เป็นส่วนหนึ่งของการศึกษาตามหลักสูตรปริญญาวิศวกรรมศาสตรดุษฎีบัณฑิต
สาขาวิชาวิศวกรรมนิวเคลียร์ ภาควิชานิวเคลียร์เทคโนโลยี
คณะวิศวกรรมศาสตร์ จุฬาลงกรณ์มหาวิทยาลัย
ปีการศึกษา 2545

ISBN 974-17-1175-1

ลิขสิทธิ์ของจุฬาลงกรณ์มหาวิทยาลัย

THE EFFECT OF FLOW LOOP CONDITIONS ON STABILITIES OF TWO-PHASE NATURAL CIRCULATION CAUSED BY BOILING

Mr. Chaiwat Muncharoen

สถาบันวิทยบริการ
จุฬาลงกรณ์มหาวิทยาลัย

A Dissertation Submitted in Partial Fulfillment of the Requirements
for the Degree of Doctor of Engineering in Nuclear Engineering
Department of Nuclear Technology
Faculty of Engineering
Chulalongkorn University
Academic year 2002

ISBN 974-17-1175-1

Thesis Title	THE EFFECT OF FLOW LOOP CONDITIONS ON STABILITIES OF TWO-PHASE NATURAL CIRCULATION CAUSED BY BOILING
By	Mr. Chaiwat Muncharoen
Field of study	Nuclear Engineering
Thesis Advisor	Associate Professor Tatchai Sumitra, Dr.Ing.
Thesis Co-advisor	Professor Masanori Aritomi, D.Eng. Assistant Professor Sunchai Nilsuwankosit, Ph.D.

Accepted by the Faculty of Engineering, Chulalongkorn University in Partial Fulfillment of the Requirements for the Doctor's Degree

…………………………………….. Dean of Faculty of Engineering
(Professor Somsak Panyakaew, D.Eng.)

THESIS COMMITTEE

……………………………………………….. Chairman
(Associate Professor Virul Mangclaviraj)

………………………………………….……. Thesis Advisor
(Associate Professor Tatchai Sumitra, Dr.Ing.)

……………………………………………….. Thesis Co-advisor
(Professor Masanori Aritomi, D.Eng.)

……………………………………………….. Thesis Co-advisor
(Assistant Professor Sunchai Nilsuwankosit, Ph.D.)

……………………………………………….. Member
(Kamol Takabut, D.Ing.)

……………………………………………….. Member
(Assistant Professor Supitcha Chanyotha, Ph.D.)

……………………………………………….. Member
(Assistant Professor Visit Thaveeprungsriporn, Ph.D.)

สถาบันวิทยบริการ
จุฬาลงกรณ์มหาวิทยาลัย

ชัยวัฒน์ มั่นเจริญ : ผลกระทบของสภาพวงจรการไหลต่อเสถียรภาพของการไหลเวียนโดยธรรมชาติแบบสองเฟสเนื่องจากการเดือด (THE EFFECT OF FLOW LOOP CONDITIONS ON STABILITIES OF TWO-PHASE NATURAL CIRCULATION CAUSED BY BOILING) อ. ที่ปรึกษา: รองศาสตราจารย์ ดร. ธัชชัย สุมิตร, อ.ที่ปรึกษาร่วม: Professor Dr. Masanori Aritomi, ผู้ช่วยศาสตราจารย์ ดร. สัญชัย นิลสุวรรณโฆษิต จำนวนหน้า131 หน้า ISBN 974-17-1175-1.

การศึกษาความไม่เสถียรภาพของการไหลโดยธรรมชาติแบบสองเฟสเนื่องจากผลกระทบของฟลักซ์ความร้อน ความดันของระบบ และ สภาพ subcoolingในช่องทางการไหล ที่มี riser ความยาวหนึ่งเมตรเหนือ heated section โดยกำหนดให้ฟลักซ์ความร้อนเพิ่มขึ้นจาก 50 ถึง 550 กิโลวัตต์ต่อตารางเมตร ที่ความดันของระบบ 0.1, 0.2, 0.4, 0.5 และ 0.7 เมกกะปาสคาล และที่สภาพ subcooling 5, 10 และ 15 เคลวิน และเปรียบเทียบผลการทดลองกับผลการคำนวณจากการพัฒนาแบบจำลองเชิงตัวเลขแบบ two-fluid ซึ่งเขียนด้วยภาษาฟอร์แทรน โดยใช้แบบแผนแบบกึ่งโดยนัยสำหรับ finite difference equation และวิธีการแบบ Newton Block Gauss Seidel (NBGS) เพื่อแก้สมการหาค่าที่ไม่รู้ โดยกำหนดช่วงเวลาไว้ที่หนึ่งมิลลิวินาทีตลอดเวลาและขนาดของตารางคือหนึ่งร้อยมิลลิเมตร จากนั้นทำการศึกษาผลกระทบของขนาดช่องทางการไหลต่อเสถียรภาพของการไหลโดยให้ขนาดเส้นผ่านศูนย์กลางของช่องทางการไหลเท่ากับ 18, 20, 22 และ 32 มิลลิเมตร ผลการทดลองยืนยันให้เห็นว่าการเพิ่มความดันของระบบและสภาพ subcooling ช่วยทำให้ระบบมีเสถียรภาพมากขึ้น นอกจากนี้แบบจำลองเชิงตัวเลขให้ผลที่ดีและมีความสอดคล้องกันดีกับผลจากการทดลอง การทำนายผลกระทบของขนาดช่องทางการไหลโดยใช้แบบจำลอง two-fluid พบว่าการเปลี่ยนขนาดเส้นผ่านศูนย์กลางของช่องทางการไหลมีผลกระทบกับรูปแบบของความไม่เสถียรภาพของการไหลในช่วงฟลักซ์ความร้อนมากกว่า 300 กิโลวัตต์ต่อตารางเมตร เนื่องจากความดันตกเนื่องจากแรงเสียดทานมีผลอย่างมากในช่วงฟลักซ์ความร้อนสูง ทำให้แบบแผนความไม่มีเสถียรภาพของการไหลเปลี่ยนรูปแบบจาก natural oscillation เป็น density wave oscillation การค้นพบใหม่จากการทดลองแสดงให้เห็นว่า geysering สามารถเกิดขึ้นได้ที่ความดันมากกว่า 0.35 เมกกะปาสคาลและที่ความเร็วของของไหลมากกว่า 0.2 เมตรต่อวินาที เนื่องจากผลกระทบของรูปทรงของช่องทางการไหล

สถาบันวิทยบริการ
จุฬาลงกรณ์มหาวิทยาลัย

ภาควิชานิวเคลียร์เทคโนโลยี ลายมือชื่อนิสิต...

สาขาวิชาวิศวกรรมนิวเคลียร์ ลายมือชื่ออาจารย์ที่ปรึกษา.......................................

ปีการศึกษา 2545 ลายมือชื่ออาจารย์ที่ปรึกษาร่วม.................................

ลายมือชื่ออาจารย์ที่ปรึกษาร่วม.................................

4171803521 : MAJOR Nuclear Engineering

KEY WORD: natural circulation / instabilities / natural oscillation / geysering / two-fluid model

Chaiwat Muncharoen :THE EFFECT OF FLOW LOOP CONDITIONS ON STABILITIES OF TWO-PHASE NATURAL CIRCULATION CAUSED BY BOILING THESIS ADVISOR : Associate Professor Dr. Tatchai Sumitra, THESIS CO-ADVISOR : Professor Dr. Masanori Aritomi, Assistant Professor Dr. Sunchai Nilsuwankosit, 131 pp. ISBN 974-17-1175-1.

The instability of the two-phase flow natural circulation due to the effect of heat flux, pressure, and subcooling in the proposed channel configuration was investigated. A 1 meter long non-heated riser above the heated section was proposed in this experiment. The heat flux was increased from 50 to 550 kW/m^2. The pressure was varied from 0.1, 0.2, 0.4, 0.5, and 0.7 MPaA and the subcooling was varied from 5, 10, and 15 K. The numerical model was developed by using two-fluid model written in FORTRAN programming language to investigate the effect of channel diameter, system pressure and subcooled condition on stabitlities of two-phase natural circulation, which is caused by boiling. The semi-implicit scheme was utilized for finite difference equations. Newton Block Gauss Seidel (NBGS) method was employed to solve the system equations for unknown variables. The time step was fixed at all time at 1 millisecond and the mesh size was 100 mm. The results from the two-fluid model were compared with the experimental results. The effect of channel diameter was investigated by using the two-fluid model. The channel diameter was varied from 18, 20, 22, and 32 mm. It is confirmed that the increase in system pressure and subcooling stabilize the system. In addition the two-fluid model can give the good results and are in good agreement with experimental results. The prediction of the effect of channel diameter on the flow oscillation from the two-fluid model indicated that the change in the channel diameter affected the flow instability pattern at the heat flux higher than 300 kW/m^2. As the frictional pressure drop was dominant at the high heat flux, the flow instability map changed from natural circulation to density wave oscillation. The new discovery received from the experiment indicated that the geysering can occur at the system pressure higher than 0.35 MPaA and at the velocity higher than 0.2 m/s due to the effect of channel geometry.

สถาบันวิทยบริการ
จุฬาลงกรณ์มหาวิทยาลัย

Department of Nuclear Technology Student’s signature...

Field of study Nuclear Engineering Advisor’s signature...

Academic year 2002 Co-advisor’s signature...

Co-advisor’s signature...

Acknowledgment

The author would like to acknowledge the financial support from The Thailand Research Fund under The Royal Golden Jubilee Ph.D. program to give me an opportunity to study doctoral degree and undertake the experiment in Japan. I am very appreciated to Associate Professor Dr. Tatchai Sumitra, my dissertation advisor, for kind advice and supervision. Thanks to Professor Masanori Aritomi for his financing support and guidance to accomplish my experiment in Tokyo Institute of Technology. Thanks to Assistant Professor Dr. Sunchai Nilsuwankosit for good advice and recommendation. Thanks to Associate Professor Nares Chankow for his help and coordination. Thanks to Dr. Takatoshi Takemoto for his encourage and revision of my dissertation. Thanks to Mr. Mohammad Hadid Subki for his assistance to undertake the experiment.

Finally, thanks to my father, Mr. Yuth, and my mother, Mrs. Jintana, for their encouragement and support.

สถาบันวิทยบริการ
จุฬาลงกรณ์มหาวิทยาลัย

Table of Contents

Page

Table of Contents (Continued)

Page

สถาบันวิทยบริการ
จุฬาลงกรณ์มหาวิทยาลัย

List of Figures

List of Figures (Continued)

List of Figures (Continued)

Abbreviations and Nomenclature

A : Area (m^2)
A_i : concentration of interfacial area (1/m)
C_p : specific heat (kJ/kg.K)
D_h : hydraulic diameter (m)
D_b : bubble diameter (m)
g : acceleration due to gravity (m/s^2)
H : buoyancy head (m)
H_0 : steady state buoyancy head (m)
h : heat transfer coefficient (J/m^2.K.sec)
h_{fg} : Latent heat of vaporization (kJ/kg)
L : length of heating section (m)
L_{eq} : length of equivalent section (m)
L_r : length of riser section (m)
k : conductivity (W/mK)
P : pressure (Pa)
p : wetted perimeter (m)
Q_h : heating generation (W)
q''' : calorific power per unit volume (kW/m^3)
q_e : electric heating power (W)
r : thickness (m)
T_g : temperature of gas phase (°C)
T_l : temperature of liquid phase (°C)
T^s : saturation temperature (°C)
Δt : time step (s)
V_g : velocity of gas phase (m/s)
V_l : velocity of liquid phase (m/s)
V_c : swirl velocity (m/s)
vol : volume of one cell (m^3)
U_g : specific internal energy of gas phase (kJ/kg)
U_l : specific internal energy of liquid phase (kJ/kg)
u_e : velocity at the exit (m/s)
Δz : spatial interval (m)
z_1 : incipience boiling point (m)

สถาบันวิทยบริการ
จุฬาลงกรณ์มหาวิทยาลัย

Abbreviations and Nomenclature (Continued)

Greek

ρ_h : specific density of heater (kg/m^3)
ρ_g : specific density of gas phase (kg/m^3)
ρ_l : specific density of liquid phase (kg/m^3)
α_e : void fraction at the exit (-)
α_g : void fraction of gas phase (-)
α_l : void fraction of liquid phase (-)
Γ : volumetric mass exchange rate (kg/m^3.s)
ε : wall vapor generation /condensation flag

Nondimensional number

F : Reynolds number factor
Gr : Grashof number
Nu : Nusselt number
$\Pr$: Prantl number
Re : Reynolds number
s : supression factor
We : Weber number

Superscript

(i) : ith channel
s : saturated liquid phase
$/$: associated with wall
$*$: associated with bulk
B : bulk
W : near wall

Subscript

$\max$: maximum
$\min$: minimum
mic : microscopic
mac : macroscopic
l : liquid phase
g : vapor phase
w : wall

สถาบันวิทยบริการ
จุฬาลงกรณ์มหาวิทยาลัย

Abbreviations and Nomenclature (Continued)

wg : wall to vapor

wl : wall to liquid

ig : interface to vapor

il : interface to liquid

สถาบันวิทยบริการ
จุฬาลงกรณ์มหาวิทยาลัย

Chapter I

Introduction

1. Background and Problems of Interest

Natural circulation is the phenomenon, which can be found in many industries such as in the riser tubes of the steam generators and in the boiler tubes of the power plants or in the coolant channels between the nuclear fuel elements in a boiling water reactor (Corradini, 1993). Initially, in this phenomenon the water will be heated to its saturation temperature and the heat will be transferred to the water by natural convection without boiling. At some point where the temperature exceeds the saturation temperature the vapor bubbles start to form on the wall. These bubbles will grow and depart from wall due to the buoyancy effects, which will induce the circulation of the water (Kocamusatafaogullari, 1993).

In nuclear industry, the Simplified Boiling Water Reactor (SBWR) has a promising prospect regarding to its competitive power generation costs, shortened construction time and simpler safety systems (Duncan, 1988). The method of natural circulation shown in Fig. 1.1 is proposed as an important feature to remove the heat dissipated from the core. The experiment was conducted to study the flow oscillation in natural circulation (Kataoka, 1988; Aritomi et al., 1992; Jiang et al., 1995; Tonimoto, Ishii, and Lee, 1998; Kim and Lee, 2000; Van Der Hagen, Stekelenburg, and Van Bragt, 2000; Wang and Hochreiter, 2000; Hibiki and Ishii, 2001; Kim et al., 2001; Muncharoen et al., 2002c; Subki et al., 2002) and forced circulation (Aritomi, Aoki, and Inoue, 1977a, 1977b, 1986a, 1986b, 1979). By eliminating the recirculating pumps, the potential accident resulted from the recirculating pumps trip will be eliminated. However, SBWR will face some instabilities and oscillations during the start-up operation due to the occurrence of void fractions in the system. This will have an effect on reactor reactivity. Moreover, SBWR geometry might influence the stability of the system in case of insufficient vaporization.

During the start-up of natural circulation, the major instability that can be occurred is geysering (Boure, 1973; Aritomi, Chiang, and Mori, 1993; Jiang et al., 1995; Yadigaroglu, 1998). When the heat flux is sufficiently high, the boiling is initiated. The bubbles will rise to the outlet plenum due to the decrease in hydrodynamic head. The bubbles are condensed at the outlet plenum and the

สถาบันวิทยบริการ
จุฬาลงกรณ์มหาวิทยาลัย

subcooled water will enter at the inlet plenum. The cycle then repeats. This driving mechanism is affected by the bubbles coalesce that form the slug bubbles in the channel. Furthermore, at the start-up phase, if the sufficient vaporization is not produced, the fluctuation of the void fraction in the channel that connects the outlet plenum and the separator tank may be induced. By introducing more heat flux, the geysering disappears and the other instability will dominate over the flow characteristics. This type of instability is called natural circulation oscillation, which has the characteristics of sine shape oscillation in flow rates and in pressure drops. In conclusion, the effects of these instabilities will complicate and cause the difficulty in raising reactor power.

Due to the advance in computer technology, many researchers have developed new numerical codes using the homogeneous, drift-flux or two-fluid models to investigate the instabilities in boiling channels (Lies and Reed, 1978; Ishii and Mishima, 1984; Ransom and Hicks, 1984; Wulff, 1993; Ransom et al., 1995; Lahey, Jr. and Drew, 1999; Okawa and Kataoka, 2000; Song and Hong, 2000; Muncharoen, Nilsuwankosit, and Sumitra, 2001; Song and Ishii, 2001; Zhou and Podowski, 2001; Muncharoen, Sumitra, and Takemoto, 2002c; Muncharoen et al., 2002d). The analytical models were developed for stability analysis (Lyczkowski, Gidaspow, and Solbrig, 1978; Saha and Zuber, 1978; Gurgenci, Veziroglu, and Kakac, 1983; Peng et al., 1984; Furutera, 1986; Aritomi et al., 1986a; Lahey, Jr., 1986; Lahey, Jr., and Podowski, 1989; Park et al., 1986; Rizwan-Uddin and Dorning, 1986; Bergdahl et al., 1989; Clausse, Lahey, Jr., and Podowski, 1989; Guido, Converti, and Clausse, 1991; Lee and Lee, 1991; March-Leuba and Blakeman, 1991; Fukasa and Kobori, 1993; Hashimoto, 1993; Nigamatulin, 1993; Lin and Pan, 1994; Wang et al., 1994; Uehiro, Rao, and Fukuda, 1996; Van Bragt and Van Der Hagen, 1998). The well-known codes in nuclear fields such as TRAC, RELAP5, RETRAN, CATHARE and CATHENA mostly utilize the finite difference or finite volume scheme with implicit, explicit or semi-implicit method to replace the derivatives in differential equations and turn into algebraic equations. In this scheme the void fraction, pressure, energy or scalar value will be calculated at the cell center and the velocity will be calculated at the cell boundaries. However, it is recognized that numerical diffusion introduced by this scheme has a greatly effect on accuracy of the scalar fields such as internal energy, liquid and vapor density (Araseki and Ishiguro, 1987; Mahaffy, 1993; Macian-Juan and Mahaffy, 1998; Guenther and Syamlal, 2001). To eliminate the numerical diffusion in the codes needs more efforts. As a consequence, the algorithm that limits the numerical diffusion can reduce the robustness of the codes (Mahaffy, 1993). The methods to stabilize the finite difference scheme were proposed by Van Leer (1969) and Hirt (1968). To select the proper mesh size for the model, it is still important to investigate its effect on the ill-posedness and the accuracy of the model (Stewart, 1979; Shieh and Krishnamurthy, 1984; Muncharoen et al., 2002a, 2002b). The two-fluid model employs six conservation equations of mass, momentum and energy for each phase. It requires the interaction between the liquid and vapor phase such as interfacial mass transfer and interfacial friction. To stabilize the numerical solution many techniques were applied to two-fluid models (Ramshaw and Trapp, 1978; Stewart, 1979,1981; Mahaffy, 1982; Ransom and Hicks, 1984; Trapp and Riemke, 1986; Minato and Kawabe, 1988; Minato, Takamori, and Ishida, 2000). In contrast the drift-flux model employs only 4 or 5 equations of mass, momentum and energy of the vapor and the mixture. The velocity of the mixture is calculated by the drift velocity and drift-flux coefficients. The interaction between the liquid and vapor phase is not required for this model. Because of the different characteristics of both models, therefore it is important from the engineering point of view to investigate, analyze and compare the mathematical models and the results of both models (Muncharoen et al., 2002c).

The study of flow instabilities is important because of their effects on heat transfer characteristic and flow characteristic, which may lead to physical damage in the boiling water reactor core (Belblidin, 1983; Archard, 1985; Chartoorgoon, 1986; Kim and Lee, 2000). To understand this effect, the knowledge on the instability phenomenon due to the effect of heat flux, pressure and subcooling in the proposed channel geometry is required. Moreover, the good model is needed to investigate, analyze and predict the instability, which may occur in the system.

สถาบันวิทยบริการ
จุฬาลงกรณ์มหาวิทยาลัย

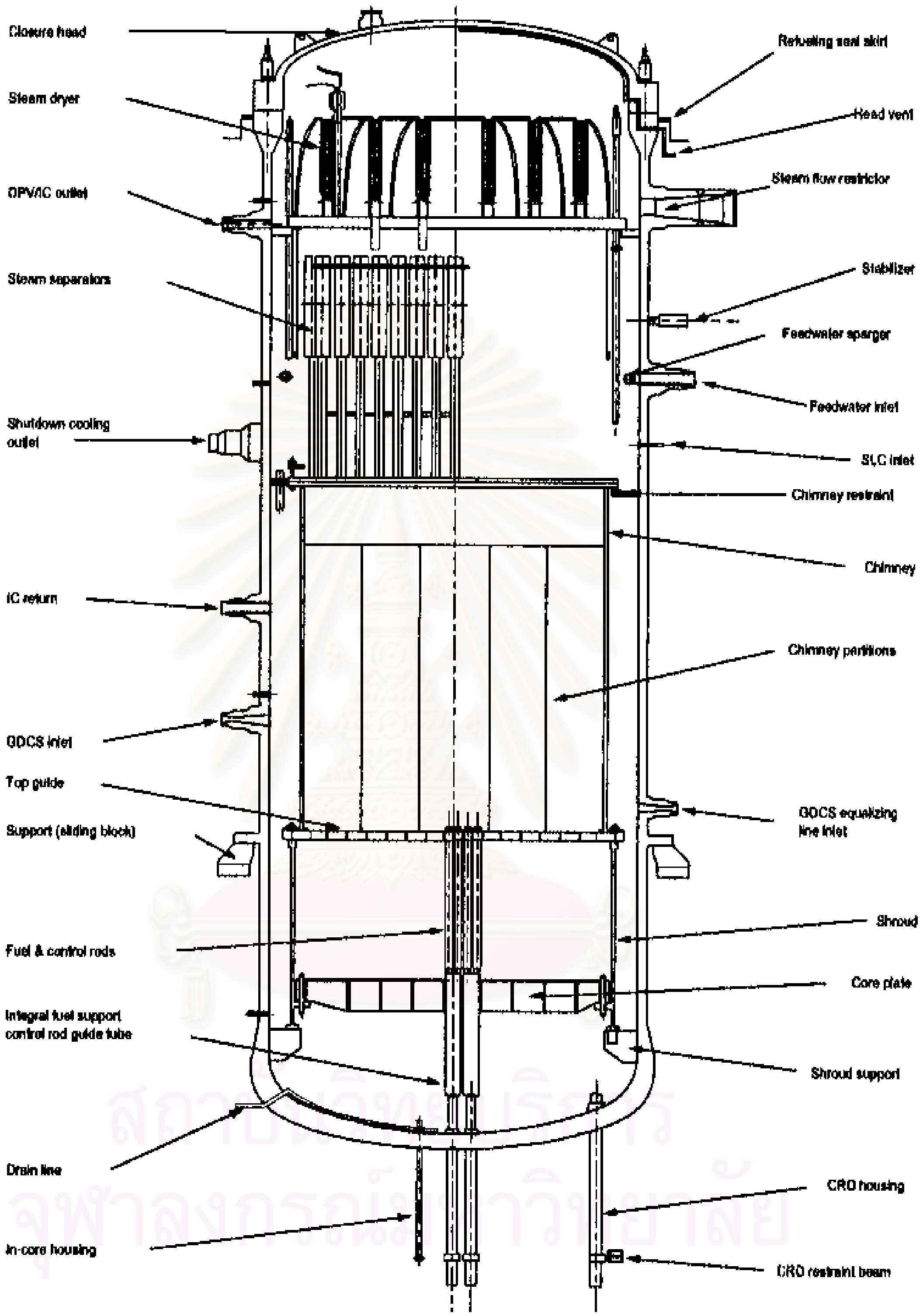

สถาบันวิทยบริการ
จุฬาลงกรณ์มหาวิทยาลัย

Fig. 1.1 Natural Boiling Water Reactor (Subki, 2002)

1.1 Objective

The purpose of this work is to develop the model of the two-phase natural circulation, which is caused by boiling, to investigate the effect of the channel diameter, system pressure and subcooled condition in the proposed channel geometry on the stability of the system. The two-phase co-current upward flow of the steam-water mixture in the vertical channels with the heat flux provided by the supplied heater shall be examined. The effect of the channel diameter including the system pressure and the subcooling on the system stability in the vertical channels shall be studied. The collected data shall be used as the database to be compared with numerical calculation and for improvement of the design for the future natural boiling water reactor. In order to analyze and predict the stability of the system, the two-fluid model shall be developed and compared with the results from the experiment. Then the effect of channel diameter will be investigated by using the two-fluid model.

1.2 Previous Works

The dynamic behavior of the two-phase flow in the vertical channel has been investigated extensively in the past. The experiments were conducted for the natural and forced circulation. Many models were developed to investigate the flow oscillation. The effect of the channel geometry has rarely been studied in natural circulation. Aritomi et al. (1977a, 1977b, 1979, 1986a, 1986b) investigated experimentally and analytically the flow instabilities in the parallel channels under forced condition. The non-linear mathematical model was proposed, which explained the results quite satisfactorily. Lies and Reed (1978) developed the drift-flux model and proposed to use the semi-implicit differencing scheme with a variation of the Newton Gauss Seidel iterative method to solve the algebraic equations. The convective terms in the mass and energy equations, the pressure gradient term in the momentum equation and the compressible work term in the energy equation all contained terms evaluated at the new time level. The Newton Block Gauss Seidel (NBGS) method represented a primary Newton iteration on the original non-linear system coupled with the secondary Block Gauss Seidel iteration for each step of the primary one. This method was more applicable than the Newton iteration or the direct inversion when the size of the matrix was large. Fukuda (1979a) conducted the experiment under natural and forced circulation conditions in two parallel channels to examine the adiabatic riser piping and classified the hydrodynamic instability of two-phase flow into Type I and Type II. Type I has a characteristic feature that it occurs at the nearly zero exit steam quality condition while as Type II occurs at the high steam quality. The gravitational pressure drop in the unheated riser section plays important role in Type I instability. However, the frictional pressure drop is dominant in Type II instability. An analysis on the hydrodynamic instability of the two-phase flow in the parallel multi-channels was conducted by Fukuda (1979b). The derived equations were applied for the prediction of the oscillation modes for the systems that was composed of a few slightly different channels. The analysis successfully predicted the modes, which had been experimentally observed. The fraction step was proposed by Stewart (1981) to solve the fully implicit difference equations and had no upper limit on time the step size. Stewart (1984) illustrated the two-phase flow model including constitutive models, heat transfer models and numerical method for solving the differential equations. Kataoka et al. (1988) investigated the effect of the separator in the natural circulation boiling water reactor with a rated capacity of 600 MW (electric). The separators are provided in the current BWR to decrease the droplet carryover into the steam dryer and steam carryunder into the downcomer region. It was shown that the void fraction in the downcomer decreased the density head in the area and also decreased the natural flow rate. The riser height required to obtain the required natural flow rate was shorten because of the elimination of the flow resistance in the separators. The recirculation rate at the core inlet increased during the pressure increasing period. This was due to the decreased void fraction and the decreased two-phase resistance in the core. The thermal-hydraulic instabilities, including the geysering, and the natural oscillation during the start-up in natural circulation has been studied by Aritomi et al. (1992). Three kinds of instabilities may occur, which are the geysering induced by condensation, the natural circulation instability induced by the hydrodynamic head fluctuation, and the density wave oscillation. It is found that geysering is dependent on both the inlet velocity and the subcooled condition in the outlet plenum. Moreover, it is induced only at the inlet velocity lower than 0.2 m/s. In 1993, Aritomi et al. investigated the geysering in the parallel boiling channel in the natural and the forced circulation. As the inlet subcooling was increased, the maximum inlet velocity where the geysering occurred was decreased. The flow reversal was independent of the inlet subcooling. The upper velocity limitation for the geysering occurrence became higher as the non-heated riser

สถาบันวิทยบริการ
จุฬาลงกรณ์มหาวิทยาลัย

length was increased. The drift flux model was developed by Chiang (1994) to predict the geysering and had provided the results that were in a good agreement with the results from the experiment. Jiang et al. (1995) conducted the experiment on the start-up of a low temperature, natural circulation nuclear heating reactor. The phenomena of flow instabilities, namely the geysering, the flashing, and the low steam quality density wave were described. It was proposed that the flashing was a process of vapor generation in which the vapor was not caused by the heating at the outside surface of the liquid but was caused by the vaporization of the liquid as it reached its local saturation value while it was flowing up. The start-up procedure was also suggested. The two-fluid model including the constitutive equations and the semi-implicit method were used to develop RELAP5/MOD3.2 as described by Ransom et al. (1995). Cheng, Hillis, and Azzorpardi (1998) investigated the flow in the concurrent vertical channels with the diameter of the 150 mm. and 28.9 mm. The results showed that traditional slug flow did not exist in the 150 mm. diameter column: instead there was a gradual transition to churn flow. The experiment on the test loop HRTL-5 that simulated the geometry and system design of the 5-MW nuclear reactor was performed to investigate the flow instabilities in the wide ranges of the inlet subcooling and the different pressure (P=0.1, 0.24, and 1.5 MPa) by Jiang et al. (2000). Several kinds of flow instabilities were observed e.g. the geysering, the flashing-related flow instability, and the high–frequency flow instability at P < 0.24 MPa, as well as the low steam quality density wave instability at P=1.5 MPa. The flow instabilities in semi-closed two-phase natural circulation loops were examined experimentally by Kim and Lee (2000). The effect of the flow restriction at the heater inlet and outlet was confirmed to be the same as those with the open loop. The flow became stable with increase in the exit restriction and with decrease in the inlet restriction. Shoukri et al. (2000) reported that slug flow was not observed in air-water flow in the large diameter vertical channel and the transition from the bubbly to intermittent flow was dependent on the pipe diameter. Wang and Hochreiter (2000) investigated the behavior of the single phase and the two phase natural circulation and developed the NATURAL computer code to predict the natural circulation flow rate of the Penn State Low Pressure Integral Test Facility (LPITF). The TRAC-PF1 was used to model the Penn State LPITF system as a benchmark to compare with the results from the NATURAL computer code. The results showed that both codes were in good agreement. Yoneda et al. (2000) studied the distribution of void fraction, bubble chord length and gas velocity of steam-water two-phase flow in a vertical pipe with the diameter of 155 mm under the steady condition. They found that the inlet condition had a great effect on the length required for the flow to be fully developed and the drift velocity characteristic depended on the diameter of the pipe. The experiment on the hot-leg U-bend two-phase natural circulation in a loop with a relatively large diameter (10.2 cm. I.D.) was performed for understanding the two-phase natural circulation and flow termination during a small break loss of accident in BWR (Hibiki and Ishii, 2001). The induced liquid natural circulation rate decreased with decreasing the gas flow rate. The gas flow rate at the flow termination decreased with the water level in the separator. The termination of the natural circulation occurred when there was insufficient hydrostatic head in the downcomer side. Kim et al. (2001) performed the experiment using scaled test facilities of system Integrated Modular Advanced Reactor (SMART) and developed the RETRAN-03/INT code to predict the characteristics of the flow oscillation. It was found that flow rates were decreased as the inclination angle increases because of decrease in thermal driving head by the elevation difference between the core and steam generator center. Analytical results by RETRAN-03/INT described the overall characteristics of the experimental results successfully.

1.3 Outline of Work

To achieve the objective, chapter 2 describes the background of the types of instabilities and previous work. The characteristics of the two major types of instabilities such as static and dynamic instabilities are explained. In chapter 3, numerical analysis for two-fluid model is described including field equations, constitutive equations, and state of equations. The numerical solution scheme and validation are illustrated. Then chapter 4 represents the experimental apparatus and procedure. The mechanical components of the equipment will be presented step by step. Next the data acquisition, which is used to acquire the data, is presented. After that the method to conduct the experiment is described. Chapter 5 shows experimental results comparing with the results from the two-fluid model and discusses the results from both experiment and model. The effect of channel diameter on the flow characteristic is investigated by using the verified two-fluid model. Finally, chapter 6 summarizes and concludes the significance of this dissertation including suggestion.

Chapter II

Two-Phase Flow Instabilities

2. Introduction

Instabilities in Boiling Water Reactor are very important due to their consequences. Instabilities may have an effect on heat transfer characteristics, which may induce boiling crisis. Moreover, they may result in mechanical vibration in the components. These instabilities have been classified into many kinds by many researchers. There are two main types of instabilities: static and dynamic or oscillation instabilities. Static instabilities cause the unsteady state due to the small fluctuation. The causes of static instabilities are related to interfacial instabilities, flow and pressure fluctuation and change in heat transfer mechanism. Only the steady state laws can predict the threshold of static instabilities. Dynamic instabilities affect the flow condition if the inertia and other feedback effects have been involved in the processes. The steady state laws are not sufficient to predict the threshold of these instabilities. The dynamic conservation equations and servo (i.e., feedback control) analysis are required to explain the dynamic instabilities.

2.1 Static Instabilities

Many kinds of static and dynamic instabilities were reported during the past. The major types of static instabilities, which commonly observe, are flow-regime transitions or fundamental relaxation instability, flow excursion (Ledinegg) instability and geysering and chugging or compound relaxation instability.

2.1.1 Flow-regime transition instability

สถาบันวิทยบริการ
จุฬาลงกรณ์มหาวิทยาลัย

The flow- regime transition instability or fundamental relaxation stability resulted from the change in flow regime such as from bubbly to slug, slug to churn, churn to annular or annular to drop-annular are related interfacial instabilities (Hetsroni, 1982). Boure (1973) described the mechanism of these phenomena due to the change in flow regime between bubbly and annular flow. The increase of bubble populations in bubbly-slug regime may change the flow regime to annular flow, which has a characteristic in low pressure drop. Thus the velocity of the flow will increase. As the bubble vaporization is not enough to maintain annular flow, the flow regime turns back to bubbly-slug flow. The cycle then repeats. This phenomenon can be found and has undesirable in system performance of Boiling Water Reactor (Lahey, Jr., 1993).

2.1.2 Flow excursion (Ledinegg) instability

This phenomenon results from the reduction in the flow rate because of an increase in the friction loss of the system. The excursion stability criteria can be obtained from the steady state pump characteristic and the internal pressure drop characteristic.

$$\frac{\partial(\Delta p)_{ex}}{\partial u} \leq \frac{\partial(\Delta p)_{int}}{\partial u} \tag{2.1}$$

This equation shows that the slope of the supply curve shall be less than that of the demand curve to prevent the excursion instability. In general, the pressure drop in a heated channel with boiling can be as follows:

$$\Delta p_{\text{int}} = \Delta p_i + \Delta p_{con} + \Delta p_F + \Delta p_g + \Delta_e \tag{2.2}$$

where the pressure drop at the right hand side are the inlet, convective-acceleration, friction, gravity and exit pressure drops, respectively.

Consider the Fig. 2.1, there are the lines indicated the supply curve and the demand curve. The intersections of these two curves determine the steady state operation. On the other words, the equilibrium can be reached when the slope of the friction loss (supply curve) crosses over the demand curve. According to the excursion stability criteria, if the flow rate at point P' or P'' increases by a small perturbation, the pressure drop of the supply curve is less than the demand curve. Thus the flow decelerates and returns to original value. On the other hand, if the flow rate at point P' or P'' decreases by a small perturbation, since the head of the supply curve is more than of the demand curve the flow accelerates to the original value. Thus both point P' or P'' are stable for operating condition. Considering at the point P, if the flow rate is increased by a small perturbation, the new stable point is point P' because the friction loss of the demand curve is more than that of the supply curve. If the flow rate at the point P is decreased by a small perturbation, the new stable point is point P'' because the friction loss of the demand curve is less than that of the supply curve.

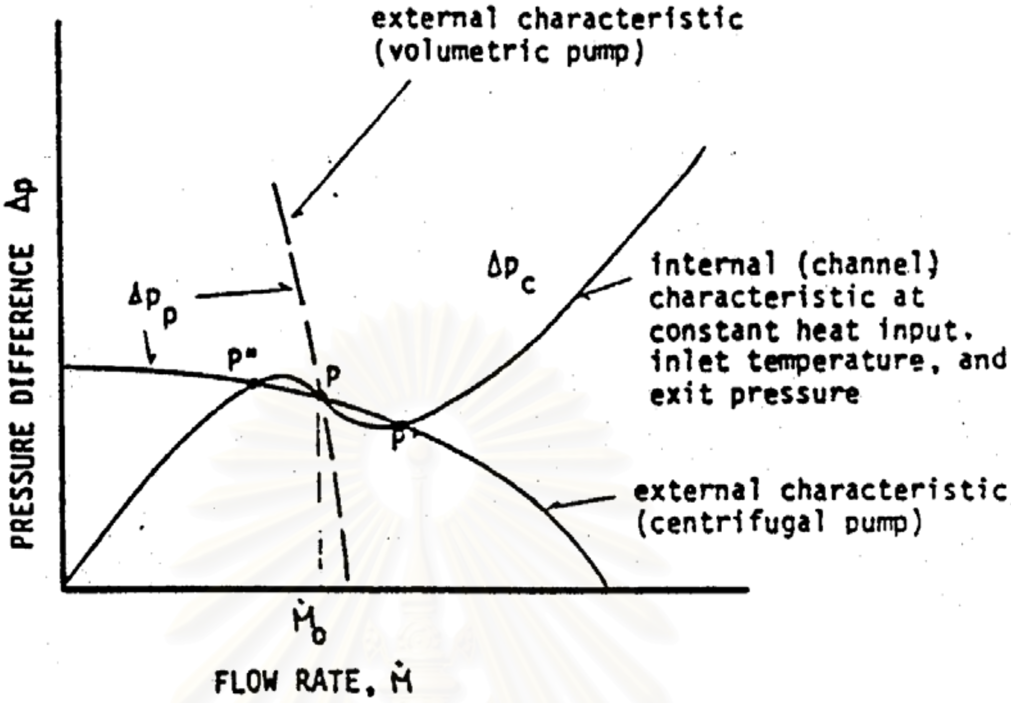

Fig. 2.1 Flow excursion characteristic (Yadigaroglu, 1998)

The effect of inlet pressure drop has been reported to stabilize the system. By adding of inlet flow restriction, the restriction will rotate the demand curve counter clockwise and rotate the supply curve clockwise. The excursion stability criterion can be achieved by this means.

2.1.3 Geysering and chugging instability

Geysering and chugging or compound relaxation stability involve static phenomena, which are coupled so as to produce a repetitive behavior, which is not necessarily periodic (Boure, 1973). The mechanism of geysering can be observed in vertical, closed end column with heater at the bottom. The driving mechanism of geysering proposed by Aritomi (1993) is as follows:

> *A large bubble covering the entire flow cross section is formed and grows towards the outlet plenum due to the decrease in hydrostatic head. As soon as the large bubble reaches the outlet plenum, it is mixed with subcooled water and condensed rapidly therein. Subcooled water reenters rapidly from the inlet plenum as the*

สถาบันวิทยบริการ
จุฬาลงกรณ์มหาวิทยาลัย

> *pressure drop corresponds to that in the other channel. If the condensation rate, that is, the reentering rate is higher than the circulation one, flow reversal is induced in the other channel. Both channels are filled with liquid and non-boiling condition is restored. After a while, a slug bubble is formed in the other channel because temperature of fluid reentering from the outlet plenum is higher than that in the channel. Such a process periodically repeats alternatively in both channels.*

The characteristic of geysering is shown in Fig.2.2. This instability is called “Geysering Induced by Condensation”. In parallel channels, geysering has the characteristic of the flow oscillation with phase difference of 180 degree between the two channels. Moreover, the whole frequency of the twin channels is twice of the frequency in each channel and flow reversal occurs in both channels (Chiang, 1994). Chugging is the phenomenon, which is characterized by the periodic explosion of the flow from the channel. Chugging instability can be observed for low-pressure liquid metals. A large ratio of liquid and vapor density and rapid evaporation from thin liquid films at the lower end of the heated section give rise to this kind of instability. With high evaporation rate at the inlet of the channel, the vapor velocity increases and then pressurizes the system. On the other hand, the pressurization pushes the level of the liquid at the inlet down and reduces the vapor velocity and evaporation rate. This will result in depressurization of the system, the liquid reenters the channels. The process then repeats. The degree of the explosion can be ranged from simple variation to violent ejection.

สถาบันวิทยบริการ
จุฬาลงกรณ์มหาวิทยาลัย

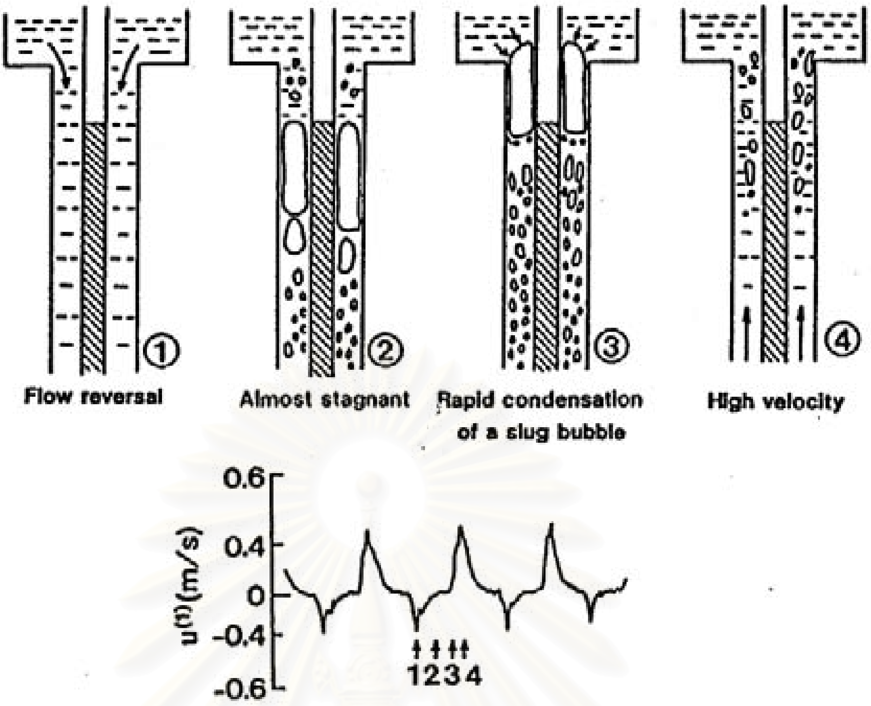

Fig. 2.2 Characteristic of geysering (Aritomi, 1993)

2.1.3.1 Parameter effects of Geysering stability

As shown by Chiang (1994), subcooling condition is indispensable for the occurrence of geysering. If the fluid in the outlet plenum is saturated, geysering will not occur. To investigate artificial geysering phenomenon, the subcooling must be controlled. An increase in the subcooling in the outlet plenum results in longer period of geysering because of longer delay time for boiling due to lower temperature fluid entering from the outlet plenum. Moreover, if the subcooling increases, the condensation rate becomes larger. Consequently the flow reversal rate and amplitude of the oscillation increases. Consider for non-heated riser length effect. A larger bubble can be formed in long non-riser and therefore the condensation rate becomes greater. In multiple boiling channels, the same feature for single channel is derived exception of the phase lag. It was revealed that the 180°, 120° and 90° phase lags exist for twin, three and four channels, respectively.

2.2 Dynamic instabilities

Dynamic instabilities can be classified into buoyancy wave, pressure wave, density wave, pressure-drop and thermal instabilities.

2.2.1 Buoyancy wave instability

Buoyancy wave or thermosiphon instability was proposed by Hsu and Graham (1986). The disturbance occurred during the flow regime change may produce the oscillation. This kind of instabilities usually occurs in natural circulation loop. The buoyancy force interrelates with the void fraction, which is the function of local heating, cooling rate and the fluid velocity. In these phenomena the system can be over and under the equilibrium point. As suggested by Hayama (1967), cited in Chiang (1994), buoyancy head is the function of the void fraction along the channel. The void fraction can be divided into the void fraction in heating channel and the void fraction in the riser. His analysis of the susceptibility to the oscillation is presented as follows. If the buoyancy head are defined by

$$H = \int \alpha dx = \int_{z_1}^{L} \alpha dx + \alpha_e L_r \tag{2.3}$$

where α is the local void fraction at z beyond the incipience point z_1, L is the length of heating section, α_e is the exit void and L_r is the riser length. Using the second mean theorem, the first term of the right hand can be achieved as

$$\int_{z_1}^{L} \alpha dx = \alpha_e L_{eq} \tag{2.4}$$

where $z_1 < L_{eq} < L$. Thus,

$$H = \alpha_d (L_{eq} + L_r) \tag{2.5}$$

The buoyancy head (H) depends on channel length, the fluid velocity and the rate of change of the buoyancy head can be shown from the conservation equations of mass and energy.

$$\frac{\partial H}{\partial t} = \frac{Q_h}{A \rho_l h_{fg}} \left(1 - \frac{z_1}{L} \right) - \alpha_e u_e \tag{2.6}$$

สถาบันวิทยบริการ
จุฬาลงกรณ์มหาวิทยาลัย

Combining with the previous equation to eliminate α_e yields

$$\frac{\partial H}{\partial t}=\frac{Q_h}{A\rho_l h_{fg}}\left(1-\frac{z_1}{L}\right)-\frac{u_e}{L_{eq}+L_r}H \tag{2.7}$$

Under steady state, $\partial H/\partial t=0$

$$\frac{Q_h}{A\rho_l h_{fg}}\left(1-\frac{z_1}{L}\right)=\frac{u_e H_0}{L_{eq}+L_r} \tag{2.8}$$

Therefore, the buoyancy equation is

$$\tau_B\frac{\partial H}{\partial t}=H_0-H \tag{2.9}$$

with

$$\tau_B=\frac{L_{eq}+L_r}{u} \tag{2.10}$$

considered as the time a particle travels through the void section. The steady state buoyancy head H_0 is determined by heat flux and boiling length, which in turn is determined by the flow rate and subcooling as well as heat flux. If a small perturbation in buoyancy ($\Delta H = H_0 - H$) caused by the small perturbation in velocity ($\Delta v = \in e^{\omega t}$), the resulting quadratic equation, which is yielded from combining the buoyancy head equation and the friction loss equation together with the small perturbation in velocity, is

$$I\omega^2+\left(a+\frac{I}{\tau_g}\right)\omega+\frac{c+a}{\tau_g}=0 \tag{2.11}$$

where

$$a=\left(\frac{\partial F_f}{\partial u}\right)_0 \tag{2.12}$$

$$c=\left(\frac{\partial H}{\partial u}\right)_0 \tag{2.13}$$

If ω is positive, a Ledinegg instability occurs. This happen when

$(c+a) < 0$ or $\left(\frac{\partial F_f}{\partial u}\right)-\left(\frac{\partial H}{\partial u}\right)<0$

However, the flow is to develop into neutral oscillation, ω must be imaginary as when

$(c+a) > 0$ and $a+\frac{I}{\tau_B}=0$

or

สถาบันวิทยบริการ
จุฬาลงกรณ์มหาวิทยาลัย

$$\frac{\partial F_f}{\partial u} + \frac{I}{\tau_B} = 0 \quad \text{and} \quad \frac{\partial F_f}{\partial u} - \frac{\partial H}{\partial u} > 0$$

2.2.2 Pressure wave or acoustic instability

This is the high frequency (10-100 Hz) wave oscillation with the period of the same order of magnitude for the pressure wave to pass through the system. This oscillation encounters in subcooled boiling, bulk boiling and film boiling. The amplitude of the oscillation is significant for high subcooled condition and it will diminish in bulk boiling region.

2.2.3 Density wave instability

Density wave normally can be observed in two-phase flow. It is the common type of instability due to the multiple feedback from the flow rate, vapor generation rate and pressure drop in a boiling channel. This low frequency oscillation period is approximately one to two times the time required for a fluid particle to travel through the channel. In this phenomenon, as the flow rate in the boiling channel reduces, the rate of enthalpy rise will increase. Thus the average density will be reduced. Consider the heating channel in Fig. 2.3. Yadigoroglu and Bergles (1972) showed that the heating channel was separated into 2 regions: single-phase and two-phase at the boiling boundary, which is the point where the bubbles occur. With the small perturbation of the oscillation of subcooled liquid entering the channel, the enthalpy perturbation will be produced at the point where the flow reaches the saturation point. Change in the flow and the length of the single-phase region give rise to the single-phase pressure drop perturbation. Due to enthalpy perturbation, the quality and the void fraction appear as another perturbation. The combination of quality and void perturbations with the variation of the two-phase region results in the two-phase pressure drop perturbation. This perturbation, which has the external characteristic of the channel, will create the feedback flow perturbation. With proper timing, this perturbation can acquire appropriate phase and become self-sustained.

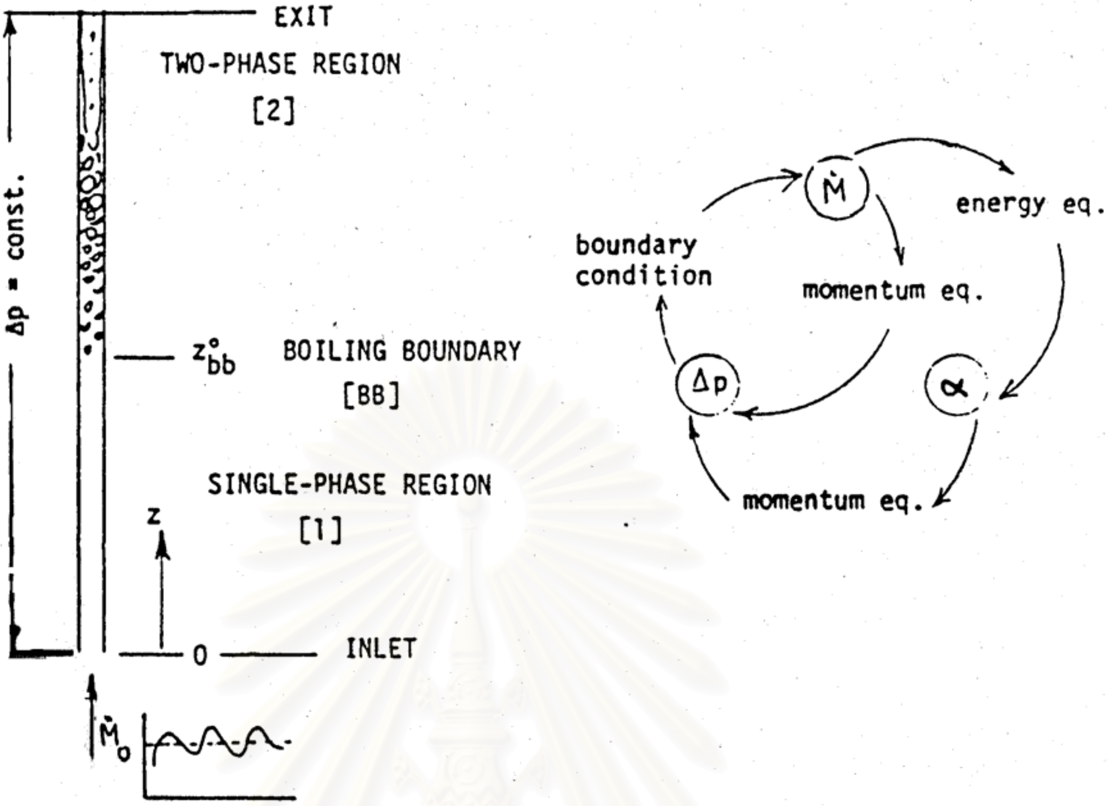

Fig. 2.3 Boiling channel and schematic of the various feedbacks (Yadigaroglu, 1998)

2.2.3.1 Parametric effects on density wave instabilities

Several important parameters including heat flux, inlet and exit restriction, subcooled condition, inlet flow and system pressure have been investigate because the density wave instability are strongly related to the total pressure drop. As previously described, the single-phase pressure drop has the stabilizing effect, since the pressure drop is in-phase with the inlet flow. Therefore the inlet restriction will help to stabilize instability. However, the two-phase pressure drop has the destabilizing effect, since it is out-of –phase with the inlet flow. Thus the outlet restriction reduces the flow stability. By decrease in heat flux or increase in inlet flow, these reduce the void fraction and two-phase region and have the effect on exit quality so the flow stability increases. An increase in subcooling condition reduces the void fraction and increases the non-boiling length, thus it has the stabilizing effect. Consider for the system pressure, this depresses the void fraction and reduces two-phase flow pressure drop. As a consequence, it will stabilize the flow stability.

2.2.4 Pressure-drop oscillations

Pressure-drop oscillations or compound dynamic instability as secondary phenomenon are triggered by a static instability phenomenon. These kinds of oscillations occur due to the interaction between the inertia mass and compressible volume like the spring-mass system. The conclusion from many researchers showed that the compressibility have the effect on critical heat flux, which will be reduced as the compressibility is increased. It also showed that the system is oscillated if the compressibility is large and inertia is small.

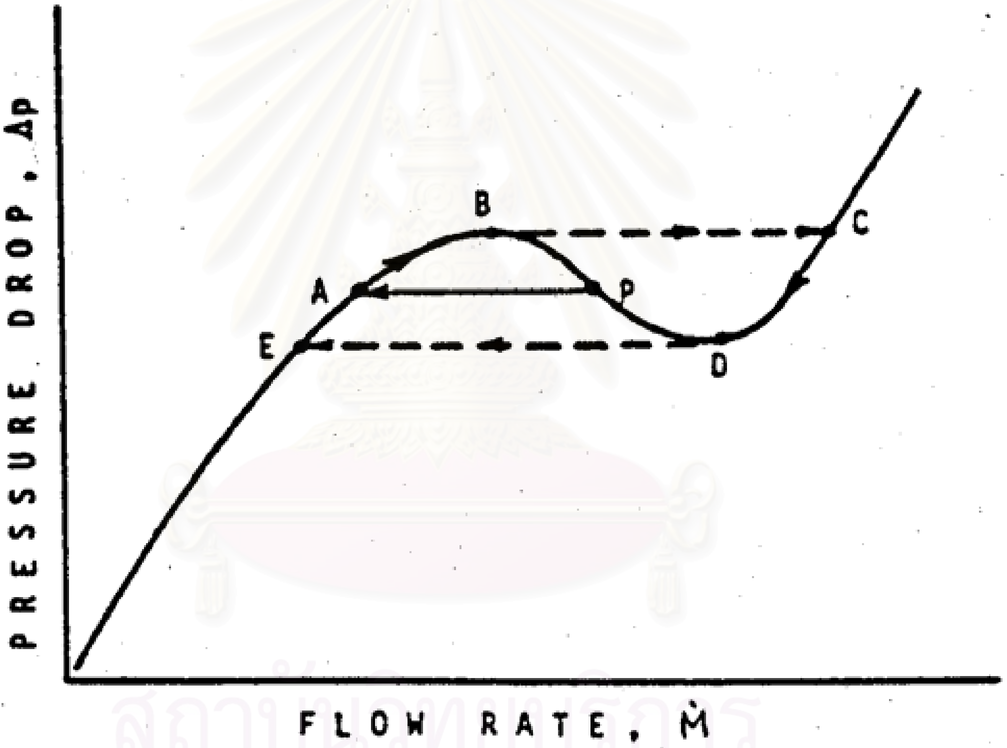

Fig. 2.4 Internal characteristic of pressure drop oscillation (Yadigaroglu, 1998)

Consider the characteristic of pressure-drop oscillations in Fig. 2.4, the unstable point P results in an initial excursive reduction of the flow rate through the heated section, along the line PA. Due to the flow imbalance the mass flow through the heating channel and store in the compressible volume. As the pressure in the control volume rises, the point moves along the segment AB. At point B the second excursion occurs, the point moves along BC. This results in the mass flow through the heating section. Consequently the pressure in the control volume reduces and the point moves along the segment CD. A flow excursion happens again at point D moving the point to E. The limit cycle ABCDEA repeats itself thereafter. These oscillations can be eliminated by throttling between the control volume and the heated channel.

2.2.5 Thermal oscillations

Thermal oscillations or compound dynamic instability are characterized by the instability of the liquid film that result from the flow oscillation between the film boiling and transition boiling, which give rise to high amplitude temperature oscillations at constant heat flux. Normally the thermal oscillations are triggered by other hydrodynamic instabilities, such as density wave or liquid-film instabilities. The higher frequency of density wave destabilized the stability of the liquid film boiling. The periods of these oscillations are quite long. On the contrary, the amplitudes of the oscillations are very high.

สถาบันวิทยบริการ
จุฬาลงกรณ์มหาวิทยาลัย

Chapter III

Numerical Analysis

3. Introduction

Two-fluid model will be developed by modified one-dimensional, transient drift-flux model of Chiang (1994). That drift-flux model consists of four equations of mixture mass, vapor mass, mixture motion and mixture thermal energy equations and constitutive equations. Volume void fraction, pressure, mixture velocity and specific internal energy of liquid phase are selected as primary dependent variables. To modify that drift-flux model to two-fluid model, six equations of phasic mass, momentum and energy will be used and six primary dependent variables are selected as described below. Constitutive equations and semi-implicit solution scheme are employed as same as Chiang's model. However, solution procedure will be changed so as to calculate the effect of flow loop conditions on stability of two-phase natural circulation.

3.1 Field Equations

This model solves six field equations for six primary dependent variables. Pressure, specific internal energy of vapor and liquid phase, vapor volume void fraction, velocities of liquid and vapor phase are selected as primary dependent variables. While density, temperature of vapor and liquid phase, saturation temperature are used as secondary dependent variables. The independent variables are time and distance. The basic six field equations (Ransom, 1995) are two phasic continuity equations, two phasic momentum equations and two phasic energy equations.

สถาบันวิทยบริการ
จุฬาลงกรณ์มหาวิทยาลัย

3.1.1 Phasic Mass Continuity Equations

$$\frac{\partial}{\partial t}(\alpha_l \rho_l) + \frac{1}{A}\frac{\partial}{\partial z}(\alpha_l \rho_l V_l A) = \Gamma_l \tag{3.1}$$

$$\frac{\partial}{\partial t}(\alpha_g \rho_g) + \frac{1}{A}\frac{\partial}{\partial z}(\alpha_g \rho_g V_g A) = \Gamma_g \tag{3.2}$$

The right hand sides of Equation (3.1) and (3.2) are mass transfers due to phase changes. In case of no mass sources or sinks, mass transfer due to phase change of liquid phase equals to negative of the vapor phase.

$$\Gamma_l = -\Gamma_g \tag{3.3}$$

The interfacial mass transfer is separated into mass transfer at the vapor/liquid interface in the bulk fluid and mass transfer at the vapor/liquid interface in the boundary layer near the walls.

$$\Gamma_g = \Gamma_{ig} + \Gamma_w \tag{3.4}$$

3.1.2 Phasic Momentum Conservation Equations

$$\begin{aligned}
&\alpha_l \rho_l A \frac{\partial V_l}{\partial t} + \frac{1}{2} \alpha_l \rho_l A \frac{\partial V_l^2}{\partial z} = -\alpha_l A \frac{\partial P}{\partial z} + \alpha_l \rho_l A B_z \\
&- (\alpha_l \rho_l A) FWF\ (V_l) - \Gamma_g A (V_{lI} - V_l) - (\alpha_l \rho_l A) \\
&FIF\ (V_l - V_g) - C \alpha_l \alpha_g \rho_m A [\frac{\partial (V_l - V_g)}{\partial t} + V_g \frac{\partial V_l}{\partial z} \\
&- V_l \frac{\partial V_g}{\partial z}]
\end{aligned} \tag{3.5}$$

$$\begin{aligned}
&\alpha_g \rho_g A \frac{\partial V_g}{\partial t} + \frac{1}{2} \alpha_g \rho_g A \frac{\partial V_g^2}{\partial z} = -\alpha_g A \frac{\partial P}{\partial z} + \alpha_g \rho_g A B_z \\
&- (\alpha_g \rho_g A) FWG\ (V_g) + \Gamma_g A (V_{gI} - V_g) - (\alpha_g \rho_g A) \\
&FIG\ (V_g - V_l) - C \alpha_g \alpha_l \rho_m A [\frac{\partial (V_g - V_l)}{\partial t} + V_l \frac{\partial V_g}{\partial z} \\
&- V_g \frac{\partial V_l}{\partial z}]
\end{aligned} \tag{3.6}$$

The forces on the right hand sides of Equation (3.5) and (3.6) are the pressure gradient, the body force, wall friction, momentum transfer due to interface mass transfer, interface frictional drag, and force due to virtual mass, respectively. The virtual mass is added to the solid mass to force the surrounding fluid to move (Kazimi and No, 1986). The virtual mass has the large influence on the mathematical characteristics and numerical stability of the two-fluid model (Drew et al., 1979; Watanabe and Kukita, 1992). Jump conditions at the interface due to conservation of momentum is as following:

สถาบันวิทยบริการ
จุฬาลงกรณ์มหาวิทยาลัย

$$\begin{aligned}&\Gamma_g A V_{gI} - (\alpha_g \rho_g A) FIG (V_g - V_l) - C\alpha_g \alpha_l \rho_m A[\frac{\partial (V_g - V_l)}{\partial t}]\\&-\Gamma_l A V_{lI} - (\alpha_l \rho_l A) FIF (V_l - V_g) - C\alpha_l \alpha_g \rho_m A[\frac{\partial (V_l - V_g)}{\partial t}] = 0\end{aligned} \tag{3.7}$$

The virtual mass terms are simplified by neglecting the spatial derivative portion without any effect (Ransom, 1995). In addition, the interface momentum transfer due to friction and due to mass transfer independently sum to zero.

$$V_{gI} = V_{lI} = V_I \tag{3.8}$$

and

$$\alpha_g \rho_g FIG = \alpha_l \rho_l FIF = \alpha_g \alpha_l \rho_g \rho_l FI \tag{3.9}$$

3.1.3 Phasic Energy Conservation Equations

$$\begin{aligned}&\frac{\partial}{\partial t}(\alpha_l \rho_l U_l) + \frac{1}{A}\frac{\partial}{\partial z}(\alpha_l \rho_l U_l V_l A) = -P\frac{\partial \alpha_l}{\partial t} - \frac{P}{A}\frac{\partial}{\partial z}(\alpha_l V_l A)\\&+ Q_{wl} + Q_{il} - \Gamma_{ig} h_l^* - \Gamma_w h_l' + DISS_L\end{aligned} \tag{3.10}$$

$$\begin{aligned}&\frac{\partial}{\partial t}(\alpha_g \rho_g U_g) + \frac{1}{A}\frac{\partial}{\partial z}(\alpha_g \rho_g U_g V_g A) = -P\frac{\partial \alpha_g}{\partial t} - \frac{P}{A}\frac{\partial}{\partial z}(\alpha_g V_g A)\\&+ Q_{wg} + Q_{ig} + \Gamma_{ig} h_g^* + \Gamma_w h_g' + DISS_g\end{aligned} \tag{3.11}$$

The right hand sides of Equations (3.10) and (3.11) are static pressure, wall heat transfer, interfacial heat transfer, heat transfer due to phase changes and energy dissipation, respectively. The total wall heat transfer rate to fluid per unit volume is as following.

$$Q = Q_{wg} + Q_{wf} \tag{3.12}$$

3.2 Constitutive Equations

The six field equations of mass, momentum and energy for each phase can be used to solve for primary dependent variables. However, it requires other equations such as flow regime maps, interfacial heat transfer, wall heat transfer, vapor

ศูนย์วิทยทรัพยากร
จุฬาลงกรณ์มหาวิทยาลัย

generation etc. to achieve closure of the solution. Thus constitutive equations are provided to calculate for those variables.

3.2.1 Flow regime maps

Following the flow regime maps, which are based on the work of Taitel and Dukler and Ishii, the vertical flow regime maps of bubbly, slug and annular mist regimes are modeled. According to Taitel and Duker, the dimensionless tube diameter is computed to check the validity of the bubbly flow in a small tube. They suggested that the bubbly flow may not exist if the dimensionless tube diameter is less than 19.11. The dimensionless tube diameter is expressed as

$$D^{*} = D[g(\rho_l - \rho_g)/\sigma]^{0.5} \tag{3.13}$$

For low mass fluxes of $G_m \leq 2000$ kg/m^2.s, the bubbly-slug transition will occur at void fraction $\alpha_g = 0.25$. The bubbly-slug criteria can be yielded

$$\alpha_L = 0.25\,min[1.0,(D^{*}/22.22)^{8}] \tag{3.14}$$

The number of 22.22 is used instead of 19.11 based on the data obtained from the development assessment of RELAP5/MOD2. This criteria shows that if the void fraction, $\alpha_{g,}$ exceeds α_L in the above equation, the bubbly flow can not exist because the rise velocity of small bubbles exceeds that of Taylor bubbles. At high mass fluxes of $G_m \geq 3000$ kg/m^2.s, a void fraction of 0.5 is used. To set up the bubbly-slug criteria, the upper and lower void limits are linearly interpolated. The bubbly-slug criteria can be shown as

$$\alpha_{BS} = \alpha_L \tag{3.15}$$

for mass fluxes of $G_m \leq 2000$ kg/m^2.s,

$$\alpha_{BS} = \alpha_L + 0.001(G_m - 2000)(0.5 - \alpha_L) \tag{3.16}$$

for mass fluxes of $2000 \leq G_m \leq 3000$ kg/m^2.s,

$$\alpha_{BS} = 0.5 \tag{3.17}$$

for mass fluxes of $G_m \geq 3000$ kg/m^2.s, if α_g is less than α_{BS}, the flow regime is bubbly regime otherwise the flow regime is slug regime. For slug to annular transition, the critical velocity is required to suspend a liquid droplet. The critical velocity suggested by Taitel and Duker in RELAP5/MOD2 can be written as

สถาบันวิทยบริการ
จุฬาลงกรณ์มหาวิทยาลัย

$$u_c = 3.1[\sigma g(\rho_l - \rho_g)]^{0.25} / \rho_g^{0.5} \tag{3.18}$$

The void fraction must be more than 0.75 to give good results between experiment and code recommended in RELAP5/MOD2. The slug to annular transition criteria is

$$\alpha_{SA} = MAX\left\{0.75, 1.4[\sigma g[(\rho_l - \rho_g)]^{0.25} / \upsilon_g \rho_g^{0.5}\right\} \tag{3.19}$$

If α_g is less than or equal to α_{SA}, the flow regime is slug regime otherwise the flow regime is annular mist regime.

3.2.2 Interfacial mass transfer rate

Interfacial mass transfer rate consists of evaporation and condensation from energy exchange at the interface and from wall heat transfer effect. It is assumed that vapor appears at saturation. The wall vaporization rate can be achieved for boiling in the boundary layer near the wall.

$$\Gamma_w = \frac{-Q_{il}^{w}}{h_g' - h_l'} \tag{3.20}$$

Similarly, it is assumed that liquid appears at saturation. The wall condensation rate can be achieved for condensation in the boundary layer near the wall.

$$\Gamma_w = \frac{-Q_{ig}^{w}}{h_g' - h_l'} \tag{3.21}$$

From phasic energy conservation equations (3.10) and (3.11), it is required that the interface terms sum to zero.

$$Q_{ig} + Q_{il} + \Gamma_{ig}(h_g^* - h_l^*) + \Gamma_w(h_g' - h_l') = 0 \tag{3.22}$$

The interface heat transfer can be expressed as

$$Q_{ig} = H_{ig}(T^s - T_g) - \frac{(1-\varepsilon)}{2}\Gamma_w(h_g' - h_l') \tag{3.23}$$

and

$$Q_{il} = H_{il}(T^s - T_g) - \frac{(1+\varepsilon)}{2}\Gamma_w(h_g' - h_l') \tag{3.24}$$

Finally, the mass transfer at the vapor/liquid interface in the bulk becomes

สถาบันวิทยบริการ
จุฬาลงกรณ์มหาวิทยาลัย

$$\Gamma_{ig} = \frac{-H_{ig}(T^s - T_g) + H_{il}(T^s - T_l)}{(h_g^* - h_l^*)} \tag{3.25}$$

and total interface mass transfer will be given as

$$\Gamma_g = \frac{-H_{ig}(T^s - T_g) + H_{il}(T^s - T_l)}{(h_g^* - h_l^*)} + \Gamma_w. \tag{3.26}$$

3.2.3 Heat Input and heat transfer models

3.2.3.1 Heat Input model

There are two options to use in this model. First, the heat flux will be released constantly to the fluid without computation of heat transfer between heater wall and fluid. Second, convection heat transfer between heater wall and fluid will be calculated and it is needed to calculate the wall temperature to solve for the solution. The heater wall temperature will be calculated from one-dimensional component radial difference approximation to the general conduction equation.

$$\frac{1}{r}[\frac{\partial}{\partial r}(rk_h \frac{\partial T}{\partial r})] + q_e = \rho_h C_{ph} \frac{\partial T}{\partial t}. \tag{3.27}$$

One dimensional and radial heat transfer, axial conduction are assumed. Temperature variation at circumference of the rod is neglected. Using those assumptions with a lump solution, the following differential equation is given:

$$\begin{aligned} T^{n+1} &= \{\frac{1}{2}(2\Delta r R_i + \Delta r^2)(\frac{\rho_h C_{ph}}{\Delta t} + q_e) - (R_i + \Delta r) \\ &[h_{wl}(T^n - T_l^{n+1}) + h_{wv}(T^n - T^{n+1})\} /[\frac{1}{2}(2\Delta r R_i + \Delta r^2)(\frac{\rho_h C_{ph}}{\Delta t}) \end{aligned} \tag{3.28}$$

where q_e is electric heating power (w), Δr is thickness, R_i is inner radius, ρ_h , C_{ph} are density and specific heat capacity of the heater, respectively.

3.2.3.2 Heat transfer model

In this model it is assumed that the wall is totally wetted by liquid and that the wall is not wetted by vapor. Consequently the heat transfer from the wall to the vapor, Q_{wg}, is equal to zero. Heat transfer from the wall to the liquid is given as

สถาบันวิทยบริการ
จุฬาลงกรณ์มหาวิทยาลัย

$$Q_{wl} = h_w A_{wl} (T_w - T_l) / V \qquad (3.29)$$

Where h_w is heat transfer coefficient obtained from the heat transfer coefficient models, A_{wl} is the heat transfer area between the wall and the liquid, and T_w, T_l are the wall and the liquid temperature, respectively.

3.2.4 Heat Transfer Coefficients

According to phasic energy field equations, the heat will transfer to the liquid from wall, Q_{wl} and $Q_{wg,}$ and interphase, Q_{il} and $Q_{ig.}$ To calculate both heat transfer from wall and interface, thus heat transfer coefficients are separated into two types. One is interface heat transfer coefficient and the other is wall heat transfer coefficient. The following equations are used for interphase heat transfer coefficients.

3.2.4.1 Interphase Heat Transfer Coefficients

For bubbly and slug flow, the heat transfer coefficients of the Plesset-Zwick is given as:

$$H_{il} = \frac{k_l}{D_h}\left[\frac{12(T_l - T^s)\rho_l C_{pl}}{\pi \rho_v h_{fg}}\right]. \qquad (3.30)$$

and a sphere convection coefficient of Lee-Ryley is given as:

$$H_{il} = \frac{k_l}{D_h}[2 + 0.74(\frac{\rho_l V_r D_b}{\mu_l})^{0.5}. \qquad (3.31)$$

and

$$H_{Ig} = 10^{14} (w / m^2 K). \qquad (3.32)$$

For annular mist flow, heat transfer coefficients given from Chiang(1994), which was modified from the constitutive equation used by TRAC and RELAP5/MOD2 are expressed as:

$$H_{ilf} = 0.02 \rho_l v_l C_{ph}. \qquad (3.33)$$

$$H_{ild} = \begin{cases} 11300 \dfrac{k_l}{D_d}, (T^s \le T_l) \\ 0.02 \rho_l v_c C_{ph}, (T^s > T_l). \end{cases} \qquad (3.34)$$

for film and droplets of liquid, respectively. Here v_c is swirl velocity and is given as

ศูนย์วิทยทรัพยากร
จุฬาลงกรณ์มหาวิทยาลัย

$$V_c = \min\left\{1 - \exp\left[0.5\frac{\mu_g}{\mu_g + \mu_l}\right]V_r, 1.4\left(\frac{\sigma}{\rho_l D_d}\right)^{0.5}, 0.5\right\}. \tag{3.35}$$

Heat transfer coefficient for liquid side can be achieved from

$$A_i H_{il} = A_{if} H_{ilf} + A_{id} H_{ild}. \tag{3.36}$$

The heat transfer coefficients of film and droplets are given as follows:

$$H_{ivf} = 0.02\rho_v C_{pv}. \tag{3.37}$$

$$H_{ivd} = \frac{k_v}{D_d}(2 + 0.74\,\mathrm{Re}_v^{1/2}\,\mathrm{Pr}_v^{1/3}). \tag{3.38}$$

Heat transfer coefficient for vapor side can be achieved from

$$A_i H_{iv} = A_{if} H_{ivf} + A_{id} H_{ivd}. \tag{3.39}$$

For transition flow which is assumed that the void fraction is between 0.5 and 0.75, the heat transfer coefficients can be obtained by interpolating and weighing between the slug and annular mist flow regimes as follows:

$$A_i H_{iv} = (1 - w)H_{iv1} + wH_{iv2}. \tag{3.40}$$

$$A_i H_{il} = (1 - w)H_{il1} + wH_{il2}. \tag{3.41}$$

The weighing factor is given as:

$$w = \begin{cases} 0, (\alpha \le 0.5) \\ (4\alpha - 2)^2(7 - 8\alpha), (0.5 < \alpha < 0.75) \\ 1, (\alpha \ge 0.75) \end{cases} \tag{3.42}$$

For transition regime, the relative velocity used in the slug regime is replaced by

$$V_r^* = w2.33\left[\frac{(\rho_l - \rho_g)\sigma We_b}{\rho_l^2}\right]^{0.25} + (1 - w)V_r \tag{3.43}$$

3.2.4.2 Wall Heat Transfer Coefficients

For wall heat transfer coefficients, the correlation equations by Dittus-Boelter for turbulent flow,Rohsenow and Choi for laminar flow, McAdams for natural convection and Chen for subcooled boiling mode are used as follows:

สถาบันวิทยบริการ
จุฬาลงกรณ์มหาวิทยาลัย

Dittus-Boelter correlation equation for turblent flow

$$h_w = 0.023 \frac{k}{D_h} Pr^{0.4} \; Re^{0.8} \tag{3.44}$$

Rohsenow and Choi correlation equation for laminar flow

$$h_w = 4.0 \frac{k}{D_h} \tag{3.45}$$

McAdams correlation equation for natural convection

$$h_w = 0.13(Gr\, Pr)^{1/3} \frac{k}{D_h} \tag{3.46}$$

Chen correlation equation for subcooled boiling

$$h_w = h_{mic} + h_{mac} \tag{3.47}$$

where

$$h_{mac} = 0.023 \frac{k}{D_h} Pr^{0.4} \; Re_l^{0.8} \; F \tag{3.48}$$

$$h_{mic} = 0.00122 \frac{k_l^{0.79} C_{pf}^{0.45} \rho_f^{0.49}}{\sigma^{0.5} \mu_l^{0.29} h_{fg}^{0.24} \rho_v^{0.24}} \Delta T_{sat}^{0.24} \Delta P^{0.75} S \tag{3.49}$$

3.2.4.3 Interfacial area

The interfacial area for different flow regimes is required to calculate interfacial heat transfer coefficients. In this model, the interfacial area is retrieved from TRAC-BD for bubbly and slug regimes. For annular mist regime, the model of the interfacial area based on TRAC-PF1 is adopted. For churn turbulent regime or transition regime, the interfacial area will be interpolated between slug and annular mist regime.

Bubbly regime:

The interfacial area can be computed in terms of Webber number, We_b, which is given as

$$We_b = \frac{\rho_l V_r^2 D_b}{\sigma} \tag{3.50}$$

สถาบันวิทยบริการ
จุฬาลงกรณ์มหาวิทยาลัย

where D_b is the bubble diameter. The Webber number has been used differently among the analysis codes. In this model, the Webber number of 7.5 is adopted to represent the average particle size. From the above equation, the bubble diameter can be calculated to find the interfacial area per unit volume assumed a uniform distribution in the volume. The interfacial area per unit volume is expressed as

$$a_{ib} = \frac{6\alpha_g}{D_b} \tag{3.51}$$

The interfacial area can be yielded as follows:

$$A_{ib} = \frac{6\alpha_g \rho_l V_r^2 (Vol)}{We_b \sigma} \tag{3.52}$$

Slug regime:

Suggested by Ishii and Mishima, the slug flow consists of the two components: an element of Taylor bubble and a number of small bubbles in the slug. The interfacial area per unit volume is given by

$$a_{is} \cong \frac{4.5}{D_h} \frac{(\alpha_g - \alpha_{gs})}{(1-\alpha_{gs})} \frac{(1-\alpha_g)}{(1-\alpha_{gs})} \tag{3.53}$$

where D_h is hydraulic diameter and α_{gs} is average void fraction in the liquid slug and is express as

$$\alpha_{gs} = \begin{cases} 0.3, G < 2000 \ kg/m^2 s \\ 0.3 + 0.2\left(G - 2000\right)/7000 \ , 2000 \le G < 2700 \ kg/m^2 s \\ 0.5, G \ge 2700 \ kg/m^2 s \end{cases} \tag{3.54}$$

The interfacial area can be calculated from

$$A_{is} = a_{is}\left(Vol\right) \tag{3.55}$$

Annular mist regime:

The annular mist regime exists when the void fraction is larger than 0.75. The interfacial area for entrained droplets and liquid wall film are necessary to compute the interphase heat transfer coefficients in annular mist regime as shown in the previous section and are expressed respectively as

สถาบันวิทยบริการ
จุฬาลงกรณ์มหาวิทยาลัย

$$A_{if} = (1-E)A_{wet}\frac{1-\alpha_g}{1-Min\,[\alpha_g, 1-1.02x10^{-3}/D_h]} \tag{3.56}$$

$$A_{id} = 6E\left(1-\alpha_g\right)\frac{Vol}{D_h} \tag{3.57}$$

where

$$E = max\left\{1-exp\left(0.50\frac{v_e - v_g}{v_e}\right), 7.75x10^{-7}We_e(Re_e We_e)^{0.25}\right\} \tag{3.58}$$

$$v_e = 2.33\left[\frac{(\rho_l - \rho_g)\sigma We_d}{\rho_g^2}\right] \tag{3.59}$$

$$We_e = \frac{\rho_g^{2/3}(\alpha_g v_g)^2 D_h(\rho_l - \rho_g)^{1/3}}{\sigma} \tag{3.60}$$

$$Re_e = \frac{\rho_l v_l D_h(1-\alpha_g)}{\mu_l} \tag{3.61}$$

3.2.5 Wall Friction

The wall friction terms in RELAP5/MOD3 are adopted to use in this model. The wall friction coefficients are used in stead of phasic wall shear stresses as follows:

$$FWF(\alpha_l \rho_l v_l)A = \tau_l \rho_l A = \alpha_l\left(\frac{dP}{dx}\right)_{2\phi}\left(\frac{z^2}{\alpha_g + \alpha_l z^2}\right)A \tag{3.63}$$

and

$$FWG(\alpha_g \rho_g v_g)A = \tau_g \rho_g A = \alpha_g\left(\frac{dP}{dx}\right)_{2\varphi}\left(\frac{1}{\alpha_g + \alpha_l z^2}\right)A \tag{3.64}$$

3.2.5.1 The two-phase friction multiplier approach

A two-phase multiplier approach is used in this model including flow regime maps of Taiel and Dukler and Ishii. By using the model of Lockhart-Martinelli, the

สถาบันวิทยบริการ
จุฬาลงกรณ์มหาวิทยาลัย

overall friction pressure drop can be calculated from the wall friction drop of liquid alone

$$\left(\frac{dP}{dx}\right)_{2\phi} = \phi_l^2 \left(\frac{dP}{dx}\right)_l \tag{3.64}$$

or from the wall friction drop of vapor alone

$$\left(\frac{dP}{dx}\right)_{2\phi} = \phi_g^2 \left(\frac{dP}{dx}\right)_g \tag{3.65}$$

where ϕ_l^2 and ϕ_g^2 are the liquid alone and vapor alone two-phase Darcy-Weisbach friction multipliers, respectively. The phasic wall friction pressure gradients are given as

$$\left(\frac{dP}{dx}\right)_l = \frac{\lambda'_l (Re'_l) M_l^2}{2 D \rho_l A^2} \tag{3.66}$$

and

$$\left(\frac{dP}{dx}\right)_g = \frac{\lambda'_g (Re'_g) M_g^2}{2 D \rho_g A^2} \tag{3.67}$$

for liquid alone and vapor alone, respectively. The Reynolds numbers where the prime indicated the liquid alone and the vapor alone Darcy-Weibach friction factors are

$$Re'_l = \frac{M_l D}{\mu_l A} \tag{3.68}$$

and

$$Re'_g = \frac{M_g D}{\mu_g A} \tag{3.69}$$

for liquid and vapor, respectively. The mass flow rates of liquid and vapor are respectively defined as

$$M_l = \alpha_l \rho_l v_l A \tag{3.70}$$

and

$$M_g = \alpha_g \rho_g v_g A \tag{3.71}$$

From above equations, the overall two-phase friction pressure gradient from the Lockhart-Martinelli ratio can be calculated from

สถาบันวิทยบริการ
จุฬาลงกรณ์มหาวิทยาลัย

$$\chi^2 = \frac{\left(\frac{dP}{dx}\right)_l}{\left(\frac{dP}{dx}\right)_g} = \frac{\phi_g^2}{\phi_l^2} \tag{3.72}$$

3.2.5.2 The HTFS two-phase friction multiplier correlation

To calculate the two-phase friction multipliers, the HTFS two-phase friction multiplier correlation is adopted. The HTFS correlation is expressed as

$$\phi_l^2 = 1 + \frac{C}{\chi} + \frac{1}{\chi^2} \tag{3.73}$$

and

$$\phi_g^2 = \chi^2 + C\chi + 1 \tag{3.74}$$

for liquid alone and vapor alone, respectively, where C is the correlation coefficient and χ is the Lockhart-Martinelli ratio. The correlation coefficient C can be calculated in term of mass flux and the Baroczy dimensionless property index, Λ.

$$2 \leq C = -2 + f_1(G)T_1(\Lambda, G) \tag{3.75}$$

where

$$f_1(G) = 28 - 0.3\sqrt{G} \tag{3.76}$$

$$T_1(\Lambda, G) = exp\left(-\frac{(log_{10}\Lambda + 2.5)^2}{2.4 - G(10^{-4})}\right) \tag{3.77}$$

$$\Lambda = \frac{\rho_l}{\rho_g}\left(\frac{\mu_l}{\mu_g}\right)^{0.2} \tag{3.78}$$

The phasic wall shear forces for liquid and vapor can be given in term of the two-phase friction factors and the unknown parameter as

$$\tau_l \rho_l = \alpha_l \left(\frac{dP}{dx}\right)_{2\phi}\left(\frac{z^2}{\alpha_g + \alpha_l z^2}\right) \tag{3.79}$$

and

$$\tau_g \rho_g = \alpha_g \left(\frac{dP}{dx}\right)_{2\phi}\left(\frac{1}{\alpha_g + \alpha_l z^2}\right) \tag{3.80}$$

สถาบันวิทยบริการ
จุฬาลงกรณ์มหาวิทยาลัย

The unknown parameter is

$$z^2 = \frac{\lambda_l(Re_l)\rho_l v_l^2 \dfrac{\alpha_{lw}}{\alpha_l}}{\lambda_g(Re_g)\rho_g v_g^2 \dfrac{\alpha_{gw}}{\alpha_g}} \tag{3.81}$$

where

$\lambda_l(Re_l)$ = liquid Darcy friction factor

$\lambda_g(Re_g)$ = vapor Darcy friction factor

Re_l = liquid Reynolds number

$$= \frac{\rho_l v_l D_l}{\mu_l} \tag{3.82}$$

Re_g = vapor Reynolds number

$$= \frac{\rho_g v_g D_g}{\mu_g} \tag{3.83}$$

α_{lw} = the liquid fraction on the wall from the flow regime factor

α_{gw} = the vapor fraction on the wall from the flow regime factor

D_l = liquid hydraulic diameter

$$= \frac{4A_l}{p_l} \tag{3.84}$$

A_l = liquid flow area

$$= \alpha_l A \tag{3.85}$$

D_g = vapor hydraulic diameter

$$= \frac{4A_g}{p_g} \tag{3.86}$$

A_g = vapor flow area

$$= \alpha_g A \tag{3.87}$$

p_l = liquid wetted perimeter

$$= \alpha_{lw} p \tag{3.88}$$

p_g = vapor wetted perimeter

$$= \alpha_{gw} p \tag{3.89}$$

สถาบันวิทยบริการ
จุฬาลงกรณ์มหาวิทยาลัย

3.2.5.3 Flow regime factors for phasic wall friction

In vertical flow regime map, the three flow regimes of bubbly, slug and annular mist are modeled. The wall liquid and vapor volume fractions are

$$\frac{p_l}{p_m} = \alpha_{lw} \tag{3.90}$$

and

$$\frac{p_g}{p_m} = \alpha_{gw} \tag{3.91}$$

where p_l, p_g and p_m are the perimeters wetted by the liquid, vapor and mixture, respectively. From the flow regime maps, the wall liquid and vapor volume fractions can be represented as follows:

Bubbly regime:

$$\alpha_{lw} = \alpha_l \tag{3.92}$$

and

$$\alpha_{gw} = \alpha_g \tag{3.93}$$

where α_l and α_g are the overall liquid and vapor volume fractions, respectively.

Slug regime:

$$\alpha_{lw} = 1 - \alpha_{gs} \tag{3.94}$$

and

$$\alpha_{gw} = \alpha_{gs} \tag{3.95}$$

where α_{gs} can be obtained from the flow regime maps.

Annular mist regime:

$$\alpha_{lw} = \alpha_{ff}^{0.25} \tag{3.96}$$

and

$$\alpha_{gw} = 1 - \alpha_{ff}^{0.25} \tag{3.97}$$

where α_{ff} can be obtained from the flow regime maps.

สถาบันวิทยบริการ
จุฬาลงกรณ์มหาวิทยาลัย

3.2.5.4 The friction factor model

In order to compute the unknown parameter, z^2, the Darcy-Weibach friction factor is used for laminar and turbulent flows with the interpolation in the transition regime. The laminar friction factor is expressed as

$$\lambda_L = \frac{64}{Re\,\phi_s}, 0 \le Re \le 2200 \tag{3.98}$$

where Re is the Reynolds number and Φ_s is a user input shape factor for noncircular flow channels. To calculate the friction factor in transition regime, the linear interpolation of the laminar and turbulent friction factor is used as

$$\lambda_{L,T} = \left(\frac{Re - 2200}{3000 - 2200}\right)\left(\lambda_{T,3000} - \lambda_{L,2200}\right) + \lambda_{L,2200}, 2200 \le Re \le 3000 \tag{3.99}$$

where $\lambda_{L,2200}$ is the laminar factor at a Reynolds number of 2200, $\lambda_{T,3000}$ is the turbulent friction factor at a Reynolds number of 3000 and the interpolation factor is defined to lie between zero and one. The turbulent friction factor by Zigrang-Sylvester approximation to the Colebrook-White correlation is adopted as

$$\frac{1}{\lambda_L} = -2\,log\left\{\frac{\varepsilon / D}{3.7} + \frac{2.51}{Re}\left[1.14 - 2\,log\left(\frac{\varepsilon}{D} - \frac{21.25}{Re^{0.9}}\right)\right]\right\} \tag{3.100}$$

where ε is the surface roughness.

3.2.6 Dissipation of Wall friction

The dissipation of wall friction will be considered in this model. The dissipation effects due to interface mass transfer, interface friction and virtual mass are neglected because these terms are small in magnitude in energy equations. Therefore, the wall friction dissipation are defined as

$$DISS_g = \alpha_g \rho_g FWG(V_g^2) \tag{3.101}$$

and

$$DISS_l = \alpha_l \rho_l FWF(V_l^2). \tag{3.102}$$

The total energy dissipation terms can be defined as

$$DISS = DISS_l + DISS_g. \tag{3.103}$$

สถาบันวิทยบริการ
จุฬาลงกรณ์มหาวิทยาลัย

3.2.7 Interphase friction

Due to the important characteristics of two-fluid model, the velocities of liquid and vapor phase are calculated separately. Therefore the interaction between the phases will be taken into account. In momentum equations, the interface friction per unit volume is utilized to calculate the velocity for each phase and can be written in terms of interphase friction coefficients as

$$F_{il} = \alpha_l \rho_l FIF\,(v_g - v_l) \tag{3.104}$$

and

$$F_{ig} = \alpha_g \rho_g FIG\,(v_g - v_l) \tag{3.105}$$

for liquid and vapor phase, respectively. The F_{il} is the magnitude of the interfacial friction force on the liquid and the F_{ig} is the magnitude of the interfacial friction force on the vapor. It is assumed that the magnitude of the interfacial friction force on the liquid be equal to the interfacial friction force on the vapor. Thus the following equation is yielded

$$\alpha_l \rho_l FIF = \alpha_g \rho_g FIG = \alpha_g \rho_g \alpha_l \rho_l FI \tag{3.106}$$

where FI is a global interfacial friction coefficient. The interfacial friction force in the difference momentum equation is given by

$$\frac{F_{ig}}{\alpha_g \rho_g} + \frac{F_{il}}{\alpha_l \rho_l} = (FIG + FIF)(v_g - v_l) \tag{3.107}$$

In terms of a global interfacial friction coefficient, the equation becomes

$$\frac{F_{ig}}{\alpha_g \rho_g} + \frac{F_{il}}{\alpha_l \rho_l} = \rho_m FI\,(v_g - v_l) \tag{3.108}$$

As a result the global interfacial friction coefficient can be defined as

$$FI = \frac{\dfrac{F_{ig}}{\alpha_g \rho_g} + \dfrac{F_{il}}{\alpha_l \rho_l}}{\rho_m (v_g - v_l)} \tag{3.109}$$

The two models of interfacial friction forces are employed: drift-flux and drag coefficient. The former uses for the bubbly and slug regime. The later uses for the annular mist regime.

3.2.7.1 Drift flux method

This method is adopted for bubbly and slug regimes in vertical flow. The drift-flux correlation, C_0, and drift velocity, v_{gj}, will be used to compute the interfacial friction force. The drift-flux correlation and drift velocity in bubbly, slug, churn and annular regimes by Zuber-Findley are as follows:

Bubbly regime:

$$C_0 = 1.2 - 0.2\sqrt{\frac{\rho_g}{\rho_l}} \tag{3.110}$$

$$V_{gj} = (1-\alpha_g)^{1.5}\sqrt{2}\left\{\frac{g(\rho_l-\rho_g)D_h}{\rho_l}\right\}^{0.25} \tag{3.111}$$

Slug regime:

$$C_0 = 1.2 \tag{3.112}$$

$$V_{gj} = 0.35\left\{\frac{g(\rho_l-\rho_g)D_h}{\rho_l}\right\}^{0.5} \tag{3.113}$$

Churn regime:

$$C_0 = 1.2 - 0.2\sqrt{\frac{\rho_g}{\rho_l}} \tag{3.114}$$

$$V_{gj} = \sqrt{2}\left\{\frac{g(\rho_l-\rho_g)D_h}{\rho_l}\right\}^{0.25} \tag{3.115}$$

Annular mist regime:

$$C_0 = 1.0 \tag{3.116}$$

$$V_{gj} = \frac{1-\alpha_g}{\alpha_g + 4\sqrt{\frac{\rho_g}{\rho_l}}}\left\{J_T + \frac{g(\rho_l-\rho_g)D_h(1-\alpha_g)}{0.015\,\rho_l}\right\} \tag{3.117}$$

where

J_T = the total volume metric flow rate

$$= J_g + J_l \tag{3.118}$$

สถาบันวิทยบริการ
จุฬาลงกรณ์มหาวิทยาลัย

J_g = the vapor volume metric flow rate

$$= \alpha_g v_g \tag{3.119}$$

J_l = the liquid volume metric flow rate

$$= (1 - \alpha_g) v_l \tag{3.120}$$

D_h = hydraulic diameter

The interfacial force can be computed from

$$F_i = C_i \left| C_1 v_g - C_0 v_l \right| \left(C_1 v_g - C_0 v_l \right) \tag{3.121}$$

where C$_i$ is the unknown coefficient and is written as

$$C_i = \frac{\alpha_l \alpha_g^3 (\rho_l - \rho_g) g}{V_{gj}^2} \tag{3.122}$$

and C$_1$ is written as

$$C_1 = \frac{1 - \alpha_g C_0}{1 - \alpha_g} \tag{3.123}$$

where the drift velocity, V_{gj}, is given in the above equations. Consider the momentum equations at steady state and neglect the effect of virtual mass and momentum flux terms. The equations are yielded as

$$0 = -\alpha_g \frac{dP}{dx} - F_{ig} - F_{wg} - \alpha_g \rho_g g \tag{3.124}$$

and

$$0 = -\alpha_l \frac{dP}{dx} + F_{il} - F_{wl} - \alpha_l \rho_l g \tag{3.125}$$

Combining both equations together by multiplying the first equation with α_g and the second equation with α_l, then subtracting the second equation from the first equation, the equation becomes

$$\alpha_l F_{ig} + \alpha_l F_{il} = \alpha_l \alpha_g (\rho_l - \rho_g) g - \alpha_l F_{wg} + \alpha_g F_{wl} \tag{3.126}$$

Because of the magnitude of the interfacial friction force on the two phases are equal, the equation in term of the interfacial friction force is

$$F_i = \alpha_l \alpha_g (\rho_l - \rho_g) g - \alpha_l F_{wg} + \alpha_g F_{wl} \tag{3.127}$$

where

$$F_i = F_{ig} = F_{il} \tag{3.128}$$

By using the drift flux correlation, which takes into account of the wall friction in that correlation, to calculate the interfacial friction force. The effect of wall friction has to eliminate. Thus the interfacial friction force is represented by the buoyancy force and becomes

$$F_i = \alpha_l \alpha_g (\rho_l - \rho_g) g \tag{3.129}$$

The global interfacial friction coefficient FI can be determined by taking into account of the relative velocity in drift flux model.

$$FI = \frac{\left(\dfrac{F_{ig}}{\alpha_g \rho_g}\right) + \left(\dfrac{F_{il}}{\alpha_l \rho_l}\right)}{\rho_m (C_1 v_g - C_0 v_l)} \tag{3.130}$$

3.2.7.2 Drag coefficient method

For annular regime, the drag coefficient method is employed. The interphase drag force per unit volume in terms of relative phasic velocity is

$$F_i = -f_{gl} \left| v_g - v_l \right| \left(v_g - v_l \right) \tag{3.131}$$

with

$$f_{gl} = \frac{1}{8} \rho_c S_F a_{gl} C_D \tag{3.132}$$

where

ρ_c = density of the continuous phase

C_D = drag coefficient

a_{gl} = interfacial area per unit volume

S_F = shape factor = 1.0

The interfacial area per unit volume can be calculated from

$$a_{gl} = \left(\frac{4 C_{an}}{D} \right) (1 - \alpha_{ff})^{1/2} + \left(\frac{3.6 \alpha_{fd}}{d_0} \right) \left(1 - \alpha_{ff} \right) \tag{3.133}$$

สถาบันวิทยบริการ
จุฬาลงกรณ์มหาวิทยาลัย

where C_n is a roughness parameter introduced to account for waves in the liquid wall film and α_{fd} is the average liquid volume fraction in the vapor core, for which

$$a_{fd} = \frac{(\alpha_f - \alpha_{ff})}{(1 - \alpha_{ff})} \qquad (3.134)$$

For vertical flow regimes, the entrainment relation is

$$\alpha_{ff} = \alpha_f C_f \, exp[-7.5x10^{-5} (\alpha_g v_g / u_c)^6] \qquad (3.135)$$

where u_c is the critical velocity. The term C_f can be expressed as

$$C_f = 10^{-4} \alpha_l \rho_l v_l \frac{D}{\mu_l} \qquad (3.136)$$

The interfacial friction factor, f_i, for the liquid film by Bharathan et. al., cited in Ransom (1995), is used instead of C_D and is written as

$$f_i = 4 [0.005 + A(\delta^*)^B \qquad (3.137)$$

where

$$log_{10} A = -0.56 + \frac{9.07}{D^*} \qquad (3.138)$$

$$B = 1.63 + \frac{4.74}{D^*} \qquad (3.139)$$

$$\delta^* = \delta \left[\frac{(\rho_l - \rho_g) g}{\sigma} \right]^{1/2} \qquad (3.140)$$

= the liquid wall film Deryagin number

3.2.8 Virtual mass

In two-phase flow, the velocity of the liquid and the vapor phase is not the same. Thus the acceleration of one phase with another phase may lead to an apparent inter-phasic force (Kazami 1986). This force caused the fluid surrounding the objects to move will take the form of virtual mass. The coefficient of virtual mass will be added in momentum equations and is determined based on the flow regime. The inertial drag force per unit volume in RELAP5/MOD3 is written as

$$FA_{gl} = -C \alpha_g (1 - \alpha_g) \rho \left[\frac{\partial (v_g - v_l)}{\partial t} \right] \qquad (3.141)$$

where

$$\rho = \alpha_g \rho_g + (1-\alpha_g)\rho_l \tag{3.142}$$

FA_{gl} = force per unit volume due to dynamic drag

The virtual mass coefficient, C, is given as

$$C = \begin{cases} \dfrac{1}{2}\dfrac{(1-2\alpha_g)}{(1-\alpha_g)}, 0 \le \alpha_g \le 1/2 \\ \dfrac{1}{2}\dfrac{(3-2\alpha_g)}{\alpha_g}, 1/2 \le \alpha_g \le 1 \end{cases} \tag{3.143}$$

for all flow regimes.

3.3 Equation of state

The equations of state are required to turn the unknown variables into the primary dependent variables. Moreover, the provisional new time level of liquid and vapor densities, liquid and vapor temperature and saturation temperature are calculated by linearization at the old time level of those properties. The linerization equations of those properties are as follows:

$$\tilde{\rho}_l^{n+1} = \rho_l^n + \left(\frac{\partial \rho_l}{\partial P}\right)^n \left(P^{n+1} - P^n\right) + \left(\frac{\partial \rho_l}{\partial U_l}\right)^n (\tilde{U}_l^{n+1} - U_l^n) \tag{3.144}$$

$$\tilde{\rho}_g^{n+1} = \rho_g^n + \left(\frac{\partial \rho_g}{\partial P}\right)^n \left(P^{n+1} - P^n\right) + \left(\frac{\partial \rho_g}{\partial U_g}\right)^n (\tilde{U}_g^{n+1} - U_g^n) \tag{3.145}$$

$$\tilde{T}_l^{n+1} = T_l^n + \left(\frac{\partial T_l}{\partial P}\right)^n \left(P^{n+1} - P^n\right) + \left(\frac{\partial T_l}{\partial U_l}\right)^n \left(\tilde{U}_l^{n+1} - U_l^n\right) \tag{3.146}$$

$$\tilde{T}_g^{n+1} = T_g^n + \left(\frac{\partial T_g}{\partial P}\right)^n \left(P^{n+1} - P^n\right) + \left(\frac{\partial T_g}{\partial U_g}\right)^n \left(\tilde{U}_g^{n+1} - U_g^n\right) \tag{3.147}$$

$$\tilde{T}_g^{s,n+1} = T_g^{s,n} + \left(\frac{\partial T_g}{\partial P}\right)^n \left(P^{n+1} - P^n\right) + \left(\frac{\partial T_g^s}{\partial U_g}\right)^n \left(\tilde{U}_g^{n+1} - U_g^n\right) \tag{3.148}$$

3.4 Numerical Solution

The semi-implicit solution scheme in Fig.3.1 is employed by replacing the system of difference equations with a system of finite-difference partially implicit in time. In this scheme, some important parameters are taken by the ones in the new time

สถาบันวิทยบริการ
จุฬาลงกรณ์มหาวิทยาลัย

step by adding increment to present initial values. To derive the finite difference equations, the concept of control volume (or mesh cell) is used. The control volumes are separated into mass and energy control volumes and momentum control volume. The velocities of momentum control volume will be calculated at the boundaries of mass and energy control volume. This will result in forming a staggered spatial mesh, which the scalar properties i.e. pressure, energies and void fraction are defined at cell centers and the vector properties i.e. velocities are defined at the cell boundaries.

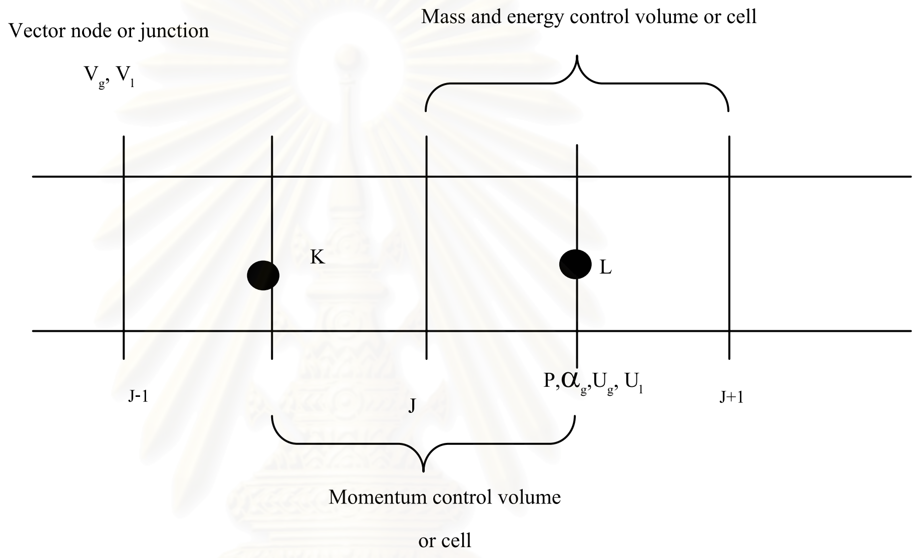

FIG. 3.1 Semi-implicit Scheme

In this model, velocity was implicitly calculated together with wall and interphase mass transfers, interphase velocity. The wall friction, interphase friction were calculated explicitly.

3.4.1 Finite Difference Equation

Finite difference equations of the sum and difference of phasic continuity equations, the sum and difference of phasic momentum equations and phasic energy equations are provided for numerical calculation. The sum and difference equations for the momentum equations are integrated with respect to the spatial variable, z from i to i+1 to calculate for the velocity at the junction j. The values of the mass and energy at the junction j are calculated in term of donor properties. The difference momentum equation is modified due to the effect of the additional wall friction terms which appear when the drift flux model is used. The sum and difference momentum equations are given by

$$
\begin{aligned}
&(\alpha_g\rho_g)_j^n(v_g^{n+1}-v_g^n)_j\,\Delta z_j+(\alpha_l\rho_l)_j^n(v_l^{n+1}-v_l^n)_j\,\Delta z_j\\
&+\frac{1}{2}(\dot{\alpha}_g\dot{\rho}_g)_j^n[(v_g^2)_L^n-(v_g^2)_K^n]\Delta t+\frac{1}{2}(\dot{\alpha}_l\dot{\rho}_l)_j^n[(v_l^2)_L^n-(v_l^2)_K^n]\Delta t\\
&-\frac{1}{2}(\dot{\alpha}_g\dot{\rho}_g)_j^n VISG_J^n\Delta t-\frac{1}{2}(\dot{\alpha}_l\dot{\rho}_l)_j^n VISF_j^n\Delta t\\
&=-(P_L-P_K)^{n+1}\Delta t+\Big[(\rho_m)_j^n B_z-(\alpha_g\rho_g)_j^n FWG_j^n(v_g)_j^{n+1}\\
&-(\alpha_l\rho_l)_j^n FWF_j^n(v_l)_j^{n+1}-(\Gamma_g)_j^n(v_g-v_l)_j^{n+1}\Big]\Delta z_j\Delta t\\
&-(\dot{\alpha}_g\dot{\rho}_g)_j^n HLOSSG_j^n(v_g^{n+1})_j\Delta t-(\dot{\alpha}_l\dot{\rho}_l)_j^n HLOSSF_j^n(v_l^{n+1})_j\Delta t
\end{aligned}
\tag{3.149}
$$

$$
\begin{aligned}
&(1+C\rho_m^2/(\rho_l\rho_g))_j^n(v_g^{n+1}-v_g^n)_j\Delta z_j\\
&+(1+C\rho_m^2/(\rho_l\rho_g))_j^n(v_l^{n+1}-v_l^n)_j\Delta z_j\\
&+\frac{1}{2}((\dot{\alpha}_g\dot{\rho}_g)/(\alpha_g\rho_g))_j^n[(v_g^2)_L^n-(v_g^2)_K^n]\Delta t\\
&-\frac{1}{2}((\dot{\alpha}_l\dot{\rho}_l)/(\alpha_l\rho_l))_j^n[(v_l^2)_L^n-(v_l^2)_K^n]\Delta t\\
&-\frac{1}{2}((\dot{\alpha}_g\dot{\rho}_g)/(\alpha_g\rho_g))_j^n VISG_J^n\Delta t+\frac{1}{2}((\dot{\alpha}_l\dot{\rho}_l)/(\alpha_l\rho_l))_j^n VISF_J^n\Delta t\\
&=-[(\rho_l-\rho_g)/(\rho_l\rho_g)]_j^n(P_L-P_K)^{n+1}\Delta t-\{FWG_j^n(v_g)_j^{n+1}-FWF_j^n(v_l)_j^{n+1}\\
&-(f_x)_j^n\left(\frac{1}{\alpha_g\rho_g}+\frac{1}{\alpha_l\rho_l}\right)_j^n[(f_{wg})_j^n(v_g)_j^{n+1}-(f_{wl})_j^n(v_l)_j^{n+1}]\\
&-[(\Gamma_g)_j^n(\rho_m^n(v_I)_j^{n+1}-\alpha_l^n\alpha_l^n v_g^{n+1}-\alpha_g^m\alpha_g^n v_l^{n+1})/(\alpha_g^2\alpha_l^2)^n]_j\\
&+(\rho_m FI)_j^n(v_g^{n+1}-v_l^{n+1})_j\}\Delta z_j\Delta t\\
&-[(\dot{\alpha}_g\dot{\rho}_g)/(\alpha_g\rho_g)]_j^n HLOSSG_j^n(v_g^{n+1})_j\Delta t\\
&+[(\dot{\alpha}_l\dot{\rho}_l)/(\alpha_l\rho_l)]_j^n HLOSSF_j^n(v_l^{n+1})_j\Delta t
\end{aligned}
\tag{3.150}
$$

สถาบันวิทยบริการ
จุฬาลงกรณ์มหาวิทยาลัย

where

$$VISG_J^n = \frac{1}{2}\{\left|v_{g,L}^n\right|[(v_g^n)_{j+1}(A_{j+1}/A_j)-(v_g^n)_j]$$
$$-\left|v_{g,L}^n\right|[(v_g^n)_j-(v_g^n)_{j-1}(A_{j-1}-A_j)]\}\tag{3.151}$$

$$VISF_J^n = \frac{1}{2}\{\left|v_{l,L}^n\right|[(v_l^n)_{j+1}(A_{j+1}/A_j)-(v_l^n)_j]$$
$$-\left|v_{l,L}^n\right|[(v_g^n)_j-(v_l^n)_{j-1}(A_{j-1}-A_j)]\}\tag{3.152}$$

$$HLOSSG_j^n = \frac{1}{2}K\left|v_{g,j}^n\right|\tag{3.153}$$

$$HLOSSF_j^n = \frac{1}{2}K\left|v_{l,j}^n\right|\tag{3.154}$$

The K is the input user loss depending on the phasic velocity direction. The f_x is the flag to select between the drift flux model and drag coefficient for interfacial friction force, f_{wl} ,f_{wg} are the additional force due to the effect of wall friction forces, for which

$$f_{wl} = \alpha_l\alpha_g\rho_g FWF\tag{3.155}$$

$$f_{wg} = \alpha_g\alpha_l\rho_l FWG\tag{3.156}$$

The donor properties shown by having the dot overscore in the sum and difference momentum equations are calculated based on the junction velocity and the scalar properties at the junction before and after velocity function and also computed depending on the pressure at the inlet and outlet of the cell. The following equations are used to calculate the donor properties.

For $v_j \neq 0$,

$$\dot{\phi}_j = \frac{1}{2}(\phi_K+\phi_L)+\frac{1}{2}\frac{\left|v_j\right|}{v_j}(\phi_K-\phi_L)\tag{3.157}$$

where $\dot{\phi}_j$ is any of the donor properties, v_j is appropriate velocity depending on liquid or vapor phase.

For $v_j = 0$ and $P_k > P_L$,

$$\dot{\phi}_j = \phi_K\tag{3.158}$$

ศูนย์วิทยทรัพยากร
จุฬาลงกรณ์มหาวิทยาลัย

For $v_j = 0$ and $P_k < P_L$,

$$\dot{\phi}_J = \phi_L \tag{3.159}$$

For $v_j = 0$ and $P_k = P_L$,

$$\dot{\phi}_j = \frac{(\rho_K \phi_K + \rho_L \phi_L)}{(\rho_K + \rho_L)} \tag{3.160}$$

Where ρ_K and ρ_L are appropriate properties based on liquid and vapor phase.

In the sum and difference momentum equations the volume average velocity is employed. The liquid and vapor velocities in the volume cells are calculated by averaging the phassic mass flow rate over the volume cells inlet and outlet junctions and are given by

$$\begin{aligned}(v_l)_L^n = {} & \frac{(\dot{\alpha}_l \dot{\rho}_l v_l)_{in}^n A_{in}^2}{[(\dot{\alpha}_l \dot{\rho}_l v_l)_{in}^n A_{in} + (\dot{\alpha}_l \dot{\rho}_l v_l)_{out}^n A_{out}] A_L} \\ & + \frac{(\dot{\alpha}_l \dot{\rho}_l v_l)_{out}^n A_{out}^2}{[(\dot{\alpha}_l \dot{\rho}_l v_l)_{in}^n A_{in} + (\dot{\alpha}_l \dot{\rho}_l v_l)_{out}^n A_{out}] A_L}\end{aligned} \tag{3.161}$$

$$\begin{aligned}(v_g)_L^n = {} & \frac{(\dot{\alpha}_g \dot{\rho}_g v_g)_{in}^n A_{in}^2}{[(\dot{\alpha}_g \dot{\rho}_g v_g)_{in}^n A_{in} + (\dot{\alpha}_g \dot{\rho}_g v_g)_{out}^n A_{out}] A_L} \\ & + \frac{(\dot{\alpha}_g \dot{\rho}_g v_g)_{out}^n A_{out}^2}{[(\dot{\alpha}_g \dot{\rho}_g v_g)_{in}^n A_{in} + (\dot{\alpha}_g \dot{\rho}_g v_g)_{out}^n A_{out}] A_L}\end{aligned} \tag{3.162}$$

for liquid and vapor phase, respectively.

To calculate intermediate phasic continuity and energy at junction i, the sum and difference of phasic continuity equations coupled with liquid and vapor energy equations will be adopted. The sum and difference of phasic continuity equations are given respectively by

$$\begin{aligned}& V_L [\alpha_{g,L}^n (\tilde{\rho}_{g,L}^{n+2} - \rho_{g,L}^n) + \alpha_{l,L}^n (\tilde{\rho}_{l,L}^{n+1} - \rho_{l,L}^n) + (\rho_{g,L}^n - \rho_{l,L}^n)(\tilde{\alpha}_{g,L}^{n+1} - \alpha_{g,L}^n)] \\ & + (\dot{\alpha}_{g,j+1}^n \dot{\rho}_{g,j+1}^n v_{g,j+1}^{n+1} A_{j+1} - \dot{\alpha}_{g,j}^n \dot{\rho}_{g,j}^n v_{g,j}^{n+1} A_j) \Delta t \\ & + (\dot{\alpha}_{l,j+1}^n \dot{\rho}_{l,j+1}^n v_{l,j+1}^{n+1} A_{j+1} - \dot{\alpha}_{l,j}^n \dot{\rho}_{l,j}^n v_{l,j}^{n+1} A_j) \Delta t = 0\end{aligned} \tag{3.163}$$

สถาบันวิทยบริการ
จุฬาลงกรณ์มหาวิทยาลัย

$$\begin{aligned}
&V_L[\alpha^n_{g,L}(\tilde{\rho}^{n+1}_{g,L}-\rho^n_{g,L})-\alpha^n_{l,L}(\tilde{\rho}^{n+1}_{l,L}-\rho^n_{l,L})+(\rho^n_{g,L}+\rho^n_{l,L})(\tilde{\alpha}^{n+1}_{g,L}-\alpha^n_{g,L})]\\
&+(\dot{\alpha}^n_{g,j+1}\dot{\rho}^n_{g,j+1}v^{n+1}_{g,j+1}A_{j+1}-\dot{\alpha}^n_{g,j}\dot{\rho}^n_{g,j}v^{n+1}_{g,j}A_j)\Delta t\\
&-(\dot{\alpha}^n_{l,j+1}\dot{\rho}^n_{l,j+1}v^{n+1}_{l,j+1}A_{j+1}-\dot{\alpha}^n_{l,j}\dot{\rho}^n_{l,j}v^{n+1}_{l,j}A_j)\Delta t\\
&=-\left(\frac{2}{h^*_g-h^*_l}\right)^n_L V_L\Delta t[H^n_{ig,L}(T^{s,n}_L-T^n_{g,L})+H^n_{il,L}(T^{s,n}_L-T^n_{l,L})\\
&+2V_L\Delta t\Gamma^n_{w,L}
\end{aligned} \tag{3.164}$$

The liquid and vapor energy equations can be expressed respectively as follows:

$$\begin{aligned}
&V_L[-(\rho^n_{l,L}U^n_{l,L}+P^n_L)(\tilde{\alpha}^n_{g,L}-\alpha^n_{g,L})+\alpha^n_{l,L}U^n_{l,L}(\tilde{\rho}^{n+1}_{l,L}-\rho^n_{l,L})\\
&+\alpha^n_{l,L}\rho^n_{l,L}(\tilde{U}^{n+1}_{l,L}-U^n_{l,L})]+[\dot{\alpha}^n_{l,j+1}(\dot{\rho}^n_{l,j+1}\dot{U}^n_{l,j+1}+P^n_L)v^{n+1}_{l,j+1}A_{j+1}\\
&-\dot{\alpha}^n_{l,j}(\dot{\rho}^n_{l,j}\dot{U}^n_{l,j}+P^n_L)v^{n+1}_{l,j}A_j]\Delta t=\{\left(\frac{h^*_l}{h^*_g-h^*_l}\right)^n_L H^n_{ig,L}(T^{s,n}_L-T^n_{g,L})\\
&+\left(\frac{h^*_g}{h^*_g-h^*_l}\right)^n_L H^n_{il,L}(T^{s,n}_L-T^n_{l,L})+H^n_{gf,L}(T^n_{g,L}-T^n_{l,L})\\
&-[\left(\frac{1+\varepsilon}{2}\right)h'^n_{g,L}+\left(\frac{1-\varepsilon}{2}\right)h'^n_{l,L}]\Gamma^n_{w,L}+Q^n_{wg,L}+DISS^n_{l,L}\}V_L\Delta t
\end{aligned} \tag{3.165}$$

$$\begin{aligned}
&V_L[-(\rho^n_{g,L}U^n_{g,L}+P^n_L)(\tilde{\alpha}^n_{g,L}-\alpha^n_{g,L})+\alpha^n_{g,L}U^n_{g,L}(\tilde{\rho}^{n+1}_{g,L}-\rho^n_{g,L})\\
&+\alpha^n_{g,L}\rho^n_{g,L}(\tilde{U}^{n+1}_{g,L}-U^n_{g,L})]+[\dot{\alpha}^n_{g,j+1}(\dot{\rho}^n_{g,j+1}\dot{U}^n_{g,j+1}+P^n_L)v^{n+1}_{g,j+1}A_{j+1}\\
&-\dot{\alpha}^n_{g,j}(\dot{\rho}^n_{g,j}\dot{U}^n_{g,j}+P^n_L)v^{n+1}_{g,j}A_j]\Delta t=\{-\left(\frac{h^*_l}{h^*_g-h^*_l}\right)^n_L H^n_{ig,L}(T^{s,n}_L-T^n_{g,L})\\
&-\left(\frac{h^*_g}{h^*_g-h^*_l}\right)^n_L H^n_{il,L}(T^{s,n}_L-T^n_{l,L})-H^n_{gf,L}(T^n_{g,L}-T^n_{l,L})\\
&+[\left(\frac{1+\varepsilon}{2}\right)h'^{,n}_{g,L}+\left(\frac{1-\varepsilon}{2}\right)h'^{,n}_{l,L}]\Gamma^n_{w,L}+Q^n_{wg,L}+DISS^n_{g,L}\}V_L\Delta t
\end{aligned} \tag{3.166}$$

สถาบันวิทยบริการ
จุฬาลงกรณ์มหาวิทยาลัย

From the sum and difference continuity equations together with liquid and vapor energy equations, the intermediate liquid and vapor internal energy and void fraction can be obtained. The intermediate liquid and vapor internal energy, void fraction will be used as the new time level values if the convergency of these values are less than 0.1 percent.

3.5 Solution Procedure

The method to solve the solution is separated into four stages: linearization of the unknowns, reduction of the numbers of unknowns, solution of Newton block Block Gauss Seidel and inverse matrix methods and finding the remaining unknowns. Two techniques are applied to solve the system of equations for the primary dependent variables such as internal energy of liquid and vapor, velocity of liquid and vapor, void fraction of vapor phase, and pressure. The first one is inverse matrix. It is used to calculate the velocity of liquid and vapor. The inverse matrix of the sum and difference equations is computed to give the intermediate velocity. The intermediate velocity will be inserted into the equations of liquid and vapor mass and energy equations to calculate the intermediate void fraction, intermediate pressure, intermediate liquid and vapor internal energy. The other one is Newton Block Gauss Seidel (NBGS) method. It is used to calculate the intermediate and the new time liquid and vapor energy, void fraction and pressure. The intermediate void fraction, pressure, liquid and vapor internal energy will be calculated inside the NBGS loop until the convergency of the system is less than 0.1 percent. Then the intermediate values will be stored as the new time values. The new times values will be used to calculate the new liquid and vapor velocity. The flow chart showing the procedure to calculate the primary variables is shown in Fig. 3.2.

สถาบันวิทยบริการ
จุฬาลงกรณ์มหาวิทยาลัย

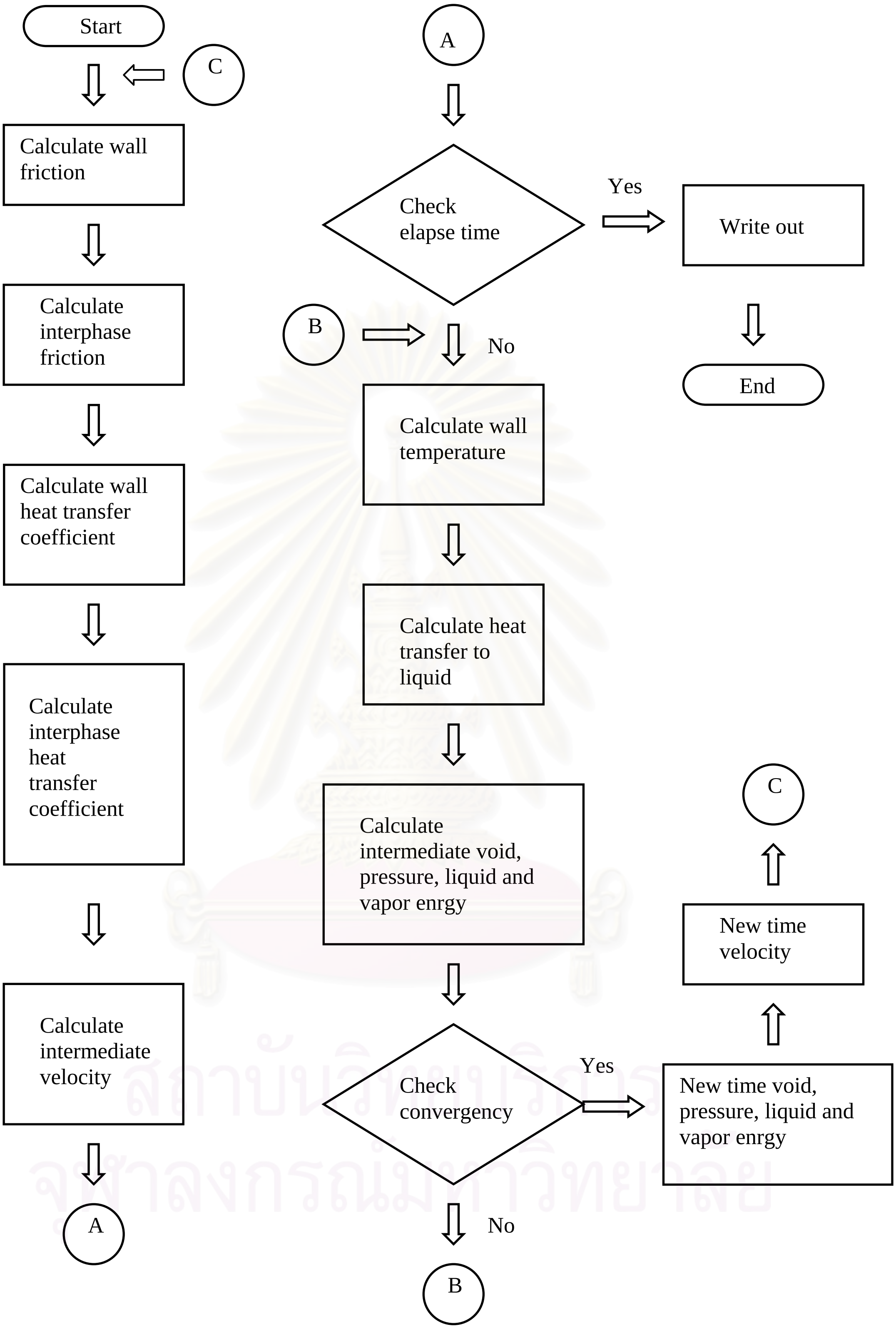

Fig. 3.2 The flow chart for calculation procedure

สถาบันวิทยบริการ
จุฬาลงกรณ์มหาวิทยาลัย

3.6 Solution Scheme

To calculate the intermediate and new time liquid and vapor velocity the sum and difference momentum equations will be arranged into the system of equations. The matrix of equations can be written as

$$AX = b$$

where

$$A = \begin{bmatrix} A_{11} & A_{12} \\ A_{21} & A_{22} \end{bmatrix} \quad X = \begin{bmatrix} v_g^{n+1} \\ v_l^{n+1} \end{bmatrix} or \begin{bmatrix} \tilde{v}_g^{n+1} \\ \tilde{v}_l^{n+1} \end{bmatrix} \quad b = \begin{bmatrix} b_1 \\ b_2 \end{bmatrix}$$

$$A_{11} = (\alpha_g \rho_g)_j^n \Delta z_j + (\alpha_g \rho_g)_j^n \Delta z_j FWG_j^n + (\Gamma_g)_j^n \Delta z_j \Delta t$$
$$+ (\dot{\alpha}_g \dot{\rho}_g)_j^n HLOSSG_J^N \Delta t$$

$$A_{12} = (\alpha_l \rho_l)_j^n \Delta z_j + (\alpha_l \rho_l)_j^n \Delta z_j FWF_J^N - (\Gamma_g)_j^n \Delta z_j \Delta t$$
$$+ (\dot{\alpha}_l \dot{\rho}_l)_j^n HLOSSF_J^N \Delta t$$

$$A_{21} = [1 + C\rho_m^2 / \rho_l \rho_g]_j^n \Delta z_j + FWG_j^n \Delta z_j \Delta t$$
$$+ (\alpha_l \alpha_g \Gamma_g / \alpha_l \alpha_g \rho_l \rho_g)_j^n \Delta z_j \Delta t$$
$$+ (\rho_m FI)_j^n (1 + f_x (C_1 - 1)) \Delta z_j \Delta t$$
$$+ (\dot{\alpha}_g \dot{\rho}_g / \alpha_g \rho_g)_j^n HLOSSG_J^n \Delta t$$
$$- f_x \left(\frac{1}{\alpha_g \rho_g} + \frac{1}{\alpha_l \rho_l} \right)_j^n f_{wg}^n$$

$$A_{22} = -[1 + C\rho_m^2 / \rho_l \rho_g]_j^n \Delta z_j + FWF_j^n \Delta z_j \Delta t$$
$$- (\alpha_l \alpha_g \Gamma_g / \alpha_l \alpha_g \rho_l \rho_g)_j^n \Delta z_j \Delta t$$
$$+ (\rho_m FI)_j^n (1 + f_x (C_0 - 1)) \Delta z_j \Delta t$$
$$+ (\dot{\alpha}_l \dot{\rho}_l / \alpha_l \rho_l)_j^n HLOSSF_J^n \Delta t$$
$$+ f_x \left(\frac{1}{\alpha_g \rho_g} + \frac{1}{\alpha_l \rho_l} \right)_j^n f_{wf}^n$$

สถาบันวิทยบริการ
จุฬาลงกรณ์มหาวิทยาลัย

$$b_1 = -\frac{1}{2}(\dot{\alpha}_g\dot{\rho}_g)_j^n[(v_g^2)_L^n - (v_g^2)_K^n]\Delta t$$

$$-\frac{1}{2}(\dot{\alpha}_l\dot{\rho}_l)_j^n[(v_l^2)_L^n - (v_l^2)_K^n]\Delta t$$

$$+\frac{1}{2}(\dot{\alpha}_g\dot{\rho}_g)_j^n VISG_J^n\Delta t + \frac{1}{2}(\dot{\alpha}_l\dot{\rho}_l)_j^n VISF_J^n\Delta t$$

$$-(P_L - P_K)^{n+1}\Delta t + (\rho_m)_j^n B_z\Delta z_j\Delta t$$

$$+(\alpha_g\rho_g)_j^n\Delta z_j + (\alpha_l\rho_l)_j^n\Delta z_j$$

$$b_2 = -\frac{1}{2}(\dot{\alpha}_g\dot{\rho}_g)_j^n[(v_g^2)_L^n - (v_g^2)_K^n]\Delta t$$

$$+\frac{1}{2}(\dot{\alpha}_l\dot{\rho}_l/\alpha_l\rho_l)_j^n[(v_l^2)_L^n - (v_l^2)_K^n]\Delta t$$

$$+\frac{1}{2}(\dot{\alpha}_g\dot{\rho}_g/\alpha_g\rho_g)_j^n VISG_J^n\Delta t - \frac{1}{2}(\dot{\alpha}_l\dot{\rho}_l/\alpha_l\rho_l)_j^n VISF_J^n\Delta t$$

$$-[(\rho_l - \rho_g)/(\rho_l\rho_g)]_j^n(P_L - P_K)^{n+1}\Delta t$$

$$+[(\Gamma_g\rho_m)_j^n v_I^{n+1}/(\alpha_l\rho_l\alpha_g\rho_g)_j^n]\Delta z_j\Delta t$$

$$+(1 + C\rho_m^2/(\alpha_g\rho_g))_j^n\Delta z_j - (1 + C\rho_m^2/(\alpha_l\rho_l))_j^n\Delta z_j$$

In case of the intermediate liquid and vapor velocity the effect of the new time pressure gradient terms in the sum and difference equations will be omitted. After the new time pressure is computed from the intermediate liquid and vapor velocity, the new time pressure gradient terms will be used to calculate the new time liquid and vapor velocity.

Similarly, the equations of vapor and liquid energy, the continuity equations of vapor and liquid will be arranged orderly into the system of equations to compute for the intermediate liquid and vapor internal energy, void fraction and pressure including the new time pressure. The matrix of equations can be achieved as

$$AX = b + g^1 v_{g,i+1}^{n+1} + g^2 v_{g,i}^{n+1} + f^1 v_{l,i+1}^{n+1} + f^2 v_{l,i}^{n+1}$$

$$A = \begin{bmatrix} A_{11} & A_{12} & A_{13} & A_{14} \\ A_{21} & A_{22} & A_{23} & A_{24} \\ A_{31} & A_{32} & A_{33} & A_{34} \\ A_{41} & A_{42} & A_{43} & A_{44} \end{bmatrix} \begin{bmatrix} X_1 \\ X_2 \\ X_3 \\ X_4 \end{bmatrix} = \begin{bmatrix} \tilde{U}_g^{n+1} - U_g^n \\ \tilde{U}_l^{n+1} - U_l^n \\ \tilde{\alpha}_g^{n+1} - \alpha_g^n \\ P^{n+1} - P^n \end{bmatrix}$$

สถาบันวิทยบริการ
จุฬาลงกรณ์มหาวิทยาลัย

Where

$$b=\begin{bmatrix} b_1 \\ b_2 \\ b_3 \\ b_4 \end{bmatrix} \quad \left[g^1\right]=\begin{bmatrix} g_1^1 \\ g_2^1 \\ g_3^1 \\ g_4^1 \end{bmatrix} \quad \left[g^2\right]=\begin{bmatrix} g_1^2 \\ g_2^2 \\ g_3^2 \\ g_4^2 \end{bmatrix} \quad \left[f^1\right]=\begin{bmatrix} f_1^1 \\ f_2^1 \\ f_3^1 \\ f_4^1 \end{bmatrix} \quad \left[f^2\right]=\begin{bmatrix} f_1^2 \\ f_2^2 \\ f_3^2 \\ f_4^2 \end{bmatrix}$$

$$A_{11}=\alpha_g\left(U_g\frac{\partial\rho_g}{\partial U_g}+\rho_g\right)+\left(\frac{h_l^*}{h_g^*-h_l^*}\right)\Delta tH_{ig}\left(\frac{\partial T^s}{\partial U_g}-\frac{\partial T_g}{\partial U_g}\right)$$
$$+\left(\frac{h_g^*}{h_g^*-h_l^*}\right)\Delta tH_{il}\left(\frac{\partial T^s}{\partial U_l}-\frac{\partial T_g}{\partial U_l}\right)+\Delta tH_{gf}\frac{\partial T_g}{\partial U_g}$$

$$A_{12}=-\left(\frac{h_g^*}{h_g^*-h_l^*}\right)\Delta tH_{il}\frac{\partial T_l}{\partial U_l}-\Delta tH_{gl}\frac{\partial T_l}{\partial U_l}$$

$$A_{13}=\rho_g U_g+P$$

$$A_{14}=\rho_g U_g\frac{\partial\rho_g}{\partial P}+\left(\frac{h_l^*}{h_g^*-h_l^*}\right)\Delta tH_{ig}\left(\frac{\partial T^s}{\partial P}-\frac{\partial T_g}{\partial P}\right)$$
$$+\left(\frac{h_g^*}{h_g^*-h_l^*}\right)\Delta tH_{il}\left(\frac{\partial T^s}{\partial P}-\frac{\partial T_l}{\partial P}\right)+\Delta tH_{gl}\left(\frac{\partial T_g}{\partial P}-\frac{\partial T_l}{\partial P}\right)$$

$$A_{21}=-\left(\frac{h_l^*}{h_g^*-h_l^*}\right)\Delta tH_{ig}\left(\frac{\partial T^s}{\partial U_g}-\frac{\partial T_g}{\partial U_g}\right)$$
$$-\left(\frac{h_g^*}{h_g^*-h_l^*}\right)\Delta tH_{il}\frac{\partial T^s}{\partial U_g}-\Delta tH_{gl}\frac{\partial T_g}{\partial U_g}$$

$$A_{22}=\alpha_l\left(U_l\frac{\partial\rho_l}{\partial U_l}+\rho_l\right)+\left(\frac{h_g^*}{h_g^*-h_l^*}\right)\Delta tH_{il}\frac{\partial T_l}{\partial U_l}$$
$$+\Delta tH_{gl}\frac{\partial T_l}{\partial U_l}$$

$$A_{23}=-\rho_l U_l-P$$

$$A_{24}=\alpha_l U_l\frac{\partial\rho_l}{\partial P}-\left(\frac{h_l^*}{h_g^*-h_l^*}\right)\Delta tH_{ig}\left(\frac{\partial T^s}{\partial P}-\frac{\partial T_g}{\partial P}\right)$$
$$-\left(\frac{h_g^*}{h_g^*-h_l^*}\right)\Delta tH_{il}\left(\frac{\partial T^s}{\partial P}-\frac{\partial T_l}{\partial P}\right)-\Delta tH_{gl}\left(\frac{\partial T_g}{\partial P}-\frac{\partial T_l}{\partial P}\right)$$

สถาบันวิทยบริการ
จุฬาลงกรณ์มหาวิทยาลัย

$$A_{31} = \alpha_g \frac{\partial \rho_g}{\partial U_g} + \left(\frac{2}{h_g^* - h_l^*} \right) \Delta t H_{ig} \left(\frac{\partial T^s}{\partial U_g} - \frac{\partial T_g}{\partial U_g} \right)$$

$$+ \left(\frac{2}{h_g^* - h_l^*} \right) \Delta t H_{il} \frac{\partial T^s}{\partial U_g}$$

$$A_{32} = -\alpha_l \frac{\partial \rho_l}{\partial U_l} - \left(\frac{2}{h_g^* - h_l^*} \right) \Delta t H_{il} \frac{\partial T_l}{\partial U_l}$$

$$A_{33} = \rho_g + \rho_l$$

$$A_{34} = \alpha_g \frac{\partial \rho_g}{\partial P} - \alpha_l \frac{\partial \rho_l}{\partial P} + \left(\frac{2}{h_g^* - h_l^*} \right) \Delta t H_{ig} \left(\frac{\partial T^s}{\partial P} - \frac{\partial T_g}{\partial P} \right)$$

$$+ \left(\frac{2}{h_g^* - h_l^*} \right) \Delta t H_{il} \left(\frac{\partial T^s}{\partial P} - \frac{\partial T_l}{\partial P} \right)$$

$$A_{41} = \alpha_g \frac{\partial \rho_g}{\partial U_g}$$

$$A_{42} = \alpha_l \frac{\partial \rho_l}{\partial U_l}$$

$$A_{44} = \alpha_g \frac{\partial \rho_g}{\partial P} + \alpha_l \frac{\partial \rho_l}{\partial P} \quad A_{43} = \rho_g - \rho_l$$

$$b_1 = -\left(\frac{h_l^*}{h_g^* - h_l^*} \right) \Delta t H_{ig} \left(T^s - T_g \right)$$

$$- \left(\frac{h_g^*}{h_g^* - h_l^*} \right) \Delta t H_{il} \left(T^s - T_l \right) - \Delta t H_{gl} \left(T_g - T_l \right)$$

$$+ \Delta t \Gamma_w \left[\left(\frac{1 - \varepsilon}{2} \right) h'_l + \left(\frac{1 + \varepsilon}{2} \right) h'_g \right] + Q_{wg} \Delta t + DISS_g \Delta t$$

$$b_2 = \left(\frac{h_l^*}{h_g^* - h_l^*} \right) \Delta t H_{ig} \left(T^s - T_g \right)$$

$$+ \left(\frac{h_g^*}{h_g^* - h_l^*} \right) \Delta t H_{il} \left(T^s - T_l \right) + \Delta t H_{gl} \left(T_g - T_l \right)$$

$$- \Delta t \Gamma_w \left[\left(\frac{1 - \varepsilon}{2} \right) h'_l + \left(\frac{1 + \varepsilon}{2} \right) h'_g \right] + Q_{wl} \Delta t + DISS_l \Delta t$$

สถาบันวิทยบริการ
จุฬาลงกรณ์มหาวิทยาลัย

$$b_3 = -\left(\frac{2}{h_g^* - h_l^*}\right)\Delta t\, H_{ig}\left(T^s - T_g\right)$$

$$-\left(\frac{2}{h_g^* - h_l^*}\right)\Delta t\, H_{il}\left(T^s - T_l\right) + 2\Delta t\, \Gamma_w$$

$$b_4 = 0$$

$$g_1^1 = -[\dot{\alpha}_{g,j+1}\left(\dot{\rho}_{g,j+1}\dot{U}_{g,j+1} + P_L\right)A_{j+1}]\Delta t / V$$

$$g_2^1 = 0$$

$$g_3^1 = -[\dot{\alpha}_{g,j+1}\dot{\rho}_{g,j+1}A_{j+1}]\Delta t / V$$

$$g_4^1 = -[\dot{\alpha}_{g,j+1}\dot{\rho}_{g,j+1}A_{j+1}]\Delta t / V$$

$$g_1^2 = [\dot{\alpha}_{g,j}\left(\dot{\rho}_{g,j}\dot{U}_{g,j} + P_L\right)A_j]\Delta t / V$$

$$g_2^2 = 0$$

$$g_3^2 = [\dot{\alpha}_{g,j}\dot{\rho}_{g,j}A_j]\Delta t / V$$

$$g_4^2 = [\dot{\alpha}_{g,j}\dot{\rho}_{g,j}A_j]\Delta t / V$$

$$f_1^1 = 0$$

$$f_2^1 = -[\dot{\alpha}_{l,j+1}\left(\dot{\rho}_{l,j+1}\dot{U}_{l,j+1} + P_L\right)A_{j+1}]\Delta t / V$$

$$f_3^1 = [\dot{\alpha}_{l,j+1}\dot{\rho}_{l,j+1}A_{j+1}]\Delta t / V$$

$$f_4^1 = -[\dot{\alpha}_{l,j+1}\dot{\rho}_{l,j+1}A_{j+1}]\Delta t / V$$

$$f_1^2 = 0$$

$$f_2^2 = [\dot{\alpha}_{l,j}\left(\dot{\rho}_{l,j}\dot{U}_{l,j} + P_L\right)A_j]\Delta t / V$$

$$f_3^2 = -[\dot{\alpha}_{l,j}\dot{\rho}_{l,j}A_j]\Delta t / V$$

$$f_4^2 = -[\dot{\alpha}_{l,j}\dot{\rho}_{l,j}A_j]\Delta t / V$$

To calculate the new time pressure, the Newton Block Gauss Seidel method is used. By substituting the liquid and velocity from the sum and difference momentum

สถาบันวิทยบริการ
จุฬาลงกรณ์มหาวิทยาลัย

equations the linear equations of NxN matrix from each cell volume are derived involved only the new time pressure. Thus the new time pressure can be achieved. The intermediate liquid and vapor energy and void fraction is obtained by substituting the new time pressure, which is calculated from the intermediate velocity.

3.7 Convergent criteria and verification of the model

After the model has been developed, it will be tested for its accuracy due to truncation and round off errors. The method of approximate percentage error will be employed. In this method, the new numerical results will be compared with the old numerical results for two times by the following equation:

$$\varepsilon_a = \frac{V_{new} - V_{old}}{V_{new}} x 100\ \% \qquad (3.167)$$

where V_{new} is the new time result and V_{old} is the old time result. The convergent criteria is expected to be less than 0.1 %. After that the model will be verified by compared the results from the model with the results from the experiment.

สถาบันวิทยบริการ
จุฬาลงกรณ์มหาวิทยาลัย

Chapter IV

Experimental Apparatus and Procedure

4.1 Introduction

This chapter describes the equipment and apparatus used in the experiment. The experiment will be performed to investigate the effect of the flow loop conditions on the stability of the two-phase natural circulation in boiling channels. The mechanical components of the equipment will be presented step by step. Then the data acquisition, which is used to acquire the data, is presented. After that the method to conduct the experiment is described.

4.2 Experimental Apparatus

The experimental apparatus consists of two major parts: a loop part and a control part.

4.2.1 Loop part

A loop part is made up of the mechanical components including lower plenum and upper plenum with double riser test sections in the middle, heater, upper tank with pre-heater, down-comer section, by-pass section, circulation pump, air compressor and control valve. Fig.4.1 shows the configuration of the system. Connected to the exit of the circulation pump, the three parallel channels with the valves connected to the lower plenum are provided for redundancy and installed with three orifices as shown in Fig.4.2. The high-range, medium-range and low-range orifices are installed to measure the total flow. Normally the orifice will be changed from the medium to high-range due to the range of the velocity. During the pre-heat period these three channels are open for fast distribution of the temperature. The lower plenum is made up of the stainless steel and equipped with a pressure gauge, a pressure sensor and a temperature sensor as shown in Fig.4.3. Above the lower plenum, one orifice is installed to measure flow oscillation in each channel. The two pyrex glass test sections, which can be extended up to 4 test sections in the future, are connected between the lower plenum and the upper plenum to investigate the two-phase flow phenomena during the experiment. The channel geometry of the test sections between inlet and upper plenum is shown on Fig.4.4. The diameter of each channel is 20 mm. O.D. with the thickness of 4 mm. The thin stainless steel electrical heater with the size of 10 mm. O.D. 1 m. long is installed inside the each channel including a temperature sensor at the end of the heater. The heater capacity is 10 kW for each channel. These heaters will be activated to simulate the fuel rod in the boiling water reactor core. Similar to the lower plenum, the upper plenum, which is shown in Fig.4.5, is made up of stainless steel and equipped with pressure sensor and a temperature sensor. From the upper plenum, the connecting channel is located to the upper tank, which is shown on Fig.4.6. The exit of the channel in the upper tank will be higher than the water level to simulate the separator in SBWR. In the upper tank, the pre-heater including the subcooled water line and condenser water line are also provided to control the subcooled condition of the system as shown in Fig.4.7. The capacity of the pre-heater is 10 kW and is controlled by the pre-heater controller shown in Fig.4.8. At the top of the upper tank, a relief valve is installed in case of over pressure and a pressure regulator and an air compressor are installed to control the pressure in the upper tank. The maximum pressure set point of the relief valve is set at 7 MPa. Fig.4.9 shows the pictures of the relief valve. The water level also installed to measure the level of the water to calculate static head of the system. The upper tank is connected to the bypass line and the down-comer line. The bypass line is installed for redundancy and is used in the pre-heat period. The make up water pipe with water filter and valve is connected to the lower section of the bypass line as shown in Fig.4.10 to fill the tank if the water level of the tank is lower than the set point. The valve is installed between the make up water pipe and the bypass line and is normally close during the normal operation. The down-comer line is 50 mm. O.D. stainless steel pipe connected between the upper tank and the suction of the circulation pump. This circulation pump is operated for the start up of the loop to achieve the operating conditions and for the forced circulation experiment. The 3-way valve is installed at the inlet of the circulation pump to change the operation of the system from forced circulation to natural circulation. The bypass connection ahead of the suction of the circulation pump is provided to operate the natural circulation phenomena after the proper operating conditions are obtained. The configuration of the circulating pump including bypass and 3-way valve is shown in Fig.4.11. To obtain the system pressure required, the air compressor is employed as shown in Fig.4.12. This air compressor will be activated when the system pressure decrease due to condensation in the upper tank. After the system pressure reach the require level the air compressor will stop by the signal from the pressure sensor at the air receiver tank.

4.2.2 Control part

A control part includes a set of data recorder system together with five amplifiers and voltage controller. Fig.4.13 shows the voltage controller, data recorder and the three amplifiers for the signal from the thermocouples of the inlet plenum, channel 1 and channel 2. The power supply for the heaters of the test sections is provided by the power converter as shown in Fig.4.14, which is converted the AC current to the DC current. Temperature at the lower plenum and the upper plenum and the upper tank is measured by thermocouple. Pressure transducers at the lower and the upper plenum are provided to measure differential pressure. All measured data will be signaled to the amplifiers and achieved by the recorder. The voltage controller is installed to remote control the power supply for the heaters.

4.3 Experimental Procedure

Before the start-up of the system, the required condition such as the pressure, the temperature, the subcooled condition will be established in pre-heat phase and the circulation pump is employed to equally distribute the temperature of the coolant. After the system condition is achieved, the circulation pump is shut down and the system is turned in to natural circulation mode. The pre-heat procedure is employed as followed:

1. Drain the measurement system as shown in Fig. 4.15 to remove the bubble for accuracy of the measurement system. All of the input (IP1 and IP2), output (OP1 and OP2), and neutral valves (N1) will be close. Then open OP1 following by IP1. Close OP1 and IP1. Open OP2 following by IP2. Close OP2 and IP2. After that open OP2, IP1, and N1, respectively. Close OP2, IP1, and N1. Finally, open OP1, IP2, and N1, respectively. Close OP1, IP2 and N1. Before the valves are closed, make sure that there is no bubble in the drain line. This procedure is applied to the measurement system of channel 1, 2, 3, 9, and 10. S1 is drained for the first start up of the system by open IP1, IP2 and close OP1, OP2 and N1.

2. Fill in the upper tank. The inlet valve on the bypass line connected to the upper tank is close. The water will fill the upper tank from the pipe connected from the upper plenum. Close the drain valve, open the valve between the make up line and the bypass line and change the direction of the 3-way valve to fill in the main riser. After that open the valve on the make up line to fill in the upper tank.
3. Measure the height of the level of the water in the upper tank. Then measure the level of the water in upper tank and the level of the separator in the upper tank to calculate static head of the system.
4. Turn on the recorder and all amplifiers of channel 1, 2, 3, 9, and 10.
5. Conduct zero adjustment for all amplifiers of all channels by closing the main riser valve, the high-range valve, the medium-range valve, and the low-range valve. Then adjust the roller to get the zero value at the corresponding channel in the recorder.
6. Prepare for starting up the circulation pump by checking the direction and the status of all following valves.
   6.1 The direction of 3-way valve to the inlet of the circulation pump
   6.2 The direction of 3-way valve to the main riser and the bypass line
   6.3 The open status of the high-range valve, the medium range valve, and the low range valve
   6.4 The open status of the main valve
   6.5 The close status of the valve between the bypass line and the make up water line
   6.6 The open status of the inlet valve on the bypass line connected to the upper tank
7. Turn on the upper heater in the upper tank to pre-heat the system. After the temperature in the upper tank reach 40 °C, turn on the circulation pump to equally distribute the temperature.
8. Turn on the air compressor and set the pressure regulator at the upper tank to the setup point. Set up the other pressure regulator between the air compressor and the upper tank to the required set point.
9. Turn on the cooling system for the upper tank.

10. When the temperature of the lower plenum reaches 60 °C, turn on the power supply for the main heater. Then turn on the voltage controller to remote control the power supply for the main heater. Adjust the voltage controller to 0.4 volt.
11. After the temperature of the lower plenum exceeds the temperature required for 10 °C, shut down the circulation pump, change the direction of the 3-way valve in 6.1 to the natural circulation line and change the direction of the 3–way valve in 6.2 to main riser only.
12. Change the valves in 6.3 and 6.4 to close status. Conduct the zero adjustment as in item 5.
13. Set up the measurement system for channel 3 to the medium-range. This will be changed to the high-range in case the value of the channel 3 in the recorder is higher than the range shown.
14. Pre-heat the system by increasing the voltage at the voltage controller from 0.4, 0.9, 1.3, 1.6, 1.9, and 2.2 volt. The time required at each step is 1 minute. After change the volt to 2.5 volt, which is the first run of the experiment, wait until the temperature of the lower plenum shown the temperature required. Record the data at the recorder and change the voltage controller to the next required volt. The pre-heat phase finishes at this stage. The experiment procedure will be described next.

In this experiment the effect of the flow loop condition such as subcooled condition, heat flux and channel configuration will be investigated. The subcooled condition will be varied from 5, 10 and 15 K. The heat flux is in the range of 1 to 500 kW/m^2. The channel configuration with the riser length at 1 meter will be kept. The experimental procedure to investigate the effects of the flow loop conditions on the stability of the two-phase natural circulation will be as follows:

1. Select the operating condition of the system at 5 K subcooled condition and 0.1 MPa with the system apparatus and the channel diameter of 20 mm as shown on FIG.4.1. The pre-heater in the separator tank and the circulating pump will be operated to get the condition. The pre-heat phase is illustrated in the previous section.

2. At the 2.5 volt record the data at the recorder when the temperature of the lower plenum is 5 K subcooled condition.
3. Change the heat flux of the heater by adjusting the voltage controller to the next heat flux.
4. After collect the data the temperature of the lower plenum will increase, to reduce this temperature open the valve on the subcooled water line. Wait until the temperature of the lower plenum reaches the subcooled condition again.
5. Repeat the item 3 and 4 until getting the maximum heat flux required.
6. Change the subcooled condition in item 1 from 5 to 10 K. Repeat the item 2 to 5.
7. Change the subcooled condition in item 1 from 5 to 15 K. Repeat the item 2 to 5.
8. Keep the subcooled condition in item at 5 K. Change the system pressure from 0.1 to 0.2 MPa. Repeat the item 2 to 5.
9. Change the system pressure in item 1 to 0.2 MPa. Change the subcooled condition from 5 to 10K. Repeat the item 2 to 5.
10. Change the system pressure in item 1 at 0.2 MPa. Change the subcooled condition from 5 to 15K. Repeat the item 2 to 5.
11. Repeat the item 8 to 10 but change the system pressure to 0.4 MPa.
12. Repeat the item 8 to 10 but change the system pressure to 0.5 MPa.
13. Repeat the item 8 to 10 but change the system pressure to 0.7 MPa.

After finish the experiment, the following procedure is employed to shut down the system.

1. Reduce the voltage to zero by using the voltage controller and turn off the voltage controller.
2. Turn of the current controller of the heater placed above the power supply of the heater.
3. Turn off the power supply.
4. Turn off the cooling system.
5. Turn off the power of the upper heater.
6. Turn off all amplifiers.
7. Turn off the recorder.
8. Do not turn off the main breaker if the temperature in the upper tank is higher than 100 °C.

สถาบันวิทยบริการ
จุฬาลงกรณ์มหาวิทยาลัย

9. Do not turn off the air compressor if the temperature in the upper tank is higher than 100 °C.

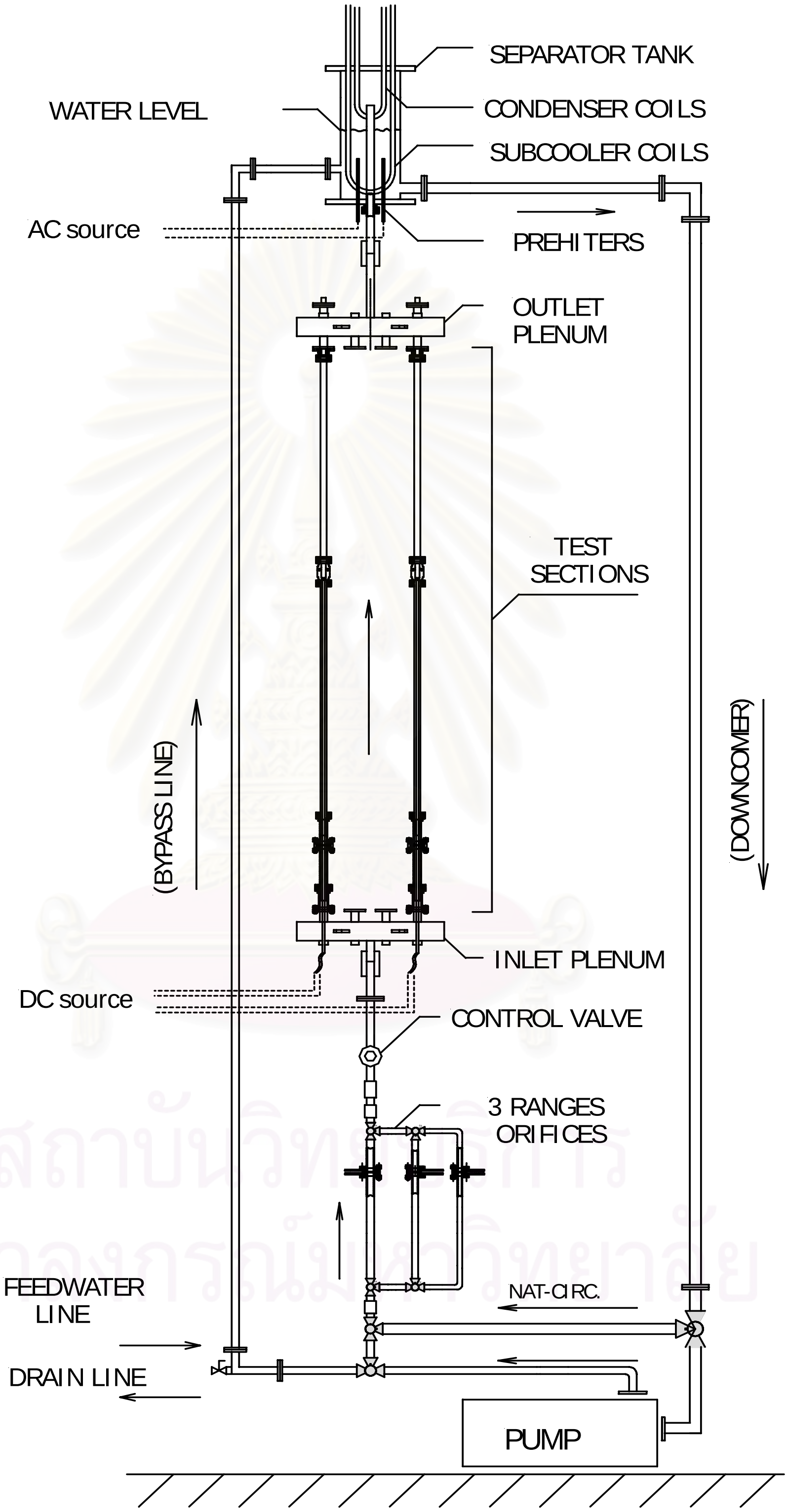

Fig.4.1 Configuration of the Equipment and apparatus

สถาบันวิทยบริการ
จุฬาลงกรณ์มหาวิทยาลัย

Fig.4.2 three parallel channels with high-, medium-, and low-range orifices

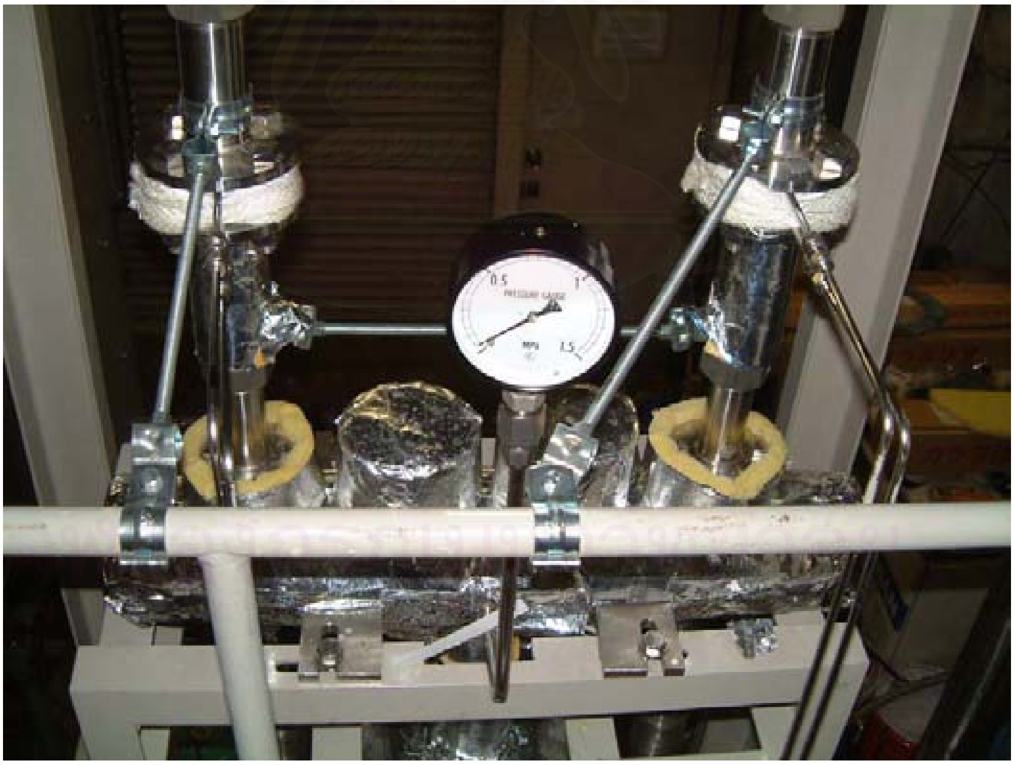

Fig.4.3 Lower plenum

Fig.4.4 Test sections

Fig.4.5 Upper plenum

Fig.4.6 Upper tank

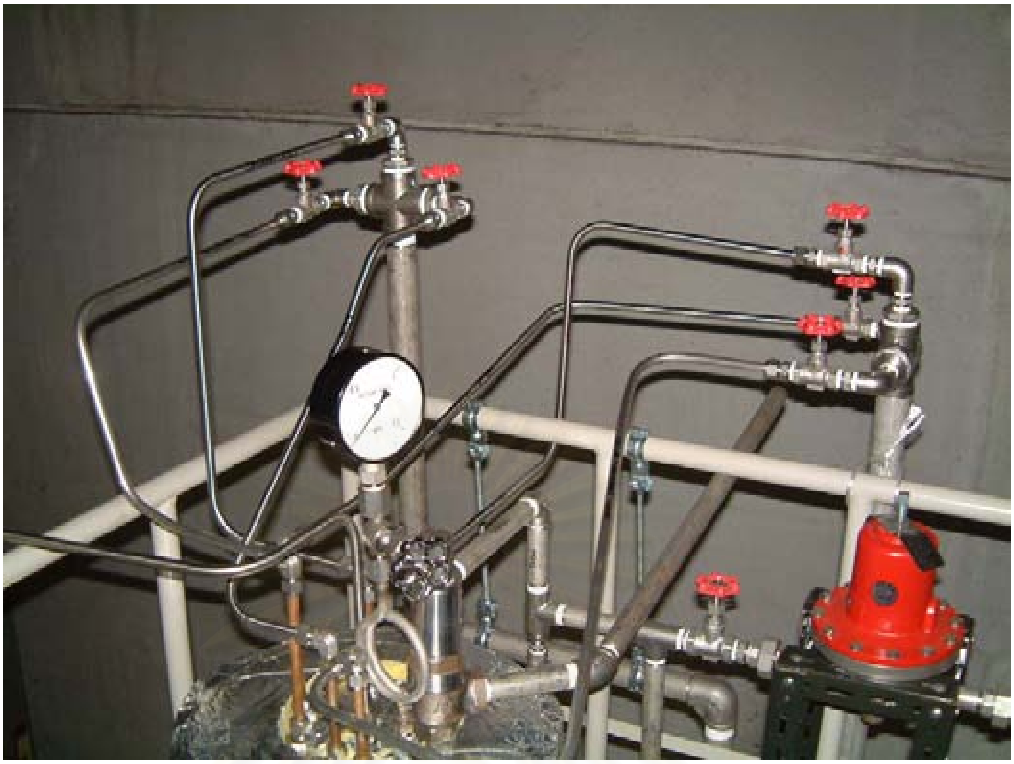

Fig.4.7 Condenser system

Fig.4.8 Pre-heater controller

Fig.4.9 Relief valve

Fig.4.10 Make-up water pipe

Fig.4.11 Configuration of circulating pump, by-pass line and 3-way valve

Fig.4.12 Air compressor

Fig.4.13 Voltage controller, amplifiers and data recorder

Fig.4.14 Power converter

Fig. 4.15 Measurement system

สถาบันวิทยบริการ
จุฬาลงกรณ์มหาวิทยาลัย

Chapter V

Experimental and Numerical Results and Discussions

5. Introduction

The numerical model has been developed as illustrated in chapter 3. The experimental facility was set up and conducted as described in chapter 4. The characteristic curve of the oscillation will be shown in this chapter. The characteristic of the oscillation such as the amplitude of the pressure drop, the amplitude of the velocity, the period of the oscillation will be investigated due to effect of the heat flux, pressure and subcooling condition. The feature of the oscillation is explained. The in-phase and out-of-phase between the maximum velocity of each channel and between the maximum velocity and pressure drop at low and high heat flux, the pressure drop between the inlet and outlet plenums, the dimensionless of the pressure drop and the head between the inlet and outlet plenums are illustrated. Then the effect of the channel geometry is described. The results from the experiment and the numerical model at pressure 0.1 MPaA and subcooling 5, 10 and 15 K are compared. Finally, the effect of the channel diameter will be investigated using the two-fluid model.

5.1 Characteristic curve

Because one experimental condition shows only one natural circulation curve, the characteristic of natural circulation for each condition can be shown by the characteristic curve of the heat flux on the x-axis and the average total inlet velocity on the y-axis. In Fig.5.1 the experiment was performed at the pressure 0.1 MPaA and subcooling10 K. The average total inlet velocity increases rapidly with the increasing heat flux from 0 to 300 kW/m^2 and remains constant at 0.38 m/s at the heat flux higher than 300 kW/m^2.

ศูนย์วิทยทรัพยากร
จุฬาลงกรณ์มหาวิทยาลัย

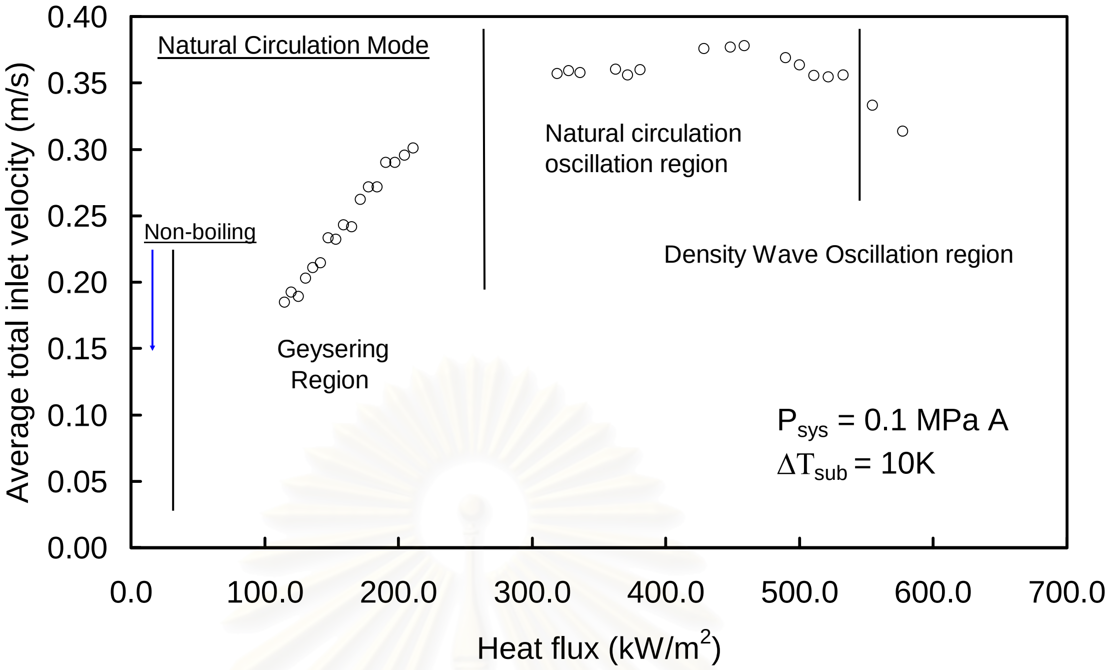

Fig. 5.1 Characteristic curve of natural circulation

5.2 Characteristic of Flow Oscillation

The characteristic of the flow oscillation can be indicated by the amplitude of the velocity, the amplitude of the pressure drop, the period and the delayed time of the flow oscillation. Moreover, the void fraction can be shown from the dimensionless of the amplitude of the pressure drop and the head between inlet and outlet plenums.

5.2.1 Amplitude of the velocity

The velocity of the flow of each channel was measured by installed the orifice at each channel. The amplitude of the velocity can be calculated from the average maximum and minimum of the velocity of each channel as follows:

$$\left(U_{max} - U_{min}\right) \tag{5.1}$$

where Umax,Umin are the average maximum and minimum velocities, respectively. From Fig. 5.2 the amplitude of the velocity at pressure 0.1 MPaA and the subcooling 10 K is shown. The amplitude of the velocity decreases from 0.7 m/s to 0.5 m/s as the inlet velocity increases from 0.18 m/s to 0.38 m/s. The average amplitude of the velocity is 0.6 m/s. At low heat flux the amplitude of the velocity is high because of the high velocity and the flow reversal during the occurrence of gerserying. At the higher heat flux the flow condition changes from geysering to natural oscillation and density wave oscillation. Therefore the amplitude of the velocity decreases.

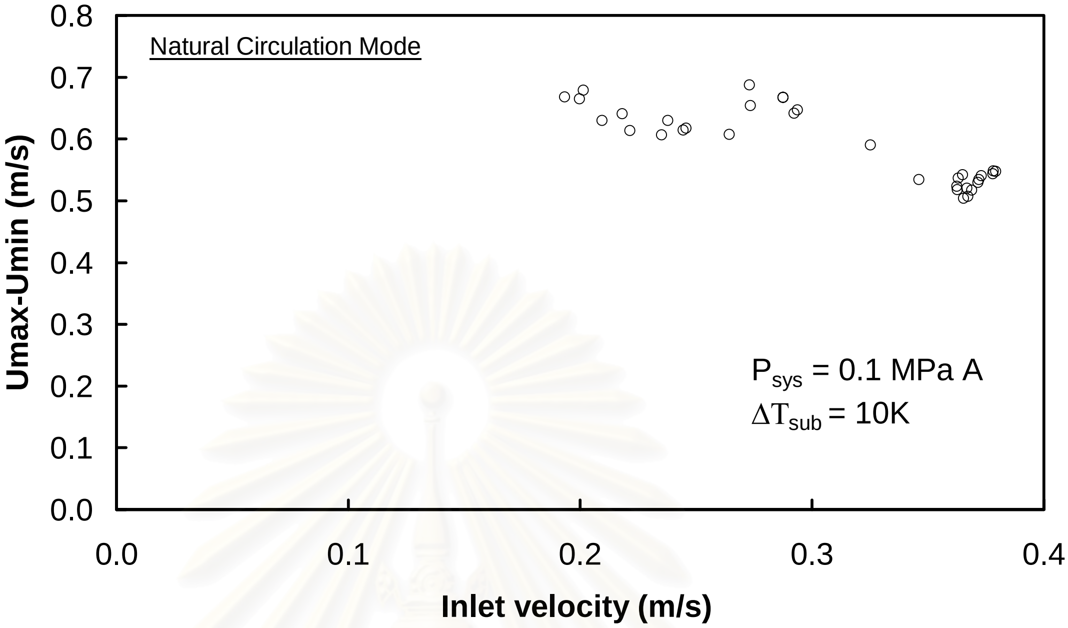

Fig. 5.2 Amplitude of the velocity

5.2.2 Amplitude of the pressure drop

The pressures at the inlet and outlet plenums were measured. The amplitude of the pressure drop can be derived from the differential pressure between the inlet and outlet plenums. The amplitude of the pressure drop increases and varies between 8 and 14 kPa with the increase inlet velocity from 0.18 to 0.38 m/s as shown in Fig.5.3. The high amplitude of the velocity at the low heat flux gives rise to high amplitude of the amplitude of the pressure drop.

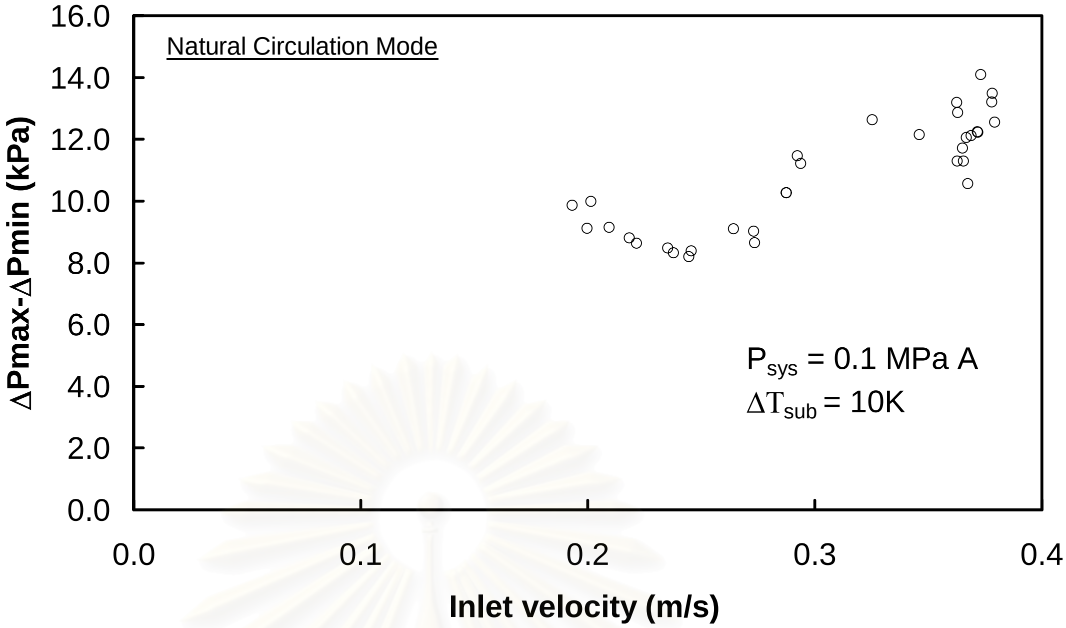

Fig.5.3 Amplitude of the pressure drop

5.2.3 Delayed time of the flow oscillation

In general, the period of the oscillation is closely related to transportation delays in the channel. The delayed time is the time for one cycle consisting of incubation, expulsion and reentry of fluid. The delayed time of the flow oscillation depends on the inlet and saturated enthalpy including the heat input. It can be calculated from Equation 5.2.

$$\tau_B = \frac{\rho_l (i' - i_{in})}{q'''} \tag{5.2}$$

where τ_B is delayed time, ρ_l is density of liquid, i' is saturated enthalpy, i_{in} is inlet liquid enthalpy, and q''' is caloric power per unit volume. The delayed time of the flow oscillation is high at the low heat flux and decreases with the increasing heat flux as shown in Fig.5.4 because at high heat flux the density of the liquid is lower than that at the low heat flux. Moreover, the caloric power per unit volume is also high at high heat flux. Therefore the delayed time of the flow oscillation is shorter at high heat flux.

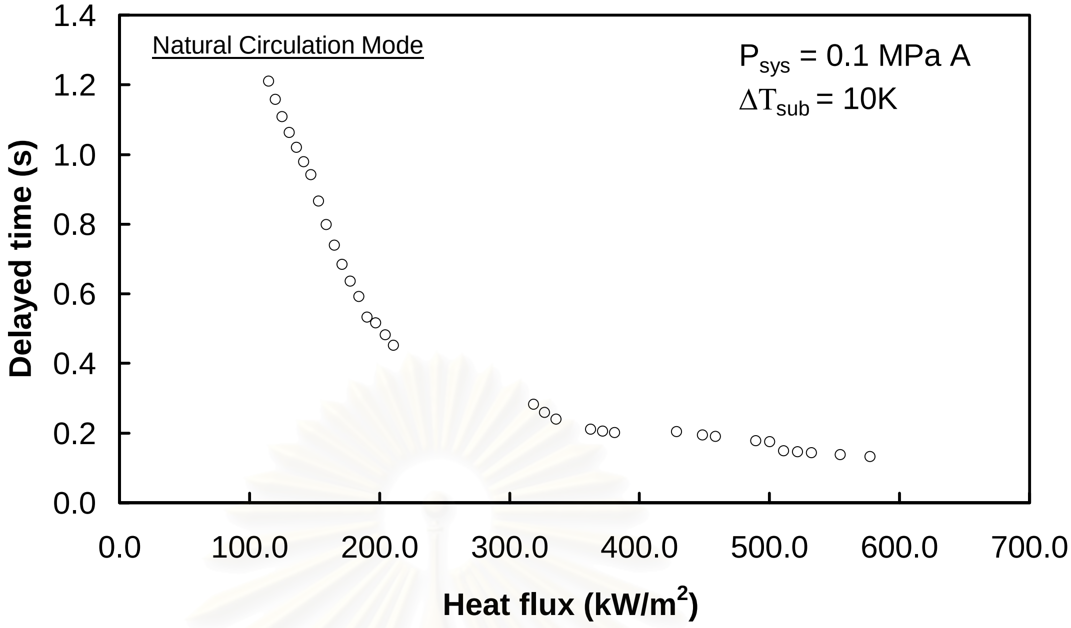

Fig.5.4 Delayed time of the flow oscillation

5.2.4 Period of the flow oscillation

The period of the flow oscillation was measured from each cycle of the oscillation at each heat flux. The period of the flow oscillation is high at the low heat flux and decreases with the increasing heat flux as shown in Fig.5.5. From Fig.5.4 and Fig.5.5 the period of the oscillation is almost equal to the delayed time of the oscillation. The period of the oscillation is high at the low heat flux because at low heat flux the heat transfer is not enough to drive the bubble to circulate through the upper tank. It needs more time for the bubble to travel through the test section. When the bubble goes toward the outlet plenum, it condenses and the flow reversal occurs. At high heat flux the natural oscillation and density wave occur and there is no flow reversal. Thus the period of the oscillation becomes shorter and shorter.

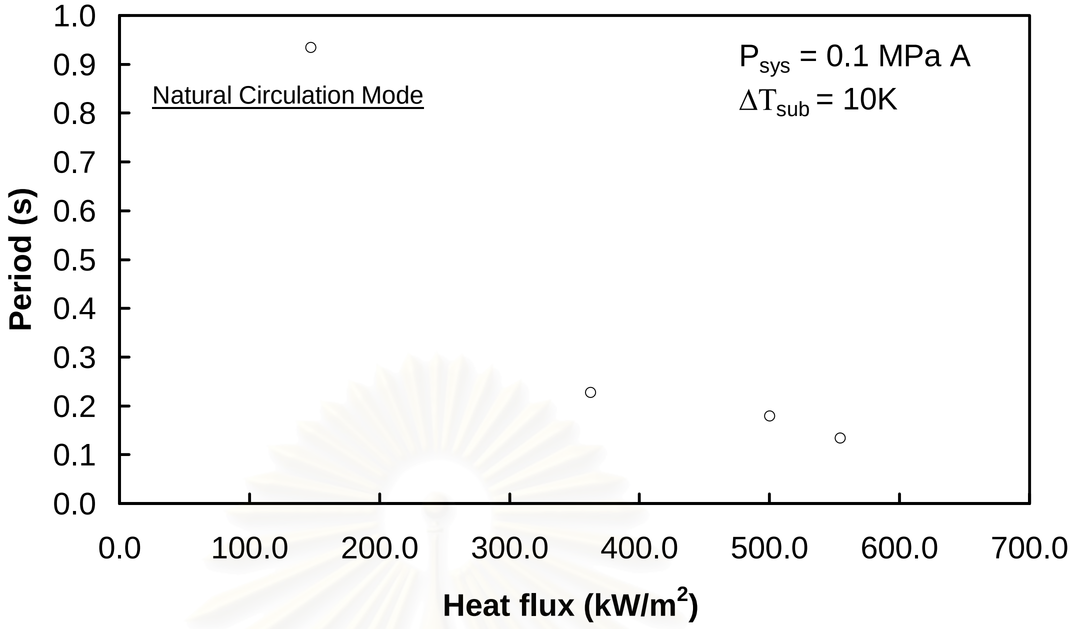

Fig.5.5 Period of the flow oscillation

5.3 Feature of the flow oscillation

The feature of the flow oscillation is shown in Fig.5.6-5.11. From the experimental results the feature of the flow oscillation changed as the heat flux increased. At the low heat flux the bubble of the test channels starts to increase toward the outlet plenum and condense at the outlet plenum. The maximum and minimum velocities of channel 1 and 2 are 0.8 and –0.4 m/s, respectively. The amplitude of the pressure drop is 3.5 kPa. The maximum velocity of each channel is 180 degree out-of-phase. The maximum velocity and the pressure drop is in-phase. After that the flow reversal occurs. The bubble starts to increase toward the outlet plenum again. The cycle then repeats. The maximum velocity and the flow reversal of the channel 1 and 2 are nearly the same. There is the fluctuation of the channel velocity after the condensation at the outlet plenum due to insufficient evaporation.

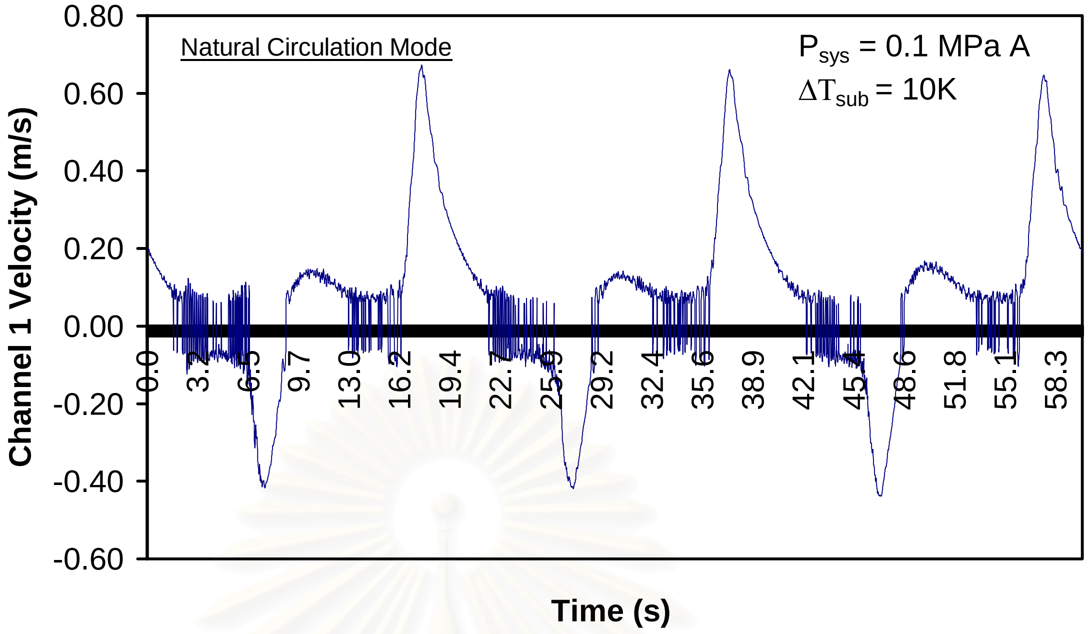

Fig 5.6 Channel 1 velocity at heat flux 54.11 kW/m^2

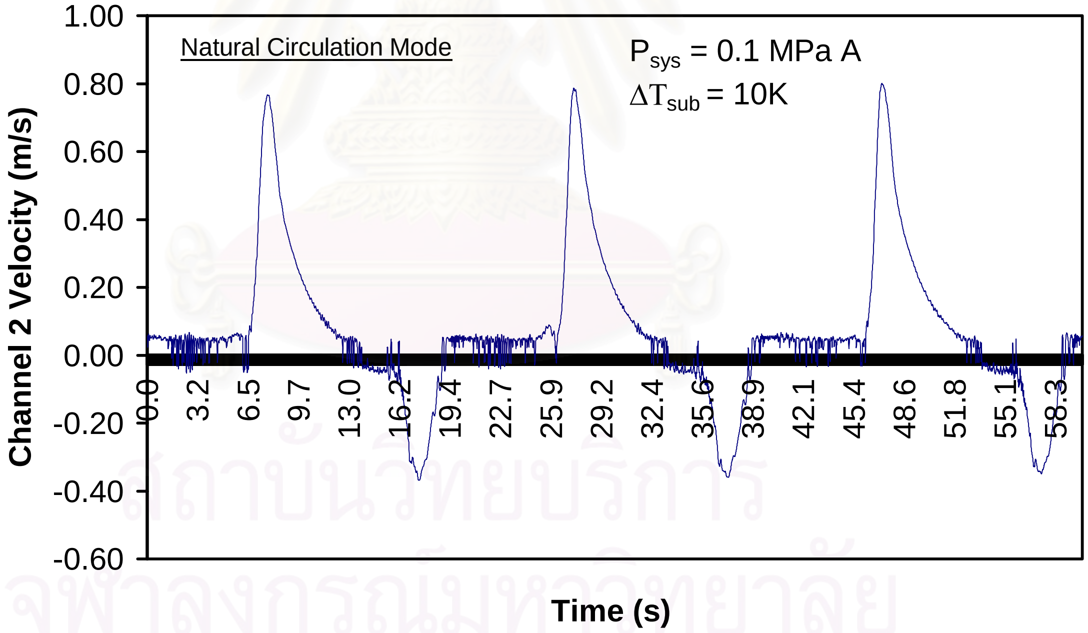

Fig 5.7 Channel 2 velocity at heat flux 54.11 kW/m^2

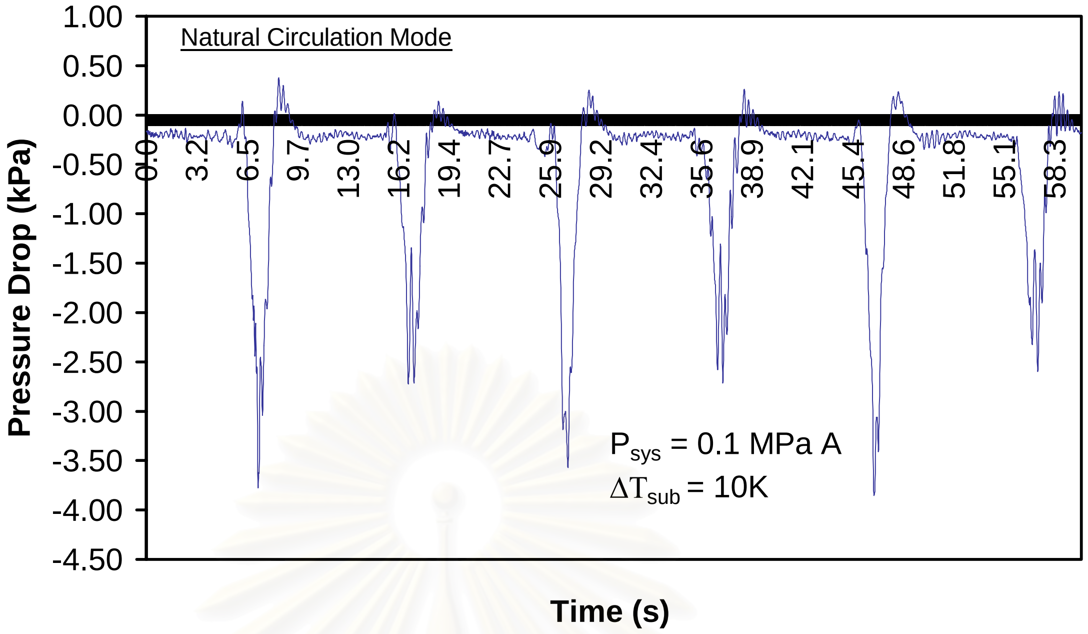

Fig 5.8 Pressure drop at heat flux 54.11 kW/m^2

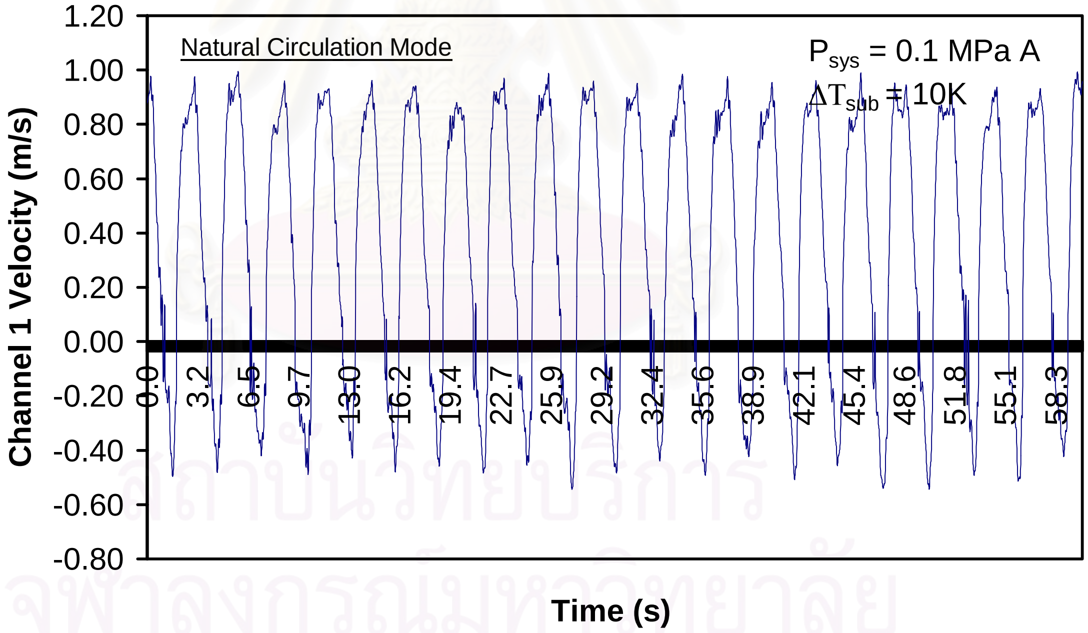

Fig 5.9 Channel 1 velocity at heat flux 285.6 kW/m^2

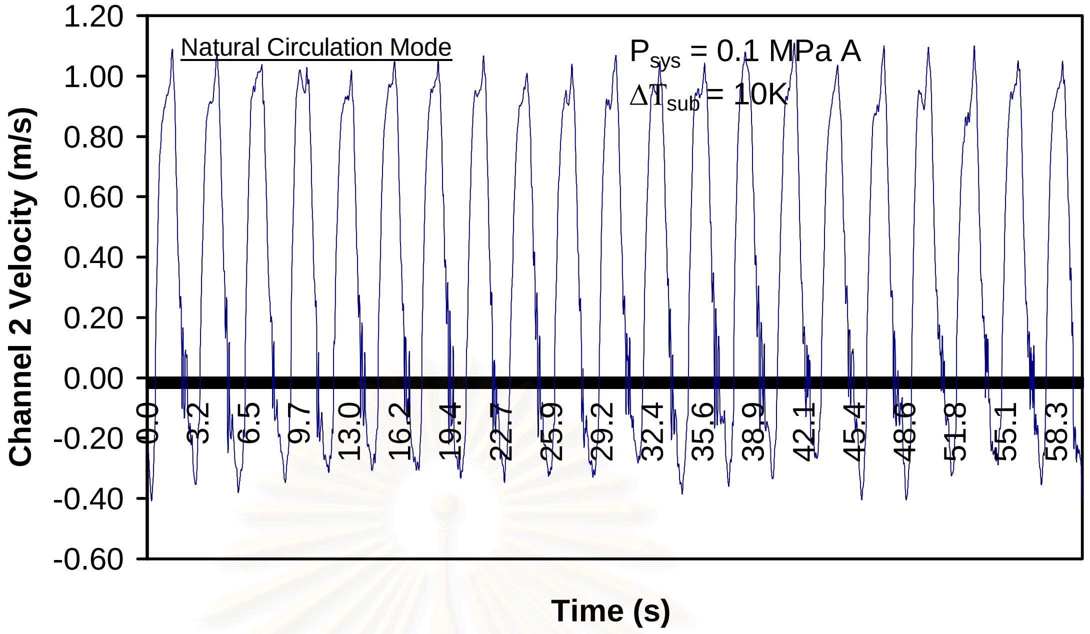

Fig 5.10 Channel 2 velocity at heat flux 285.6 kW/m^2

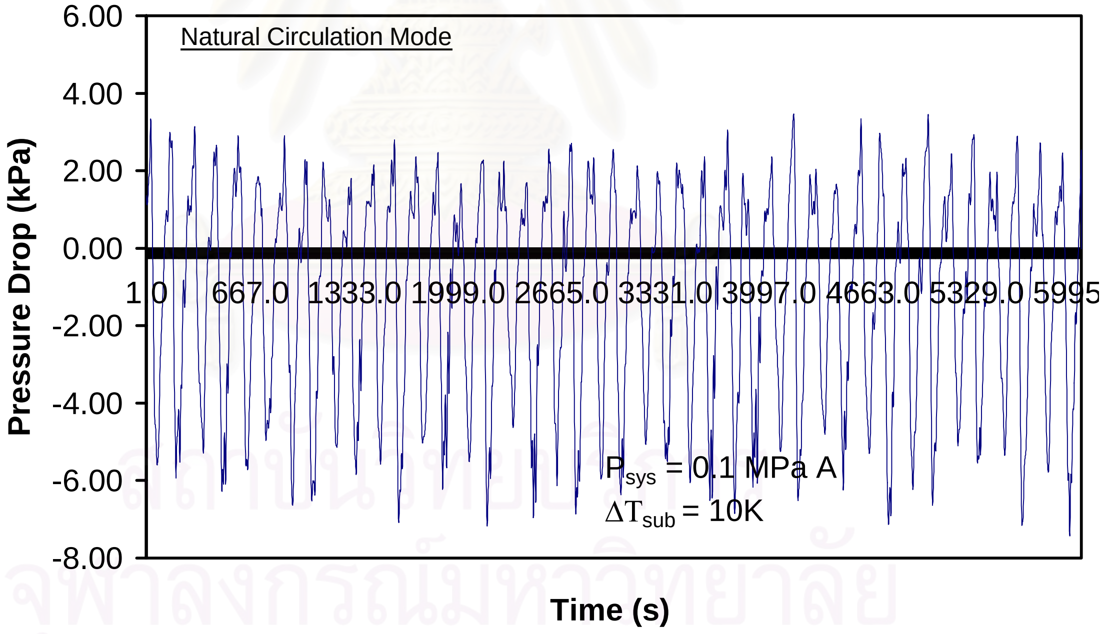

Fig 5.11 Pressure drop at heat flux 285.6 kW/m^2

At the higher heat flux the heat transfer from the heater is enough to drive the coolant from the outlet plenum through the downcommer to the inlet plenum. The more heat flux increases the less period and delayed time derives. The maximum and minimum velocities of channel 1 and 2 are 0.8 and –0.4 m/s, respectively. The amplitude of the pressure drop is 9 kPa and the period of the pressure drop at high heat flux is higher than that of the pressure drop at low heat flux. The maximum velocity between each channel is out-of-phase. The phase between the maximum velocity and the pressure drop is not clearly observed due to the high frequency of the pressure drop. Aritomi (1993) and Chiang (1994) showed that at high heat flux there was no flow reversal in the region. However, in this experiment as shown in Fig 5.9-5.10 at the heat flux 285.6 kW/m^2 the flow reversal still exists. This phenomenon occurs due to the effect of channel geometry, which will be described in section 5.6.

5.4 Effect of the system pressure

The system pressure is varied from 0.1, 0.2, 0.4, 0.5 and 0.7 MPaA to investigate the effect of the system pressure on the characteristic of the flow oscillation. The effect of the system pressure on the average total inlet velocity, the average channel velocity, the amplitude of the velocity, the amplitude of the pressure drop, the dimensionless of the pressure drop and the head, the delayed time and the period of the flow oscillation at 10 K subcooling is shown on Fig. 5.12-5.17. It can be seen from Fig.5.12 that the characteristic curves of the flow oscillation at all pressure for subcooling 10 K are alike. The average total inlet velocity increases steeply at the heat flux from 0 to 300 kW/m^2 and slightly increases at the heat flux higher than 300 kW/ m^2. At the same heat flux the difference of the maximum and the minimum of the average total inlet velocity for all pressure is 0.08 m/s. The average total inlet velocity has the tendency to decrease for the increasing pressure from 0.1 to 0.7 MPaA except at pressure 0.4 MPaA.

สถาบันวิทยบริการ
จุฬาลงกรณ์มหาวิทยาลัย

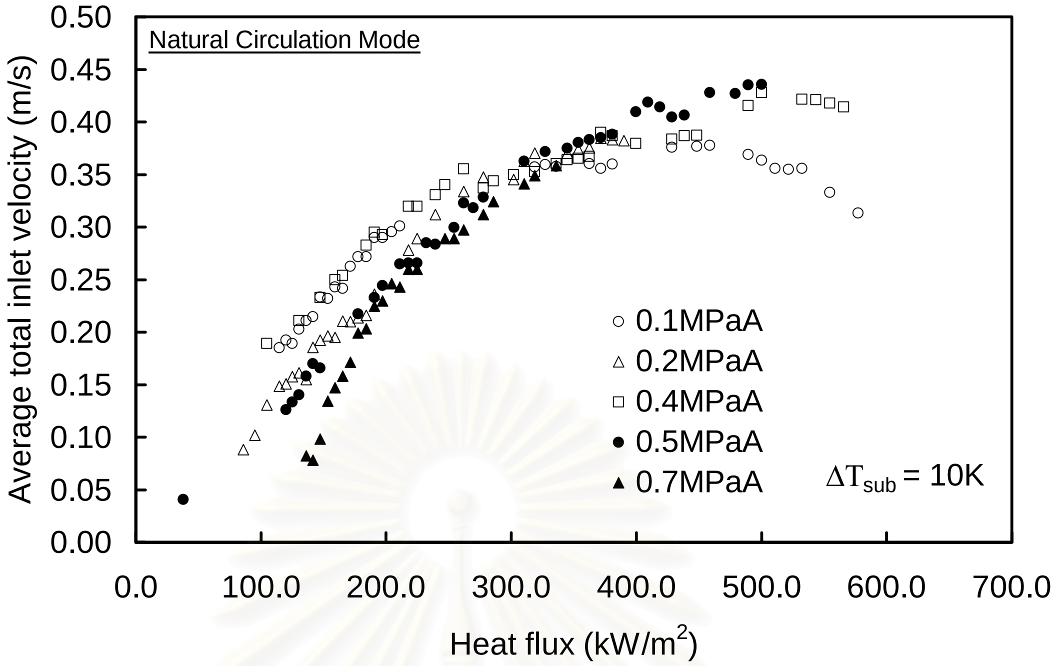

Fig.5.12 Effect of the pressure on the average total inlet velocity and the heat flux at subcooling 10 K

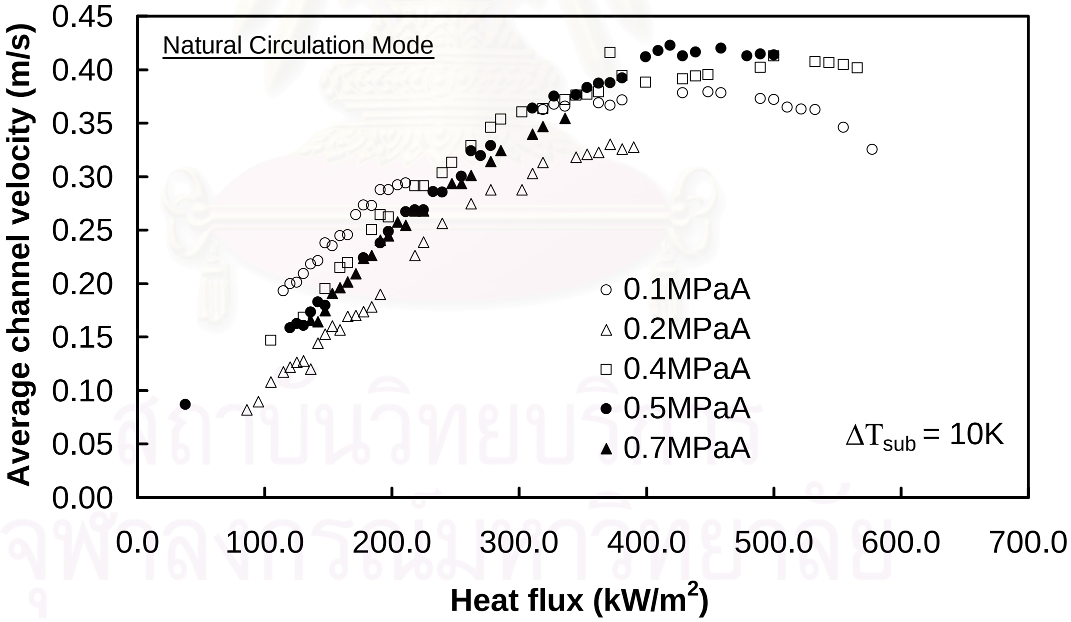

Fig.5.13 Effect of the pressure on the average channel velocity and the heat flux at subcooling 10 K

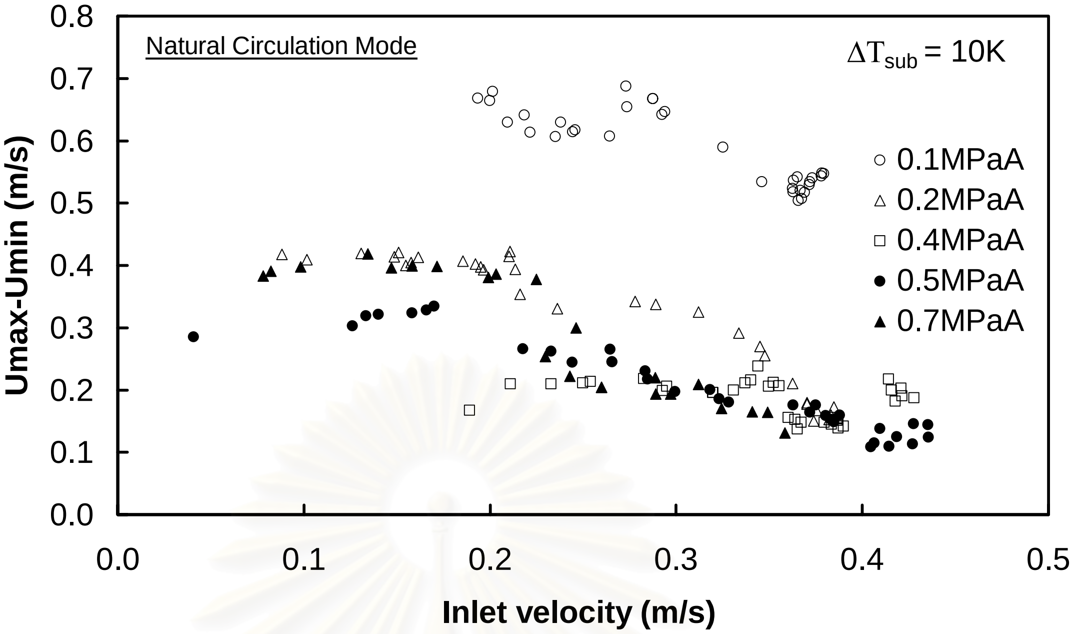

Fig.5.14 Effect of the pressure on the amplitude of the velocity and the inlet velocity at subcooling 10 K

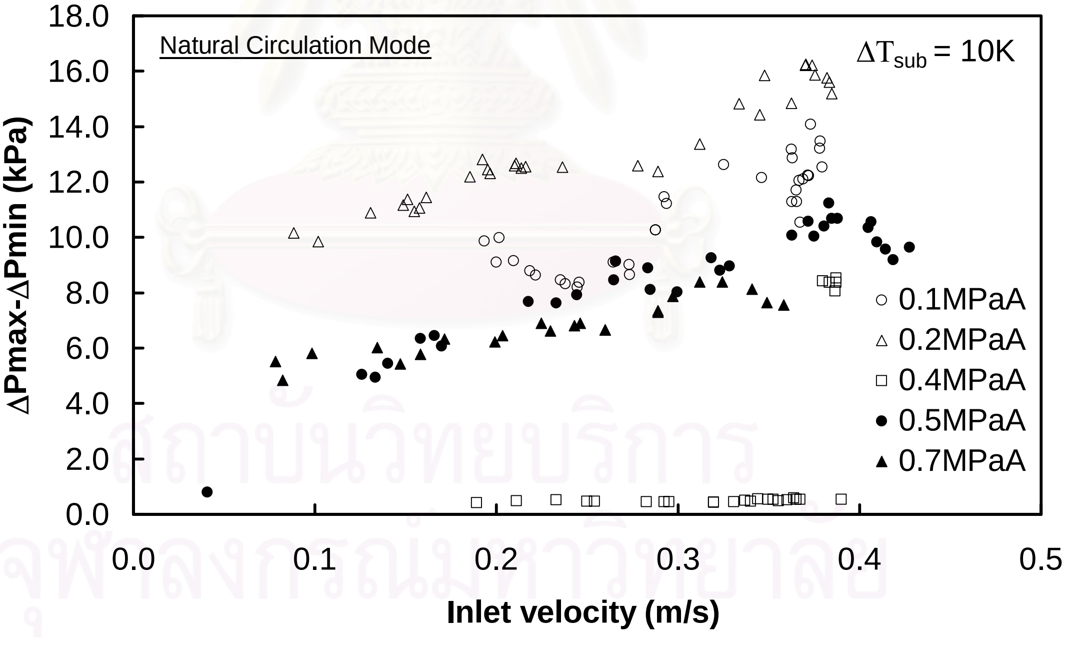

Fig.5.15 Effect of the pressure on the amplitude of the pressure drop and the inlet velocity at subcooling 10 K

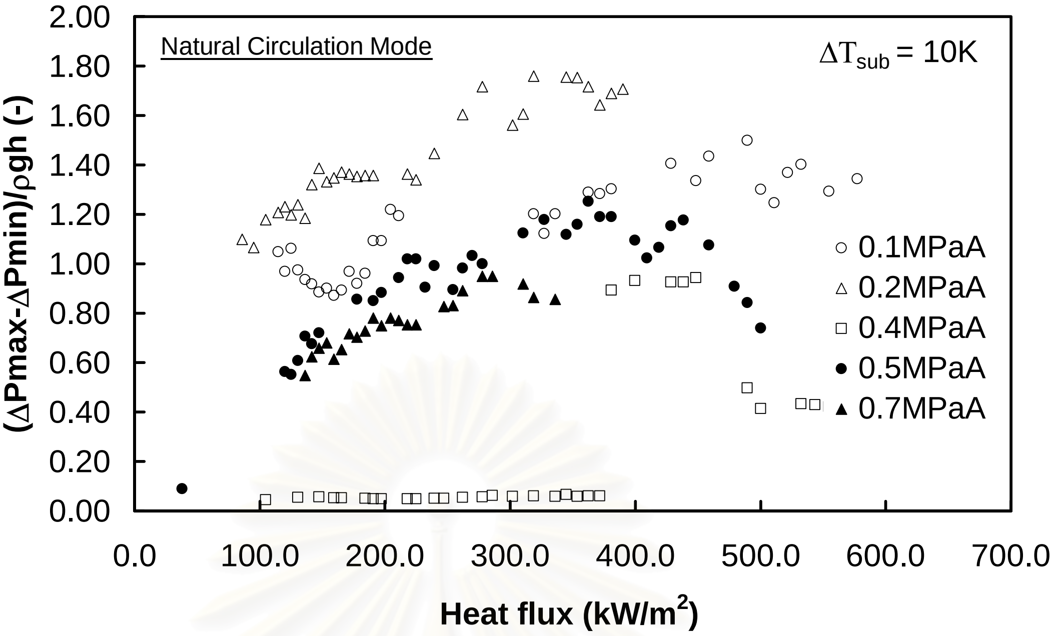

Fig.5.16 Effect of the pressure on the dimensionless of the pressure drop and the head at subcooling 10 K

The amplitude of the average channel velocity is in the range between 0.1 and 0.7 m/s corresponding with the inlet velocity between 0.08 and 0.43 m/s in Fig. 5.14. The amplitude of the average channel velocity decreases as the inlet velocity increases for all pressure. The maximum amplitude of the average channel velocity is occurred at pressure 0.1 MPaA. The amplitude of the average channel velocity has the tendency to decrease with the increasing system pressure except at the pressure 0.4 MPaA.

Contrary to the amplitude of the average channel velocity the amplitude of the pressure drop increases with the increasing inlet velocity and has the tendency to decrease with the increasing system pressure except at the pressure 0.2 and 0.4 MPaA.

Like the amplitude of the pressure drop the dimensionless of the pressure drop and the head has the tendency to decrease with increasing system pressure except at the pressure 0.2 and 0.4 MPaA.

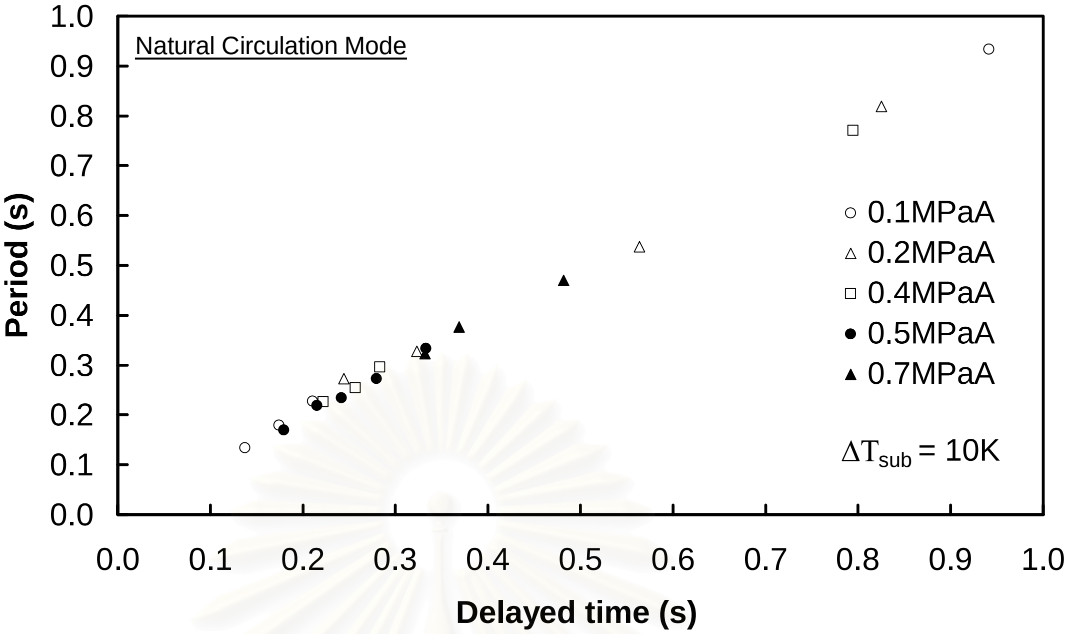

Fig.5.17 Effect of the pressure on the period and the delayed time at subcooling 10 K

The relationship between the period and the delayed time due to the effect of system pressure at subcooling 10 K is shown in Fig. 5.17. The period and the delayed time are nearly the same for all pressure. Obviously seen that the change in system pressure does not have the effect on the period and the delayed time of the flow oscillation.

Fig. 5.18-5.23 show the features of the flow ocsillation flow at pressure 0.1, 0.2, 0.4, 0.5 and 0.7 MPaA and subcooling 15 K. In Fig.5.18 except for the pressure 0.5 and 0.7 MPaA the average total inlet velocity has the tendency to decrease with the increasing pressure. The difference of the maximum and the minimum of the average total inlet velocity of all pressure is 0.12 m/s. The average of the average total inlet velocity of all pressure is 0.45 m/s.

In Fig.5.19 the average channel velocity has the tendency to decrease with the increasing system pressure except at the pressure 0.2 and 0.7 MPaA. The difference of the maximum and the minimum of the average channel velocity of all pressure is 0.1 m/s. The average of the average channel velocity of all pressure is 0.39 m/s.

Fig.5.20 shows the effect of the system pressure on the amplitude of the velocity at subcooling 15 K. The amplitude of the velocity varies between 0.15 and 1 m/s with the inlet velocity between 0.2 and 0.58 m/s. The amplitude of the velocity has the tendency to decrease with the increasing system pressure.

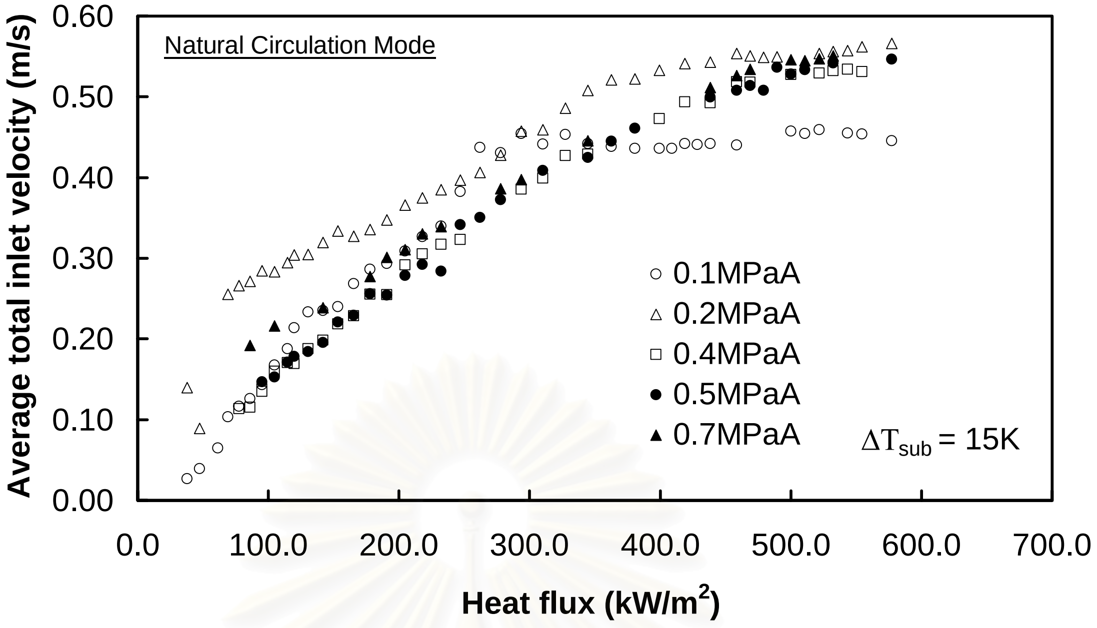

Fig.5.18 Effect of the pressure on the average total inlet velocity and the heat flux at subcooling 15 K

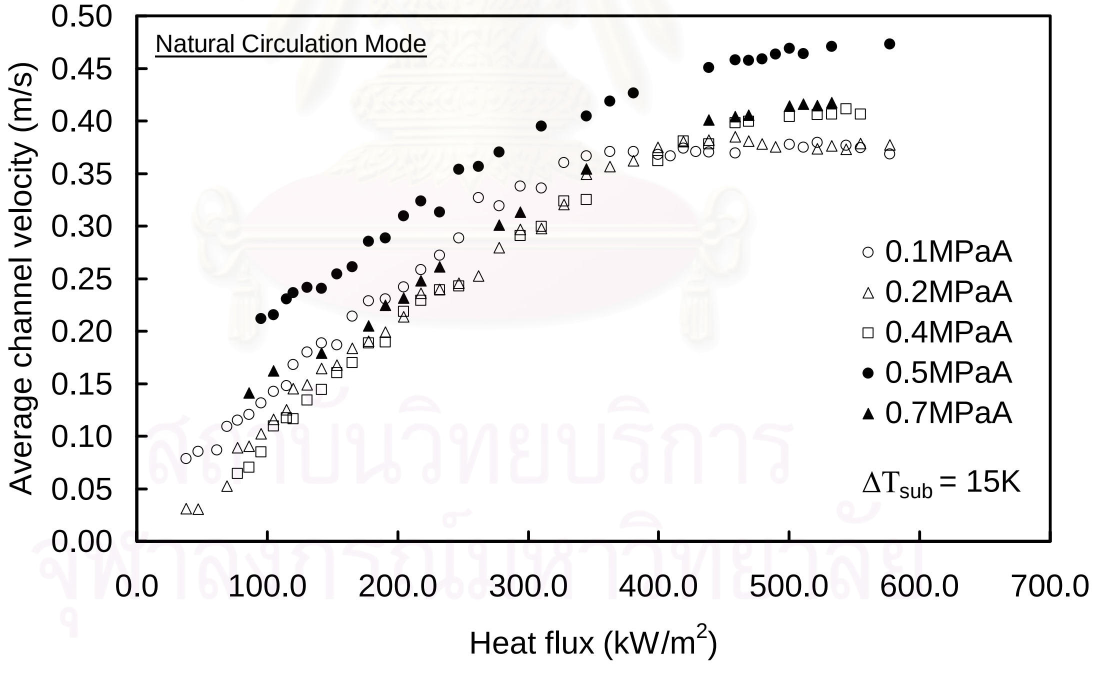

Fig.5.19 Effect of the pressure on the average channel velocity and the heat flux at subcooling 15 K

สถาบันวิทยบริการ
จุฬาลงกรณ์มหาวิทยาลัย

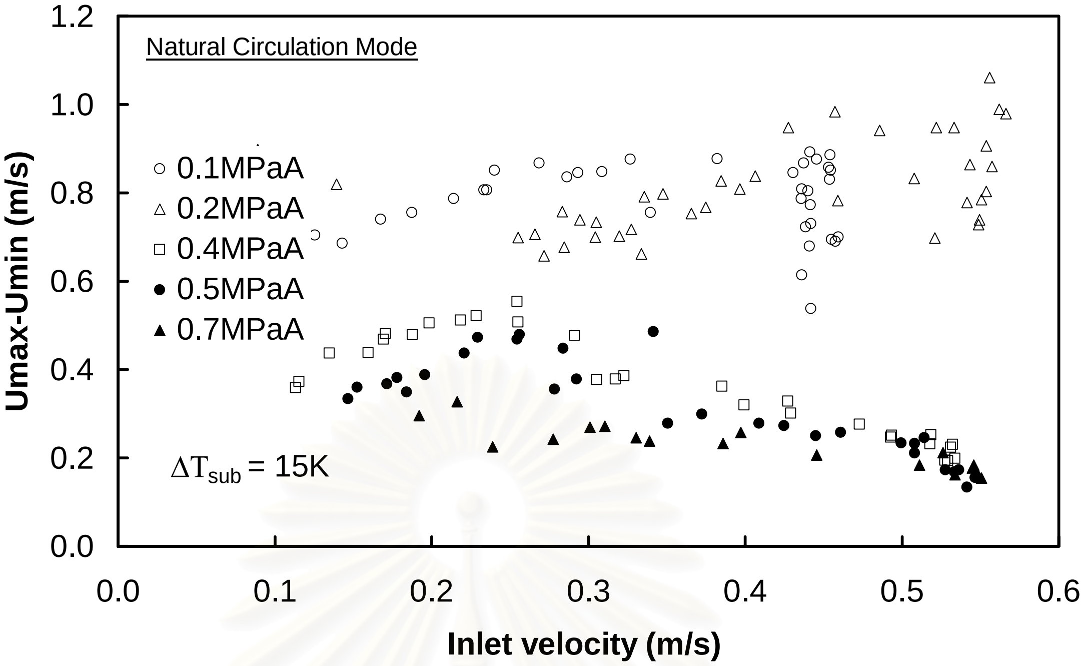

Fig.5.20 Effect of the pressure on the amplitude of the velocity and the inlet velocity at subcooling 15 K

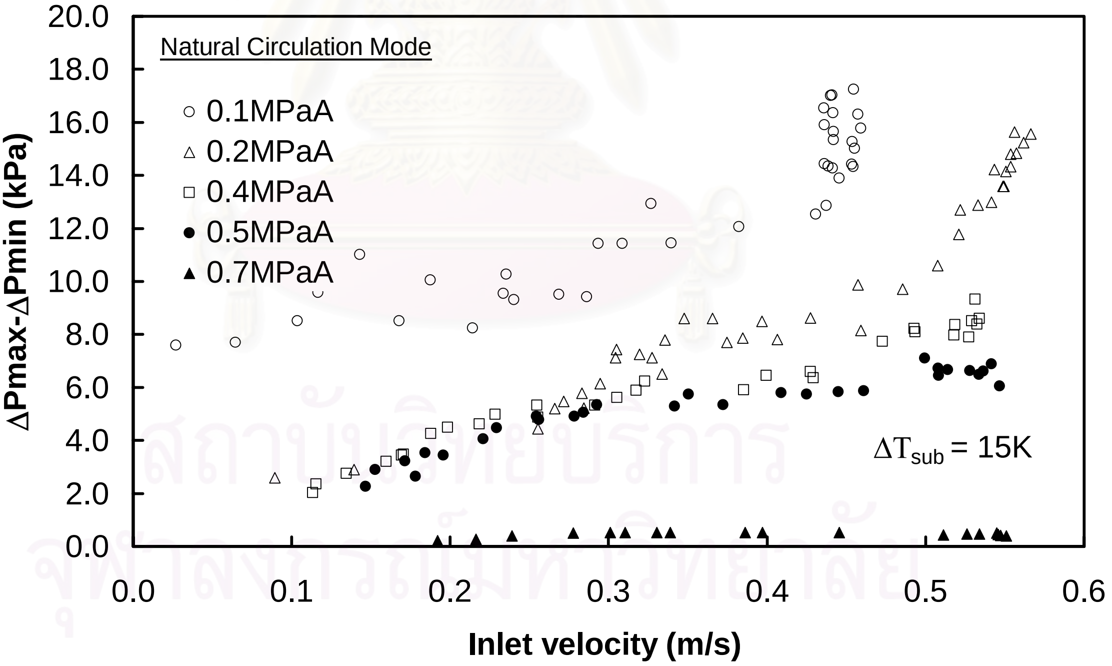

Fig.5.21 Effect of the pressure on the amplitude of the pressure drop and the inlet velocity at subcooling 15 K

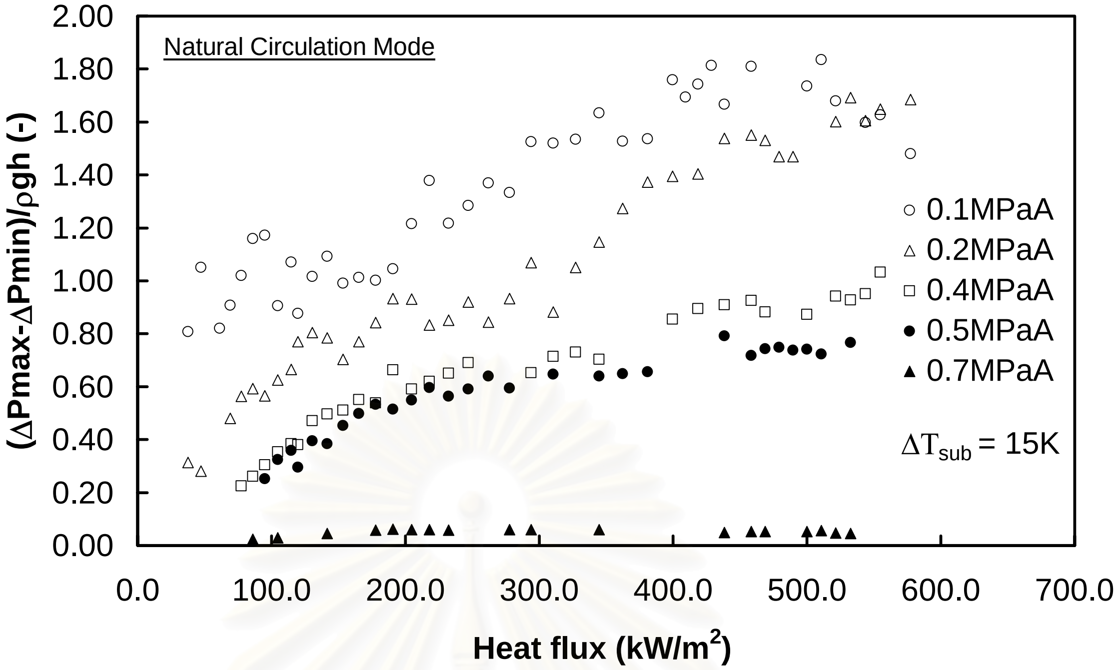

Fig.5.22 Effect of the pressure on the dimensionless of the pressure drop and the head at subcooling 15 K

Fig. 5.21 and Fig. 2.22 shows the effect of the pressure on the pressure drop and the dimensionless of the pressure drop and the head at subcooling 15 K, respectively. The pressure drop varies between 0.2 and 17 kPa with the increasing inlet velocity between 0.2 and 5.5 m/s. The pressure drop has the tendency to decrease with the increasing pressure. Similarly to the pressure drop the dimensionless of the pressure drop and the head varies between 0.2 and 1.8 with the heat flux between 50 and 550 kW/m^2 and has the tendency to decrease with the increasing pressure.

The relationship between the period and the delayed time due to the effect of system pressure at subcooling 15 K is shown in Fig. 5.23. The period and the delayed time are nearly the same. Obviously seen that the change in the system pressure does not have much effect on the period and the delayed time of the flow oscillation.

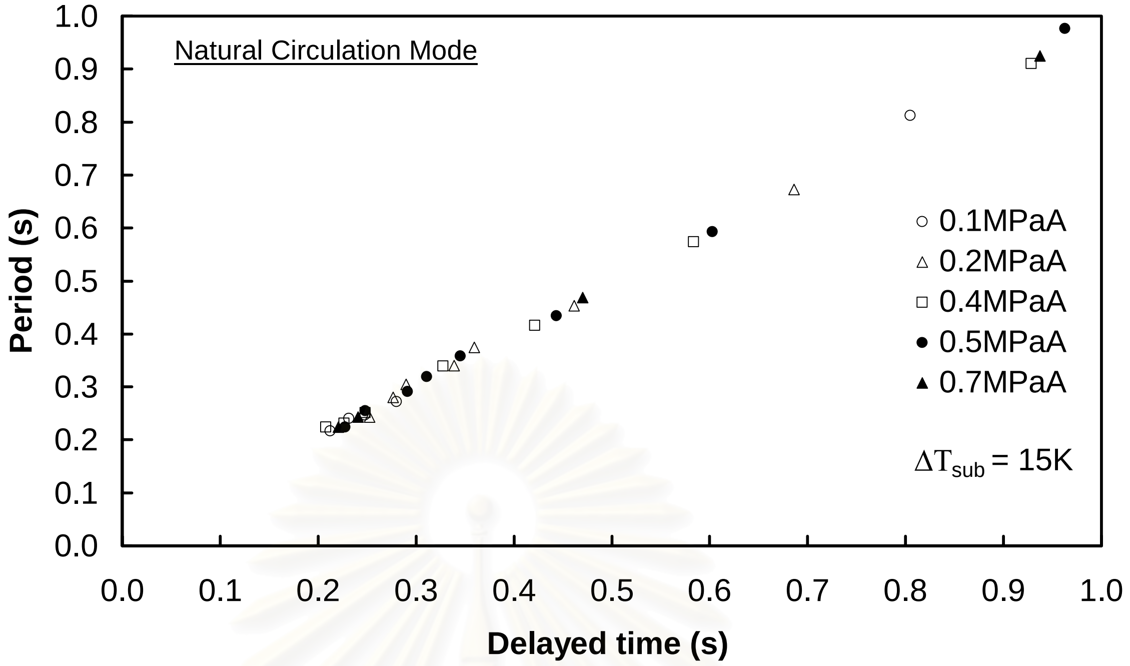

Fig.5.23 Effect of pressure on the period and the delayeded time at subcooling 15 K

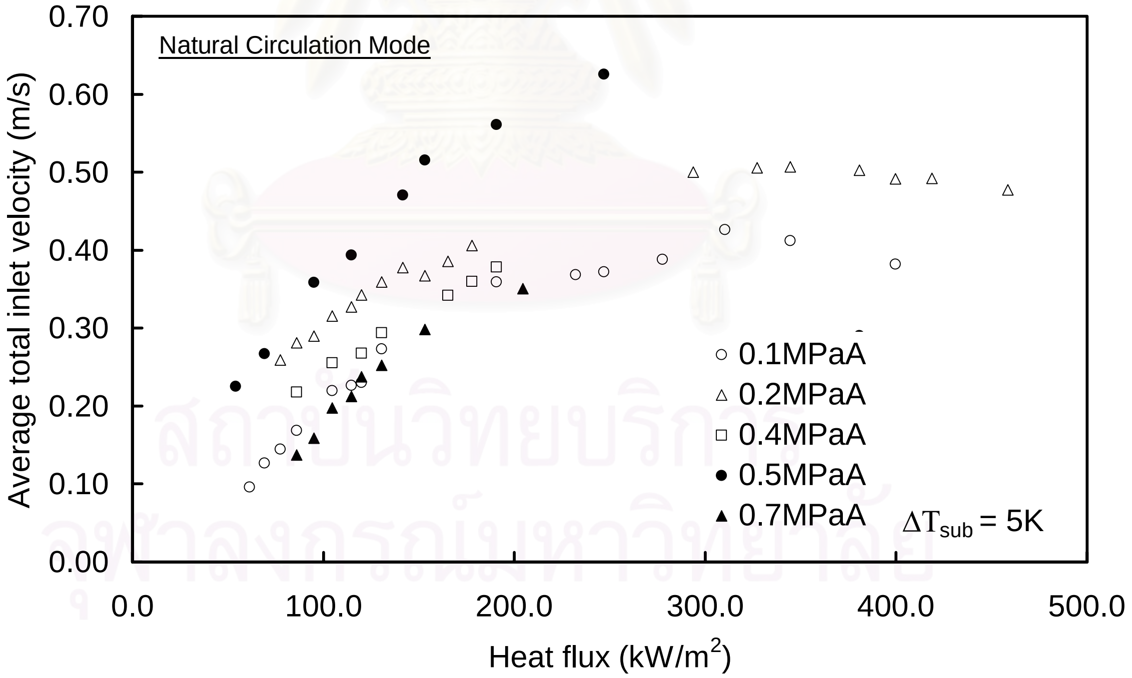

Fig.5.24 Effect of the pressure on the average total inlet velocity and the heat flux at subcooling 5 K

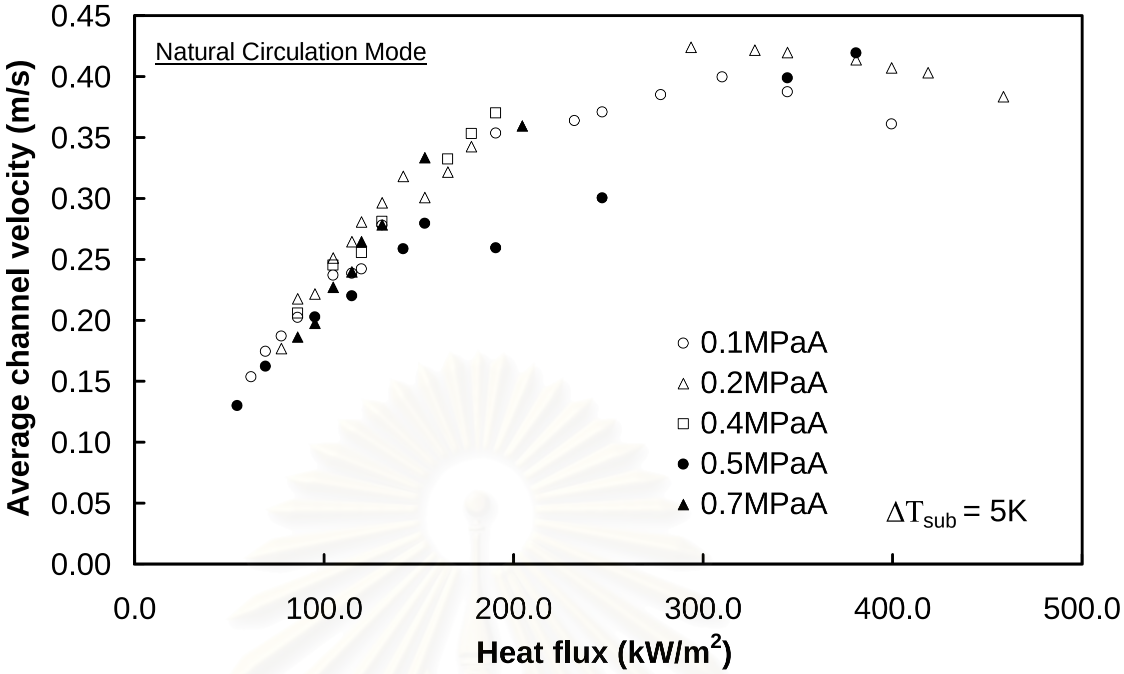

Fig.5.25 Effect of the pressure on the average channel velocity and the heat flux at subcooling 5 K

It can be seen from Fig.5.24 that the characteristic curves of the flow oscillation at all pressure for subcooling 5 K are alike. The average total inlet velocity increases steeply at the heat flux from 0 to 300 kW/m^2 and slightly increases at the heat flux higher than 300 kW/ m^2. At the same heat flux the difference of the maximum and the minimum of the average total inlet velocity for all pressure is 0.25 m/s. The average total inlet velocity has the tendency to decrease for the increasing system pressure from 0.1 to 0.7 MPaA except at pressure 0.1 and 0.4 MPaA. Fig. 5.25 shows that the average channel velocity has the same trend with the average total inlet velocity. But the difference of the maximum and the minimum of the average channel velocity among all pressure is 0.1 m/s. It is not clearly seen from Fig. 5.25 that the average channel velocity has the tendency to decrease with the increasing pressure from 0.1 to 0.7 MPaA.

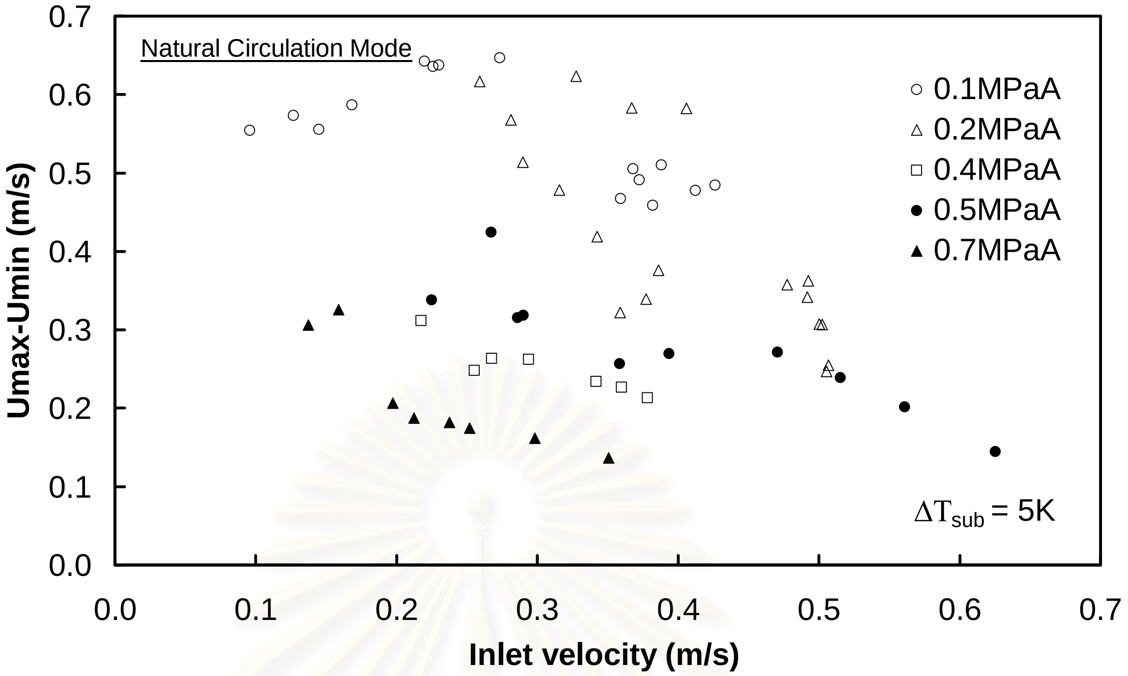

Fig.5.26 Effect of the pressure on the amplitude of the velocity and the inlet velocity at subcooling 5K

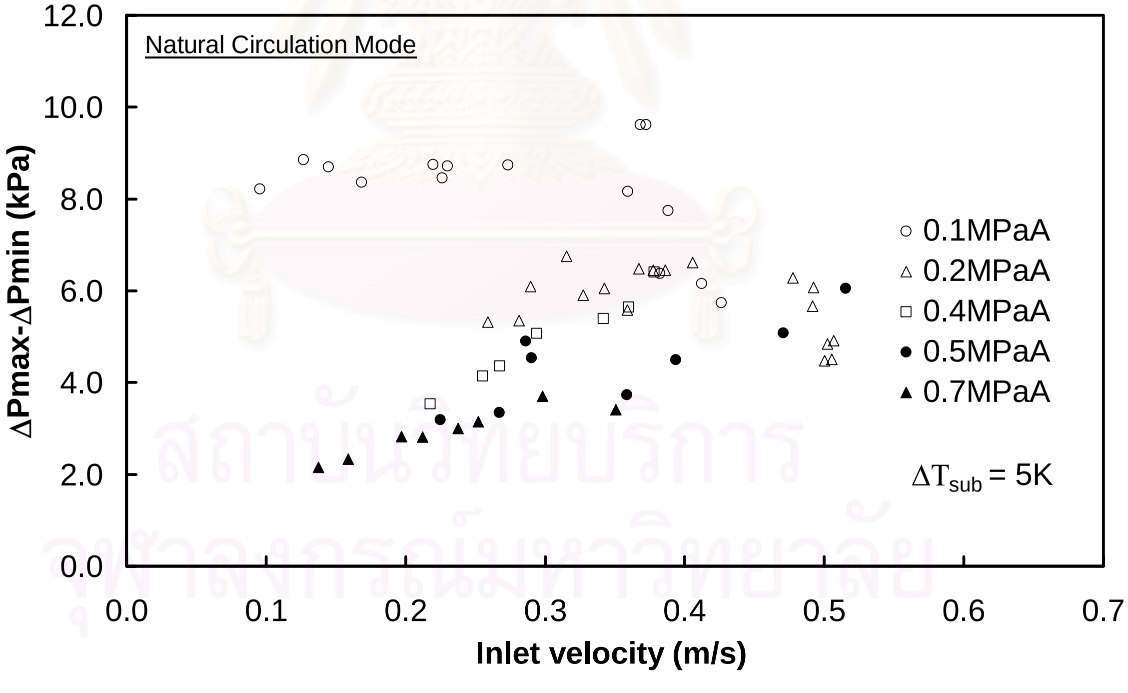

Fig.5.27 Effect of the pressure on the amplitude of the pressure drop and the inlet velocity at subcooling 5 K

สถาบันวิทยบริการ
จุฬาลงกรณ์มหาวิทยาลัย

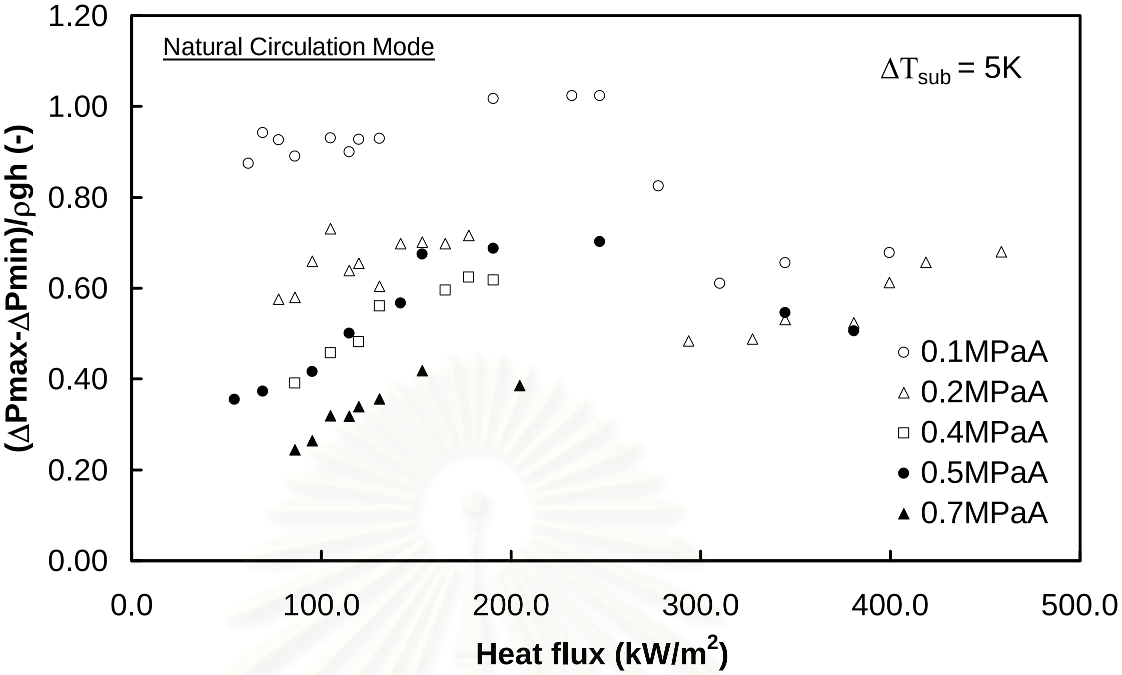

Fig.5.28 Effect of the pressure on the dimensionless of the pressure drop and the head at subcooling 5 K

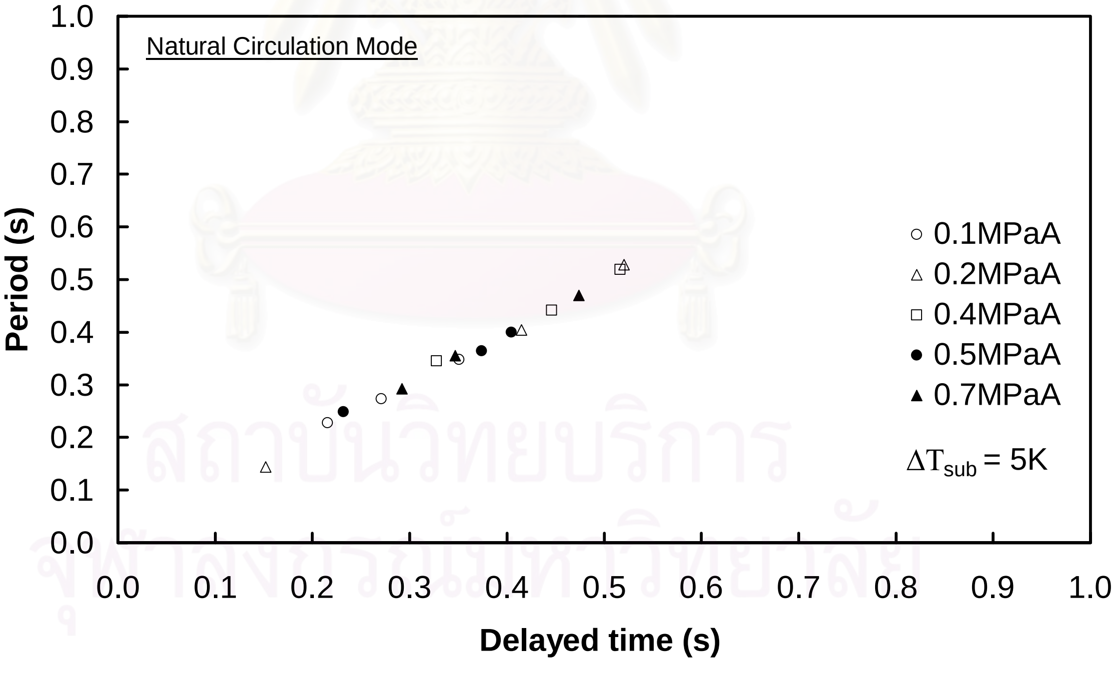

Fig.5.29 Effect of the pressure on the period and the delayed time at subcooling 5 K

The amplitude of the average channel velocity is in the range between 0.1 and 0.65 m/s corresponding with the inlet velocity between 0.1 and 0.65 m/s. The amplitude of the average channel velocity decreases as the inlet velocity increases for all pressure. The maximum amplitude of the average channel velocity is occurred at pressure 0.1 MPaA. The amplitude of the average channel velocity has the tendency to decrease with the increasing system pressure.

Contrary to the amplitude of the average channel velocity the amplitude of the pressure drop increases with the increasing inlet velocity and has the tendency to decrease with the increasing system pressure. The amplitude of the pressure drop varies between 2 and 10 kPa with the inlet velocity between 0.1 and 0.63 m/s.

Like the amplitude of the pressure drop the dimensionless of the pressure drop and the head has the tendency to decrease with increasing system pressure. The dimensionless of the pressure drop and the head varies between 0.2 and 1 with the heat flux between 50 and 550 kW/m^2.

The relationship between the period and the delayed time due to the effect of system pressure at subcooling 5 K is shown in Fig. 5.29. The period and the delayed time are nearly the same. Obviously seen that the change in system pressure does not have much effect on the period and the delayed time of the flow oscillation.

For all subcooling at the heat flux lower than 300 kW/m^2 the increase in system pressure from 0.1 MPaA to 0.7 MPaA has the effect on the decrease of the average total inlet velocity, the average channel velocity, the amplitude of the velocity, the amplitude of the pressure drop and the dimensionless of the pressure drop and the head. The increase in the system pressure reduces the void fraction, which has the effect on the two-phase friction and momentum pressure drop. Moreover it has the effect on the bubble size because of the decreased density difference and surface tension between liquid and vapor. As the saturation temperature is dependent on the system pressure, the increase in system pressure will increase the saturation temperature and thus lower the heat transfer coefficient. The decrease in heat transfer coefficient will reduce the heat transfer from the heater to coolant. Consequently, the average total inlet velocity and the average channel velocity decrease. In some cases the results from the experiment are not consistent due to the difficulty in controlling the subcooled condition and water level in the upper tank of the fluid. Especially at pressure 0.4 MPaA and subcooling 10 K the amplitude of the pressure drop and the dimensionless between the pressure drop and the head were relatively low because of the low water level in the upper tank. Chiang (1994) found that the geysering was not observed at the pressure above 0.35 MPaA. However, in these experiments it is interesting that the geysering can be observed at the system pressure upto 0.7 MPaA as shown on Fig. 5.30. The reason for this phenomenon is due to the effect of channel geometry on the condensation of the coolant in the test channels. The longer riser induces a large magnitude of the amplitude of the velocity because the geysering is more pronounced in longer risers. Thus a 1 meter long riser and the channel geometry in this experiment gives rise to the occurrence of the geysering above 0.35 MPaA. The detail of the phenomenon due to the effect of channel geometry will be described in the next section. As the amplitude of the void fraction can be indicated by the dimensionless of the pressure drop and the head between inlet and outlet plenums, the higher pressure suppress the occurrence of the void fraction. Furthermore, increase system pressure gives rise to the increase of the saturation temperature, which will has an effect on the range of the bubble-slug criteria and stabilizes the system. In natural circulation the flow rate depends on the heat flux of the heat input. The period and the delayed time decrease as the heat flux increases. The increase in system pressure doesn’t have much effect on the period and the delayed time of the oscillation. At the heat flux higher than 300 kW/m^2 the average total inlet velocity, the average channel velocity, the amplitude of the veolicty, the amplitude of the pressure drop and the dimensionless of the pressure drop and the head increase as the the system pressure increase due to the high friction pressure drop as reported by Fukuda (1979a).

สถาบันวิทยบริการ
จุฬาลงกรณ์มหาวิทยาลัย

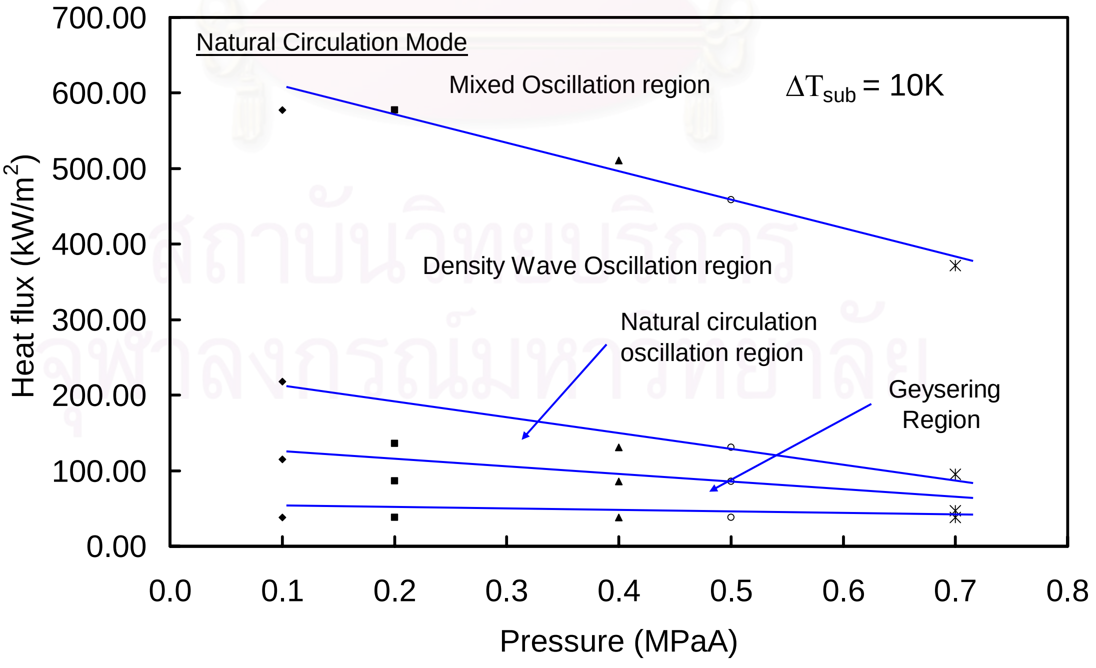

Fig. 5.30 Flow instability map

5.5 Effect of the subcooling

The effect of the subcooling at 5, 10 and 5 K is investigated. It is found that the average total inlet velocity, the average channel velocity decrease with the increasing subcooling as shown in Fig.5.31-5.32, respectively. The same characteristic curves of the average total inlet velocity at subcooling 5, 10 and 15 K are shown in Fig. 5.31. The difference of the maximum and the minimum of the average total inlet velocity for all subcooling at the same heat flux is 0.08 m/s. At the heat flux lower than 300 kW/m^2 the average total inlet velocity has the tendency to decrease for the increasing subcooling from 5 to 15 K. Fig. 5.32 shows that the average channel velocity has the same trend with the average total inlet velocity. But the difference of the maximum and the minimum of the average channel velocity among all subcooling is 0.1 m/s. At low the heat flux lower than 300 kW/m^2 the average channel velocity has the tendency to decrease with the increasing subcooling from 5 to 15 K. In general the increasing subcooling will lower the Grashof number and liquid temperature and thus reduce the heat transfer coefficient and interfacial heat transfer coefficient, respectively. As the heat and the mass transfer between liquid and vapor phases decrease, the average total inlet velocity and the average channel velocity decrease. The increase in subcooling has an effect on increase non-boiling length and decreases void fraction. At the heat flux higher than 300 kW/m^2 the maximum average total inlet velocity and and the maximum average channel velocity occurred at the subcooling 15 K because of the high friction pressure drop at the lower subcooling.

สถาบันวิทยบริการ
จุฬาลงกรณ์มหาวิทยาลัย

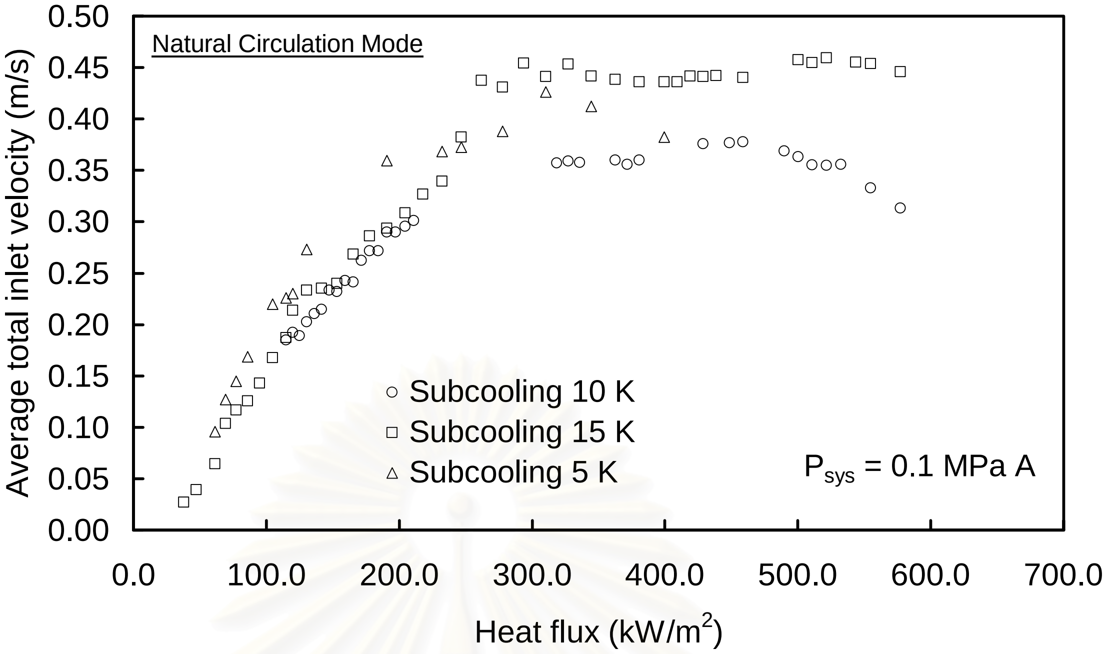

Fig. 5.31 Effect of the subcooling on the average total inlet velocity and the heat flux at pressure 0.1 MPaA

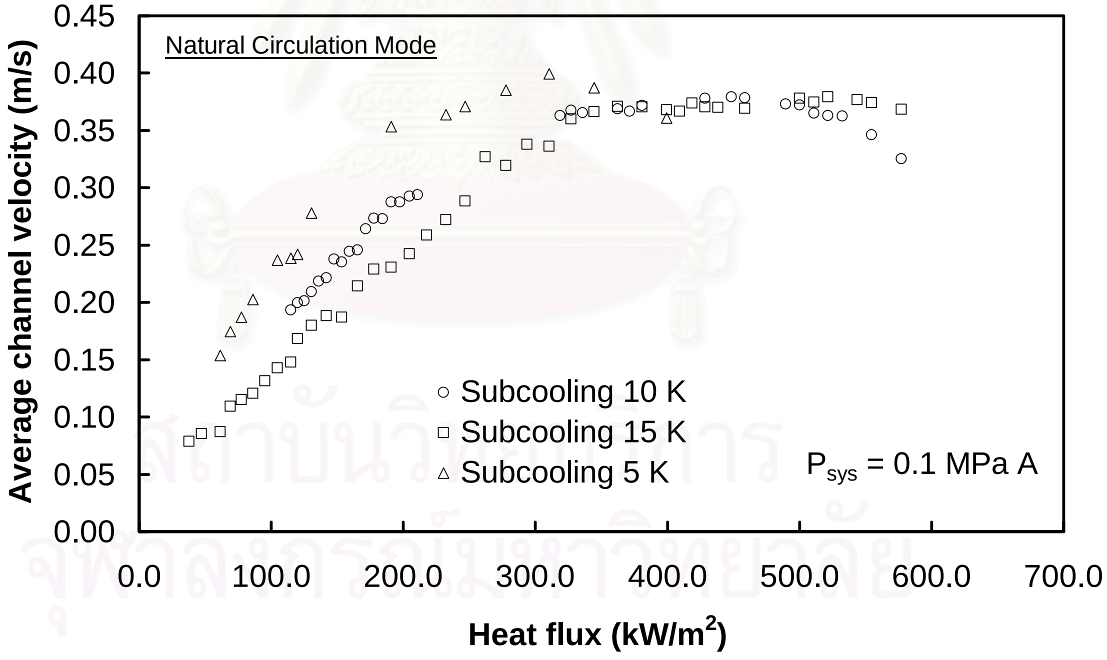

Fig. 5.32 Effect of the subcooling on the average channel velocity and the heat flux at pressure 0.1 MPaA

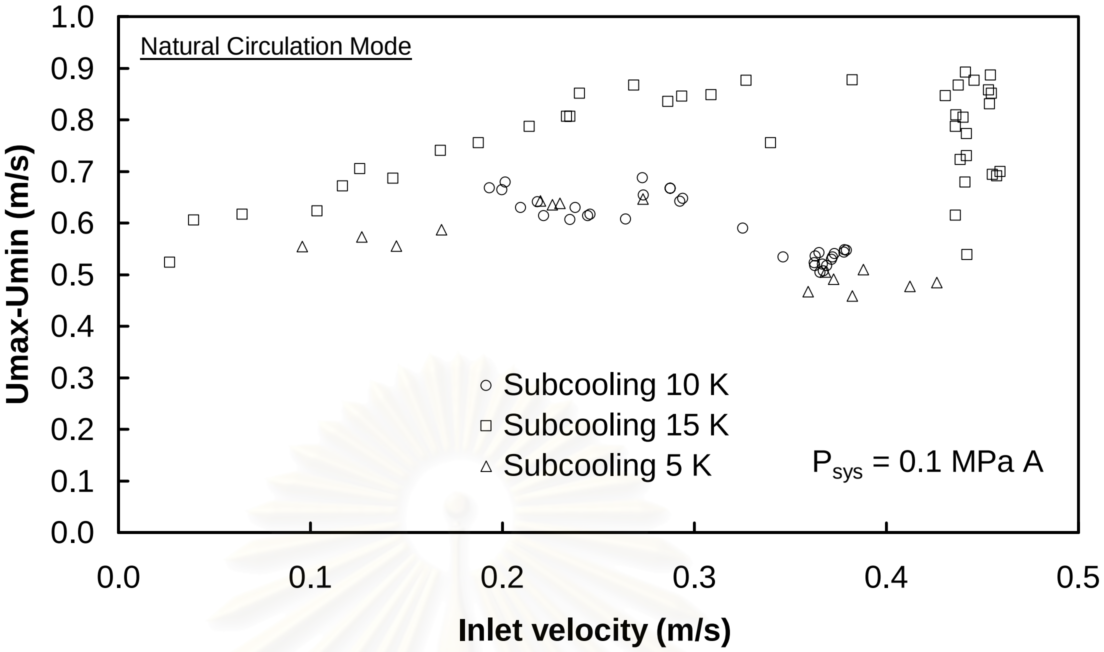

Fig. 5.33 Effect of the subcooling on the amplitude of the velocity and the inlet velocity at pressure 0.1 MPaA

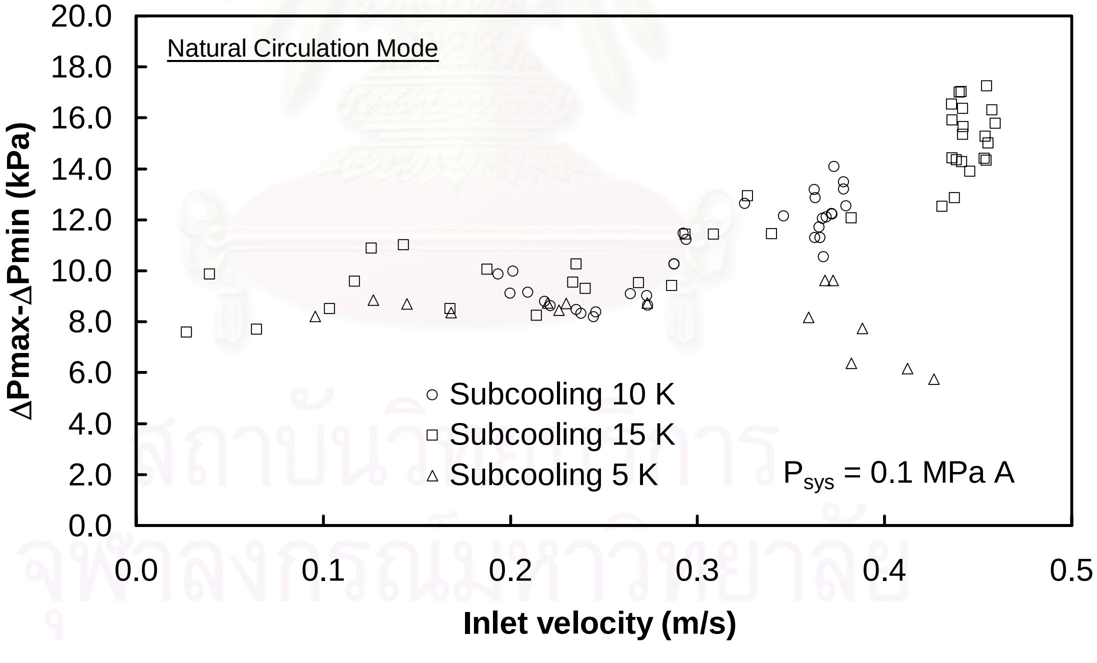

Fig. 5.34 Effect of the subcooling on the amplitude of the pressure drop and the inlet velocity at pressure 0.1 MPaA

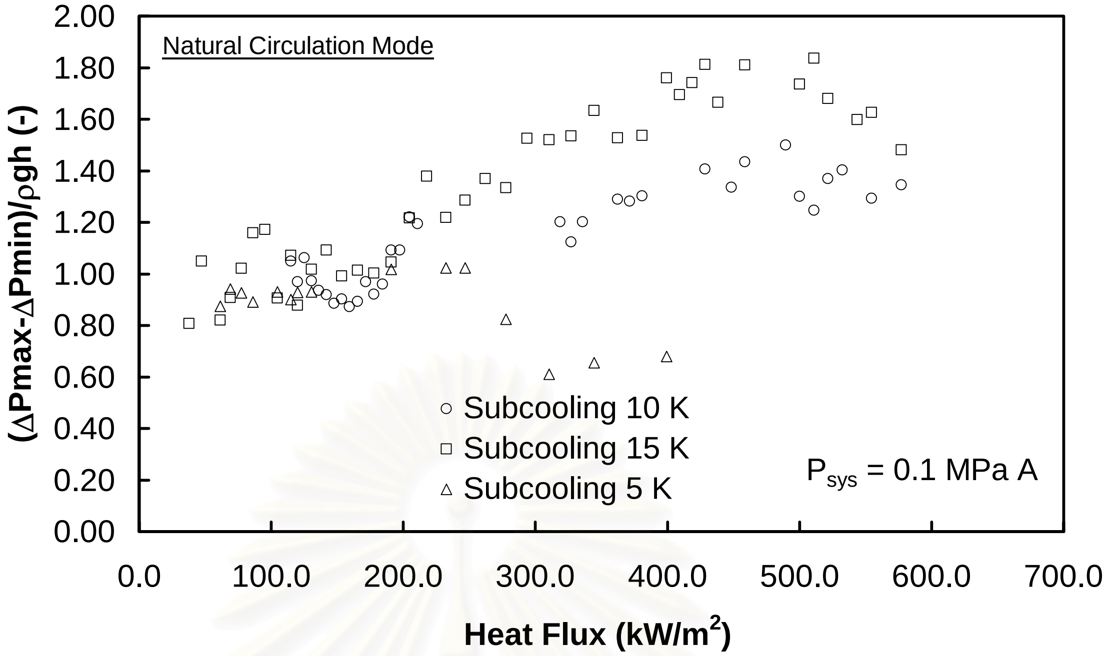

Fig. 5.35 Effect of the subcooling on the dimensionless of the pressure drop and the head at pressure 0.1 MPaA

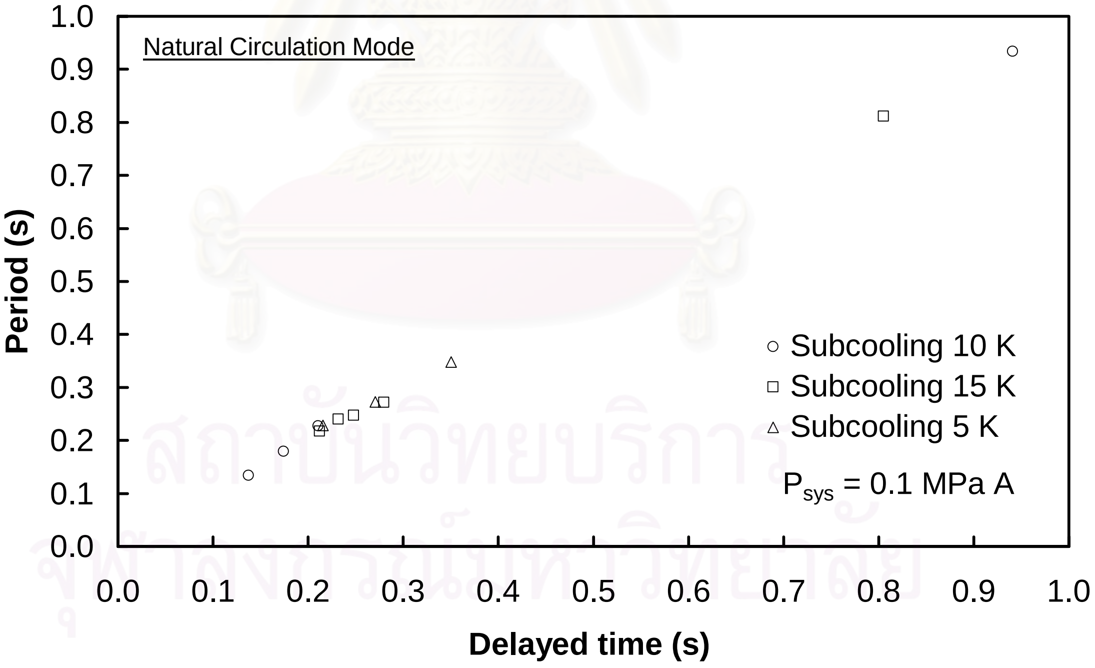

Fig. 5.36 Effect of the subcooling on the period and the delayed time at pressure 0.1 MPaA

The amplitude of the average channel velocity, shown in Fig. 5.33, is in the range between 0.45 and 0.9 m/s corresponding with the inlet velocity between 0.02 and 0.45 m/s. The amplitude of the average channel velocity has the trend to decrease with the increasing inlet velocity. The maximum amplitude of the average channel velocity is occurred at subcooling 15 K. The amplitude of the average channel velocity has the tendency to increase with the increasing subcooling.

In Contrast the amplitude of the average channel velocity the amplitude of the pressure drop increases with the increasing inlet velocity. The amplitude of the pressure drop has the tendency to increase with the increasing subcooling and varies between 4 and 16 kPa with the inlet velocity between 0.02 and 0.45 m/s.

Similar to the amplitude of the pressure drop the dimensionless of the pressure drop and the head has the tendency to increase with increasing subcooling. The dimensionless of the pressure drop and the head varies between 0.6 and 1.8 with the heat flux between 50 and 550 kW/m^2.

The relationship between the period and the delayed time due to the effect of system pressure at subcooling 5 K is shown in Fig. 5.36. The period and the delayed time are nearly the same. Obviously seen that the change in subcooling does not have much effect on the period and the delayed time of the flow oscillation.

Normally the increase subcooling stabilizes the system. However, in this experiment at the heat flux higher than 300 kW/m^2 the average total inlet velocity, the average channel velocity increase with the increasing subcooling due to the high condensation at the high subcooling, which increases the flow reversal. Therefore the amplitude of the velocity, the amplitude of the pressure drop and the dimensionless of the pressure drop increase with the increasing subcooling at the outlet plenum.

5.6 Effect of the channel geometry

As mentioned in the previous section that the length of the riser and the channel geometry have the effect on the occurrence of the geysering at the pressure above 0.35 MPaA, in this experiment as shown in chapter 4 the test section with the heater inside connected to the 1 meter long riser and the upper plenum. The slug bubble has the high velocity in the test section due to the annular shape between the test section and the heater. Because of the circular shape of the riser when the slug bubble enters into the riser, the shape of the slug bubble changes and the velocity of the slug bubble decreases. At the point where the pressure head increases it is easier for the slug bubble to collapse before entering at the upper plenum. This makes the geysering occurring at the higher pressure. Fig. 5.37 shows the bubble shape in the test section and in the riser.

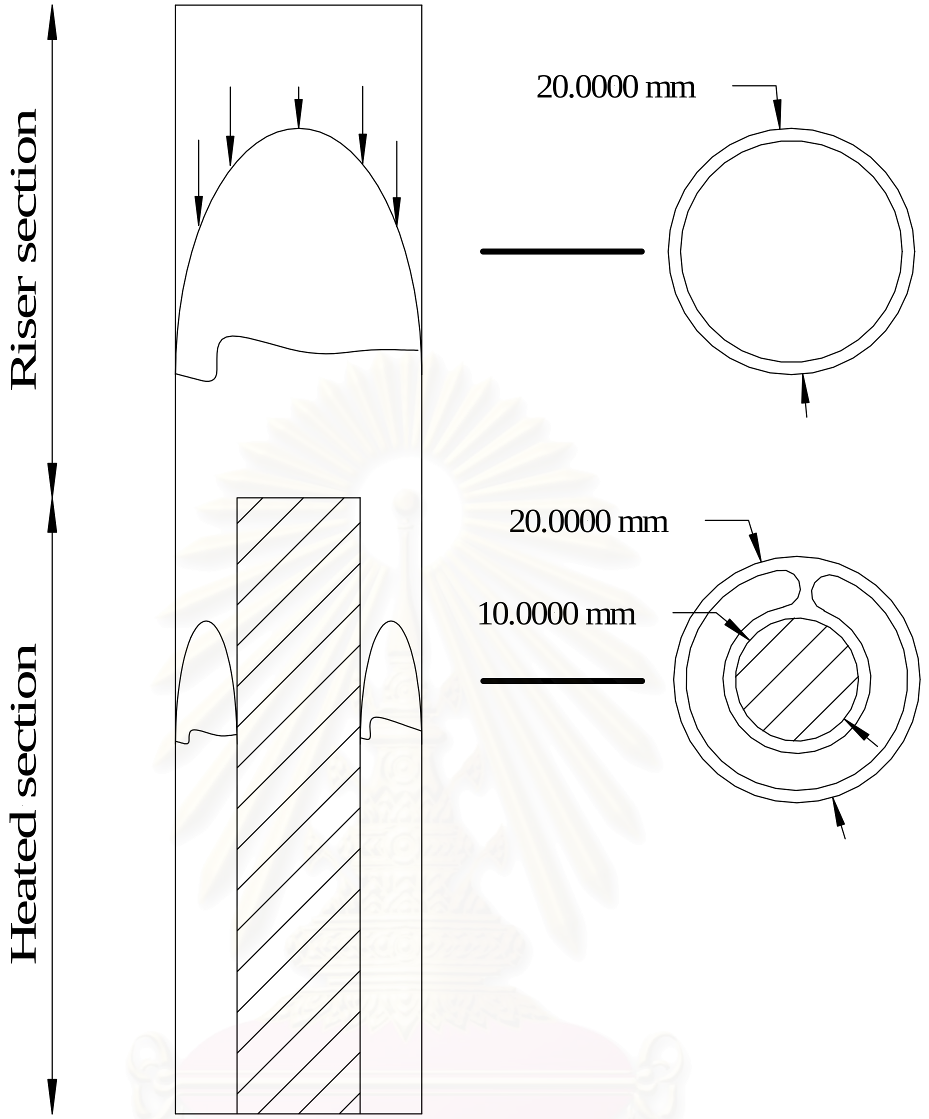

Fig. 5.37 Bubble shape in the test section and in the riser

5.7 Comparison of numerical and experimental results

The two-fluid model has been developed as described in Chapter 3. To compare the results from the two-fluid model with the experimental results, the test section between the inlet and the outlet plenums is simulated including the heater inside the test channel. The velocity of the channel, the pressure and the temperature at the inlet and the outlet plenums is calculated at the same position as in the experiment facility. Fig.5.38 shows the analytical model for the test section. The outside diameter of the channel is 20 millimeter and the inside diameter is 10 millimeter. The test section is divided in to 25 mesh size. Each mesh size is 100 millimeter. The non-heated section is 300 millimeter. The heated section is 1200 millimeter and the riser is 1000 millimeter. At the inlet it is assumed to be the inlet plenum. The inlet subcooling then can be controlled. At the exit it is assumed to be the outlet plenum and the pressure is fixed as required. The time step and the mesh size used in this model are 0.001 second and 100 millimeter, respectively. Because the oscillation easily occurs at low pressure, the analytical model at the pressure 0.1 MPaA and at subcooling 5, 10 and 15 K is analyzed and verified with the experimental results at the same conditions. Fig. 5.39-5.56 show the comparison of the numerical and experimental results.

In Fig. 5.39 to 5.44 the feature of the flow oscillation at pressure 0.1 MPaA and subcooling 5 K are shown. For the average total inlet velocity, the average channel velocity and the amplitude of the velocity, the two-fluid can give the good agreement with the experimental results. However the amplitude of the pressure drop and the dimensionless of the pressure drop and the head of the two-fluid model are slightly different from those of the experimental results. Fig. 5.44 shows the very good agreement of the delayed time of the two-fluid model and the experiment.

สถาบันวิทยบริการ
จุฬาลงกรณ์มหาวิทยาลัย

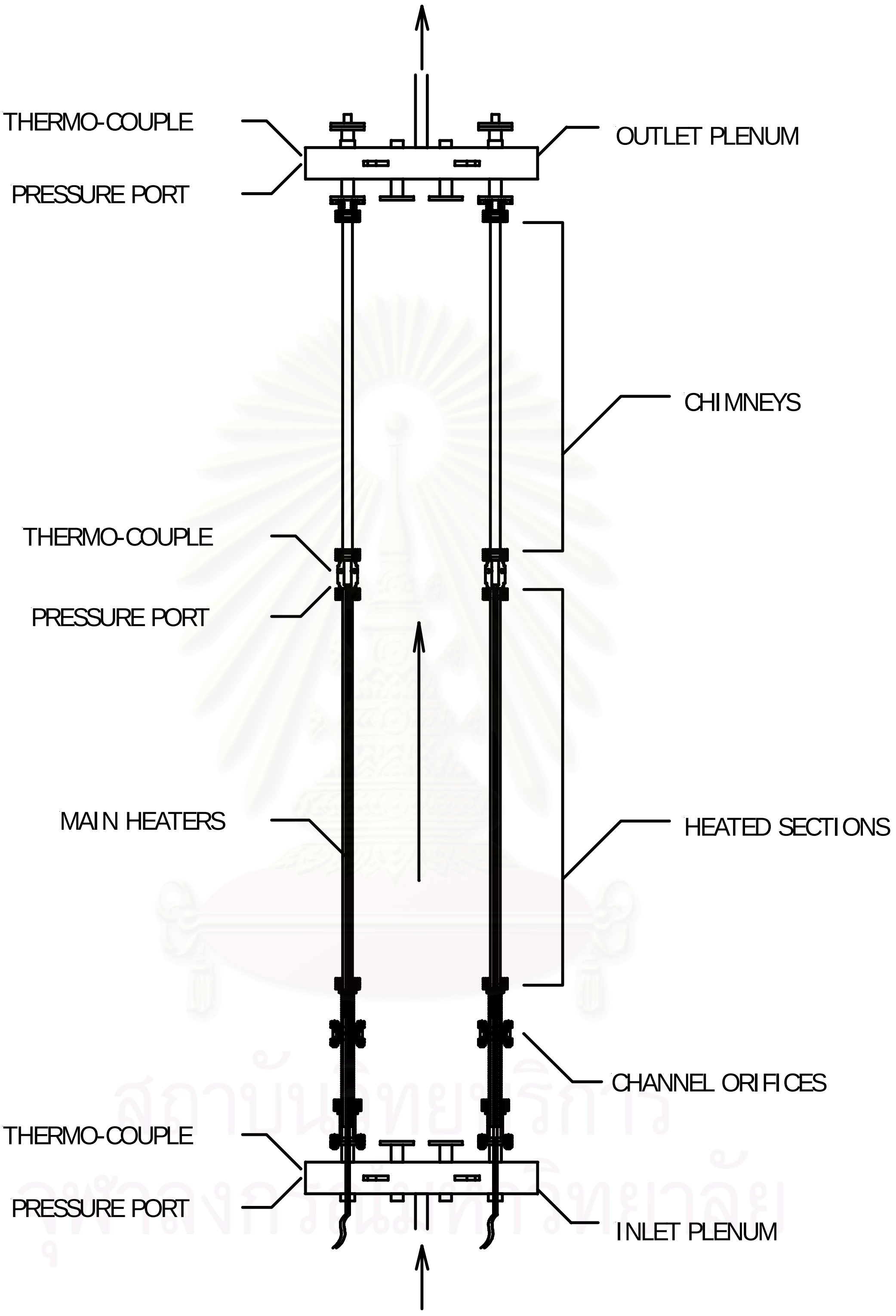

Fig.5.38 Analytical model of the test section

สถาบันวิทยบริการ
จุฬาลงกรณ์มหาวิทยาลัย

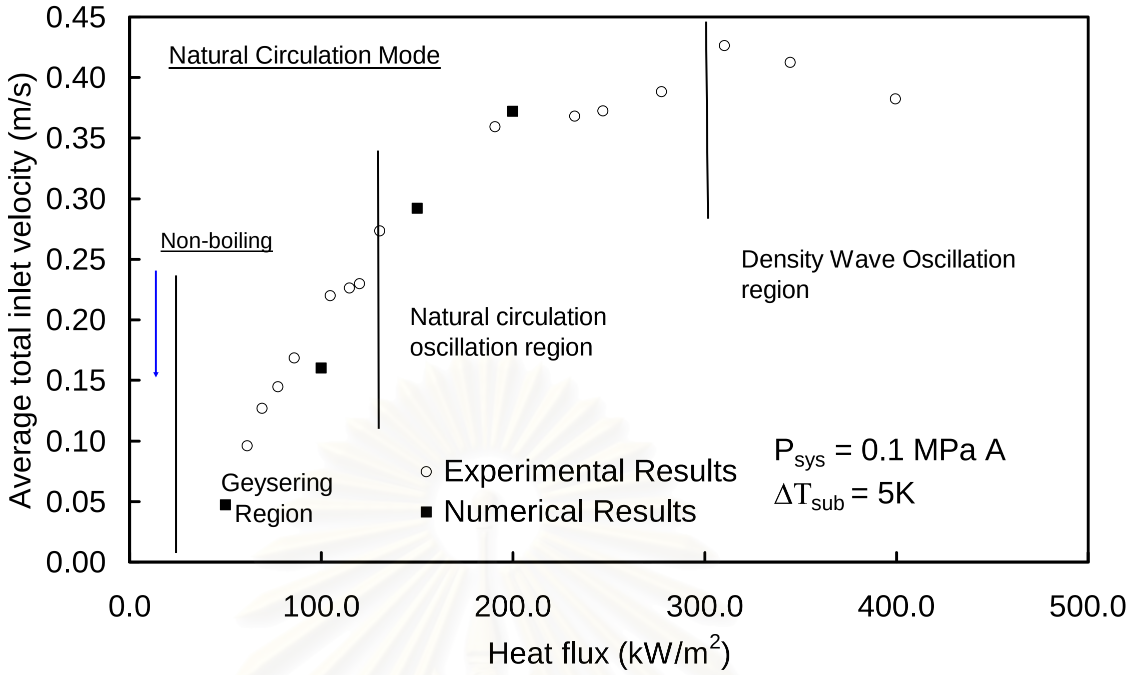

Fig.5.39 Comparison of numerical and experimental results of the average total inlet velocity and the heat flux at pressure 0.1 MPaA and subcooling 5 K

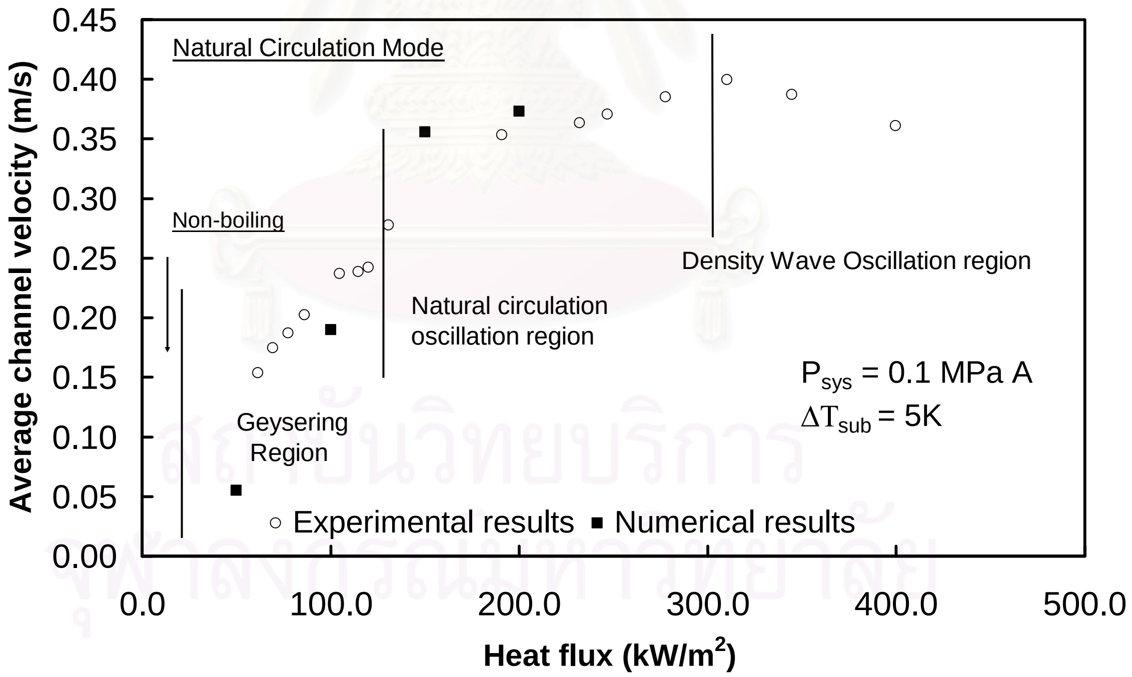

Fig.5.40 Comparison of numerical and experimental results of the average channel velocity and the heat flux at pressure 0.1 MPaA and subcooling 5 K

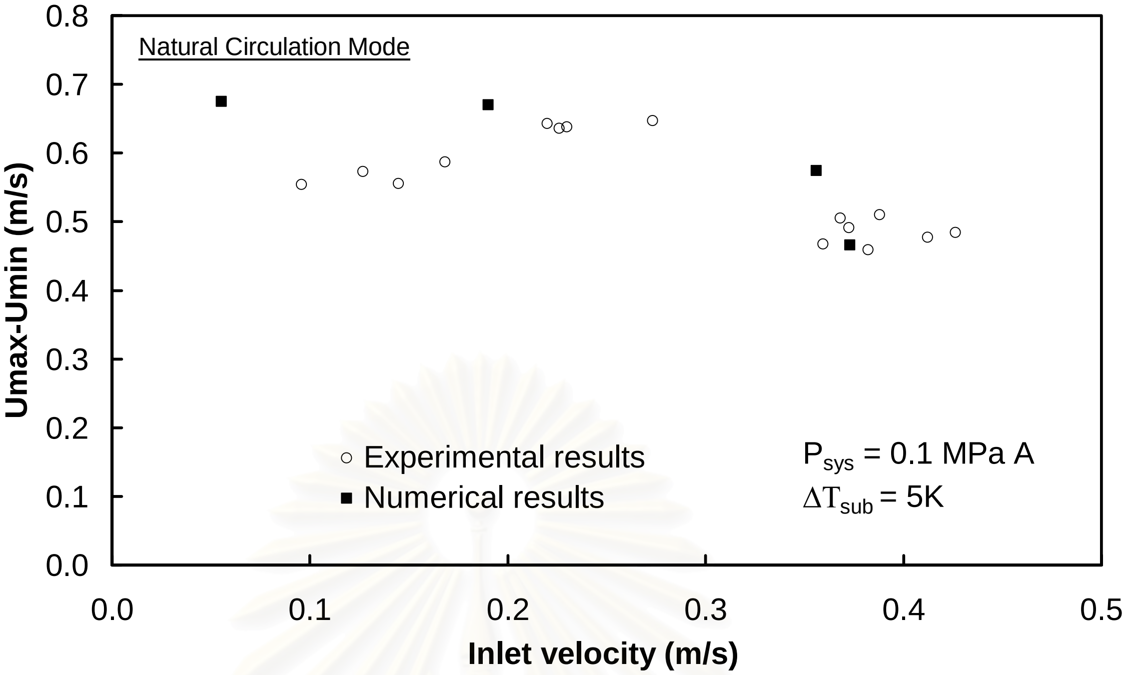

Fig.5.41 Comparison of numerical and experimental results of the amplitude of the velocity and the inlet velocity at pressure 0.1 MPaA and subcooling 5 K

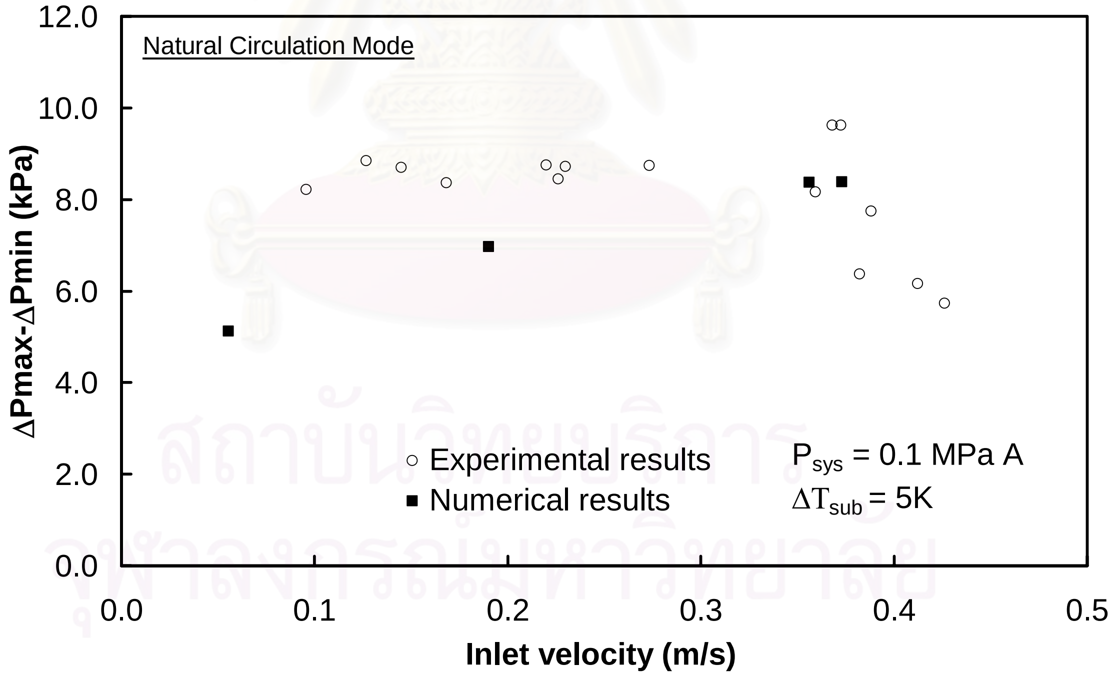

Fig.5.42 Comparison of numerical and experimental results of the amplitude of the pressure drop and the inlet velocity at pressure 0.1 MPaA and subcooling 5 K

สถาบันวิทยบริการ
จุฬาลงกรณ์มหาวิทยาลัย

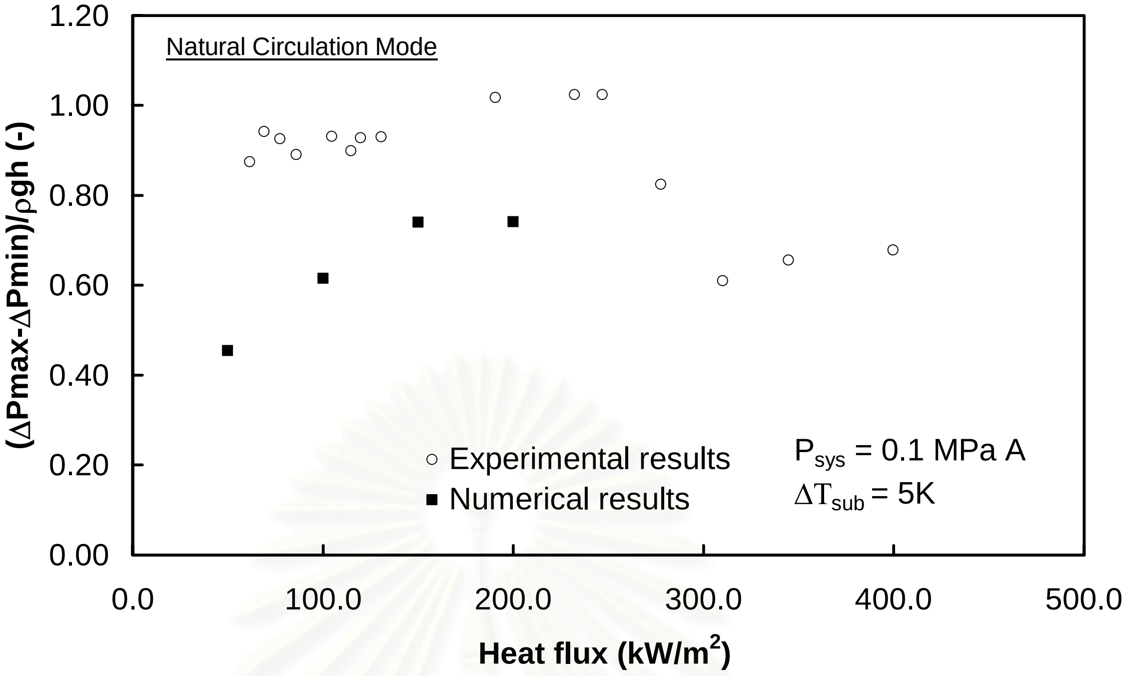

Fig.5.43 Comparison of numerical and experimental results of the amplitude of the dimensionless of the pressure drop and the head at pressure 0.1 MPaA and subcooling 5 K

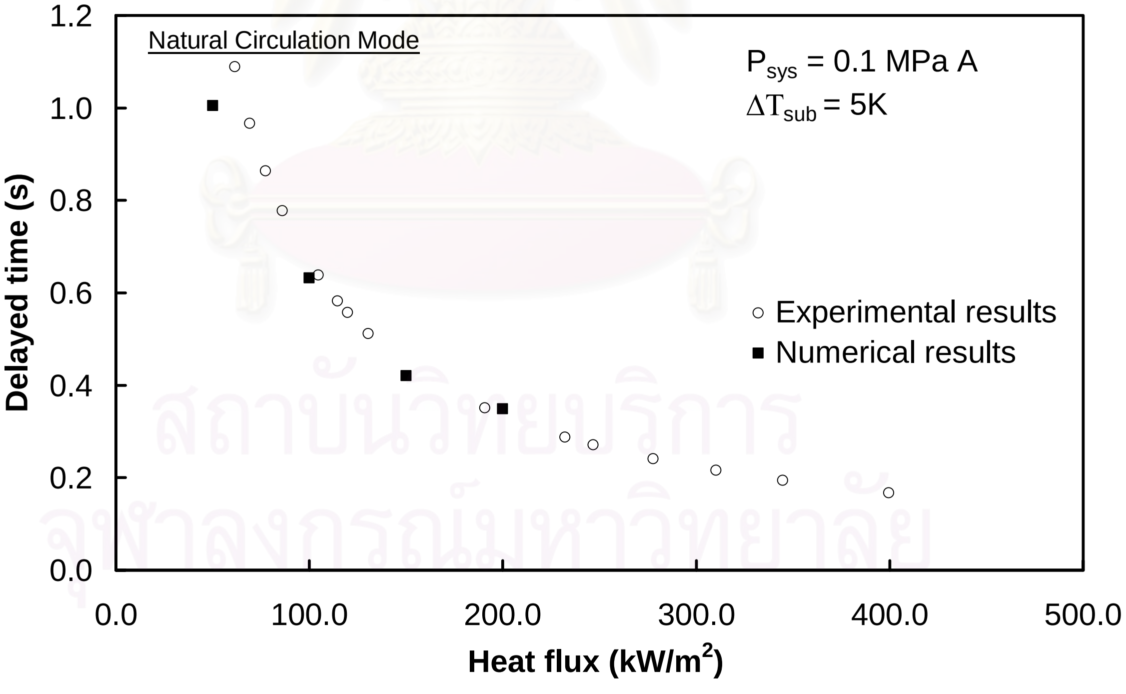

Fig.5.44 Comparison of numerical and experimental results of the delayed time and the heat flux at pressure 0.1 MPaA and subcooling 5 K

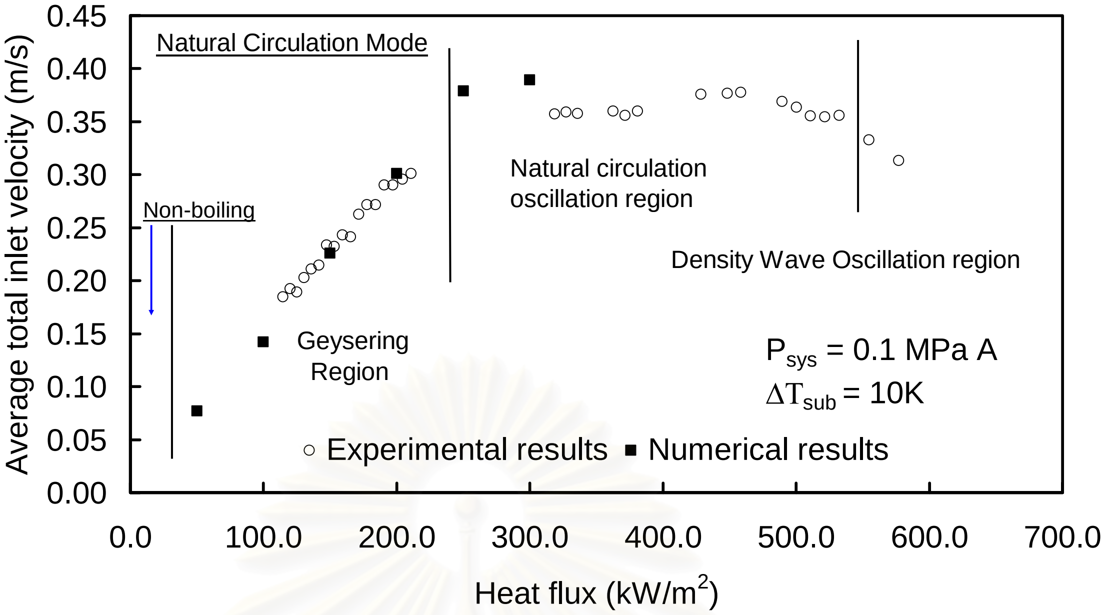

Fig.5.45 Comparison of numerical and experimental results of the average total inlet velocity and the heat flux at pressure 0.1 MPaA and subcooling 10 K

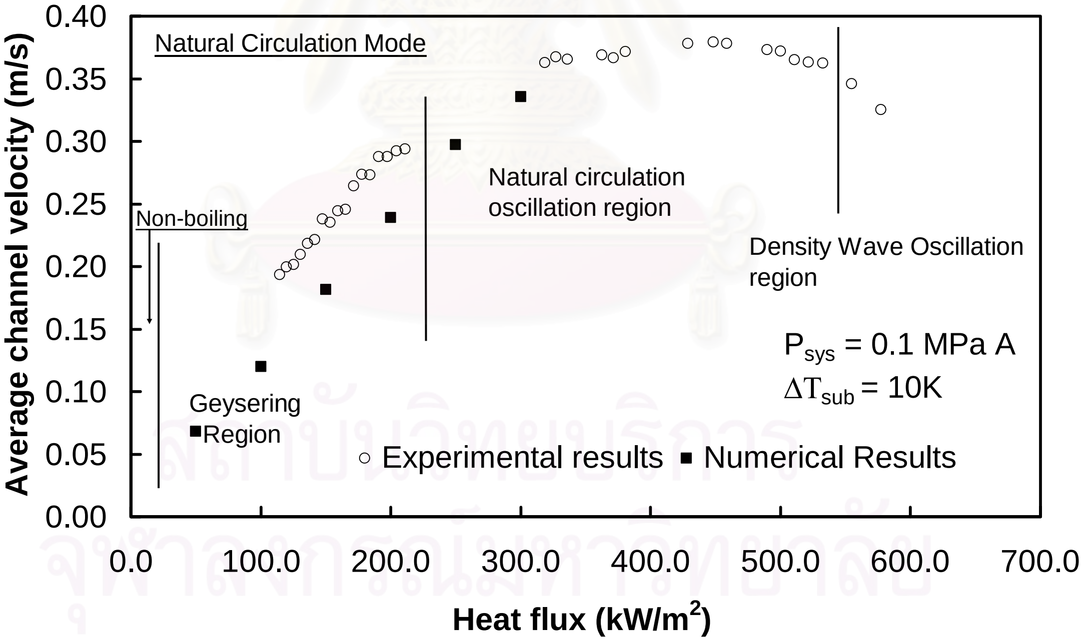

Fig.5.46 Comparison of numerical and experimental results of the average channel velocity and the heat flux at pressure 0.1 MPaA and subcooling 10 K

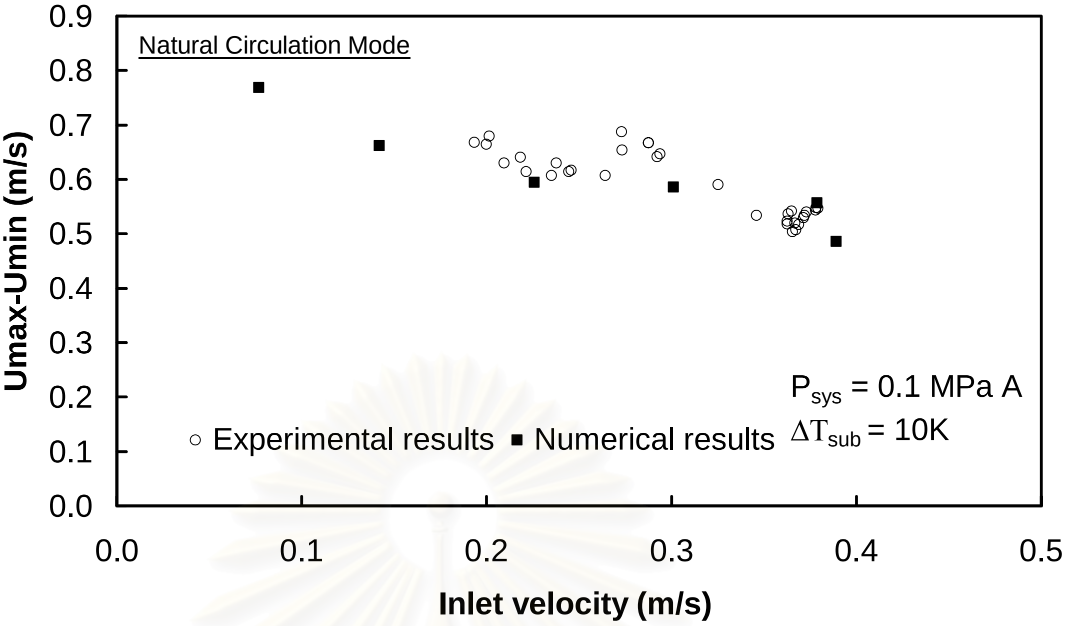

Fig.5.47 Comparison of numerical and experimental results of the amplitude of the velocity and the inlet velocity at pressure 0.1 MPaA and subcooling 10 K

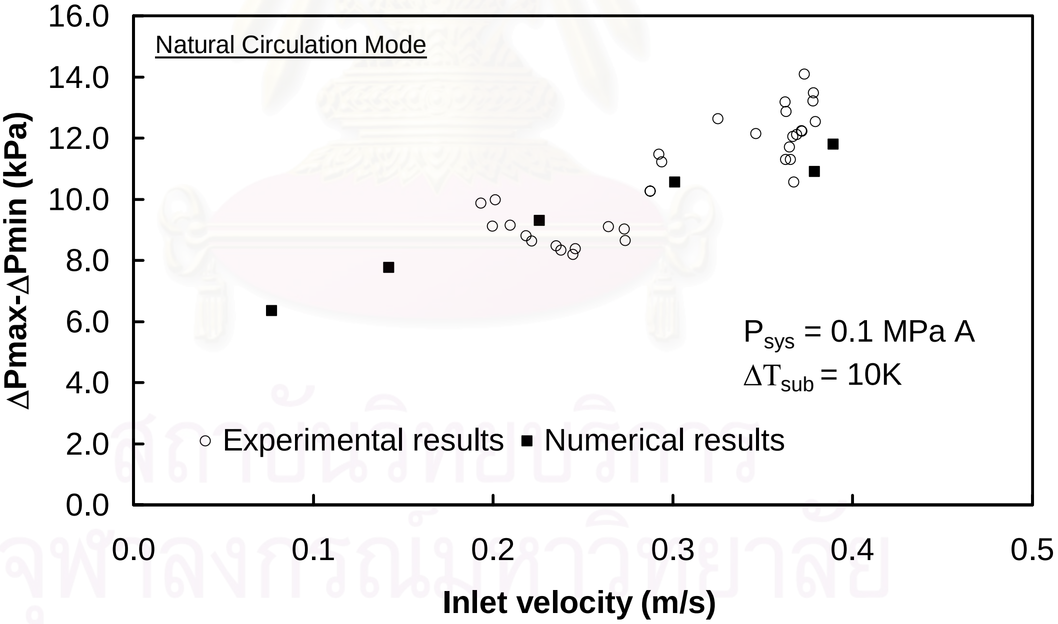

Fig.5.48 Comparison of numerical and experimental results of the amplitude of the pressure drop and the inlet velocity at pressure 0.1 MPaA and subcooling 10 K

สถาบันวิทยบริการ
จุฬาลงกรณ์มหาวิทยาลัย

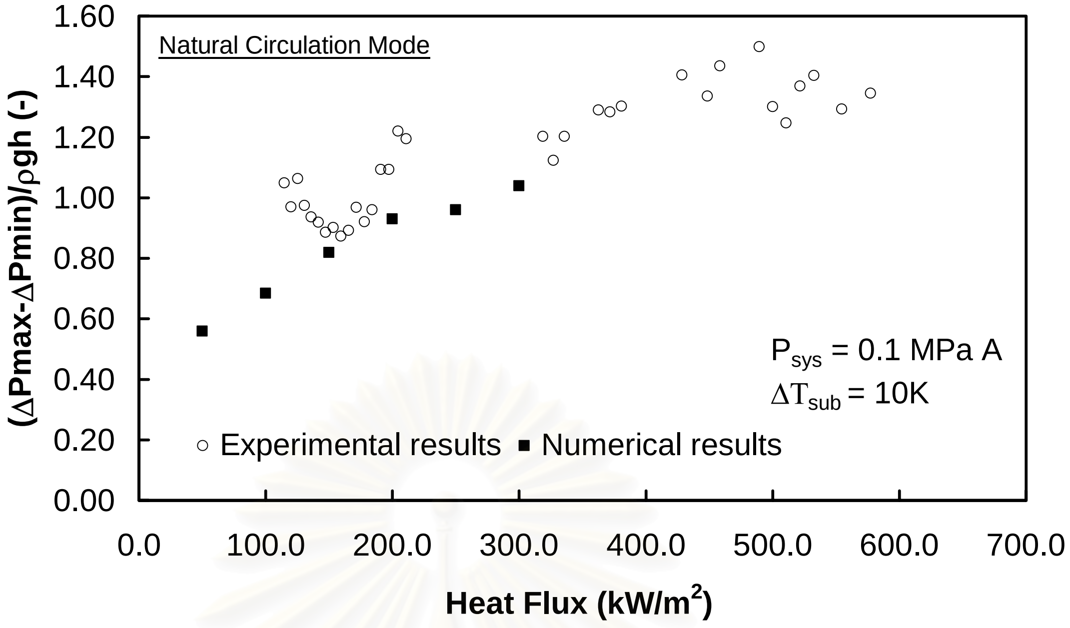

Fig.5.49 Comparison of numerical and experimental results of the amplitude of the dimensionless of the pressure drop and the head at pressure 0.1 MPaA and subcooling 10 K

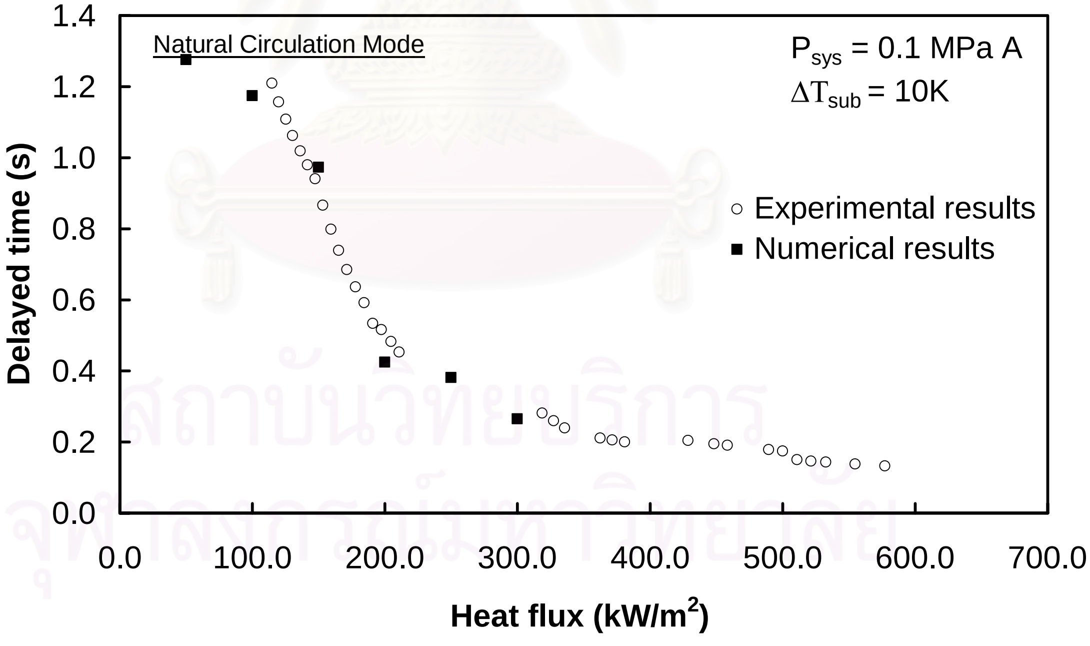

Fig.5.50 Comparison of numerical and experimental results of the delayed time and the heat flux at pressure 0.1 MPaA and subcooling 10 K

สถาบันวิทยบริการ
จุฬาลงกรณ์มหาวิทยาลัย

In Fig. 5.45 to 5.50 the feature of the flow oscillation at pressure 0.1 MPaA and subcooling 10 K are shown. For the average total inlet velocity, the amplitude of the velocity, the amplitude of the pressure drop and the delayed time, the two-fluid can give the good agreement with the experimental results. However, the average channel velocity and the dimensionless of the pressure drop and the head of the two-fluid model are slightly different from those of the experimental results. Fig. 5.50 shows the very good agreement of the delayed time of the two-fluid model and the experiment.

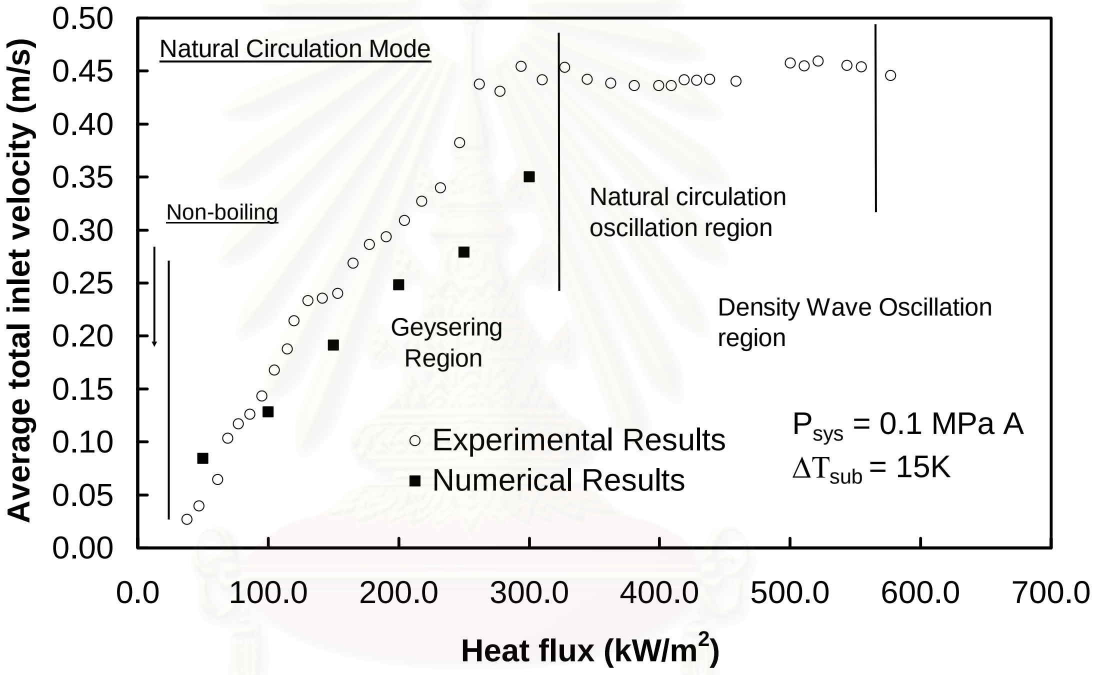

Fig.5.51 Comparison of numerical and experimental results of the average total inlet velocity and heat flux at pressure 0.1 MPaA and subcooling 15 K

สถาบันวิทยบริการ
จุฬาลงกรณ์มหาวิทยาลัย

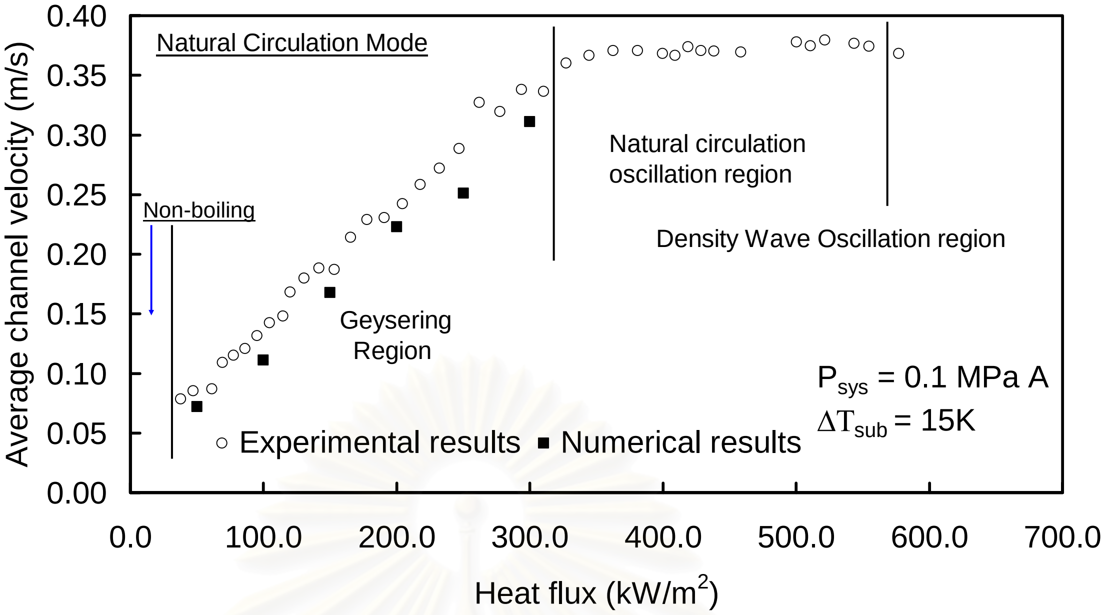

Fig.5.52 Comparison of numerical and experimental results of the average channel velocity and the heat flux at pressure 0.1 MPaA and subcooling 15 K

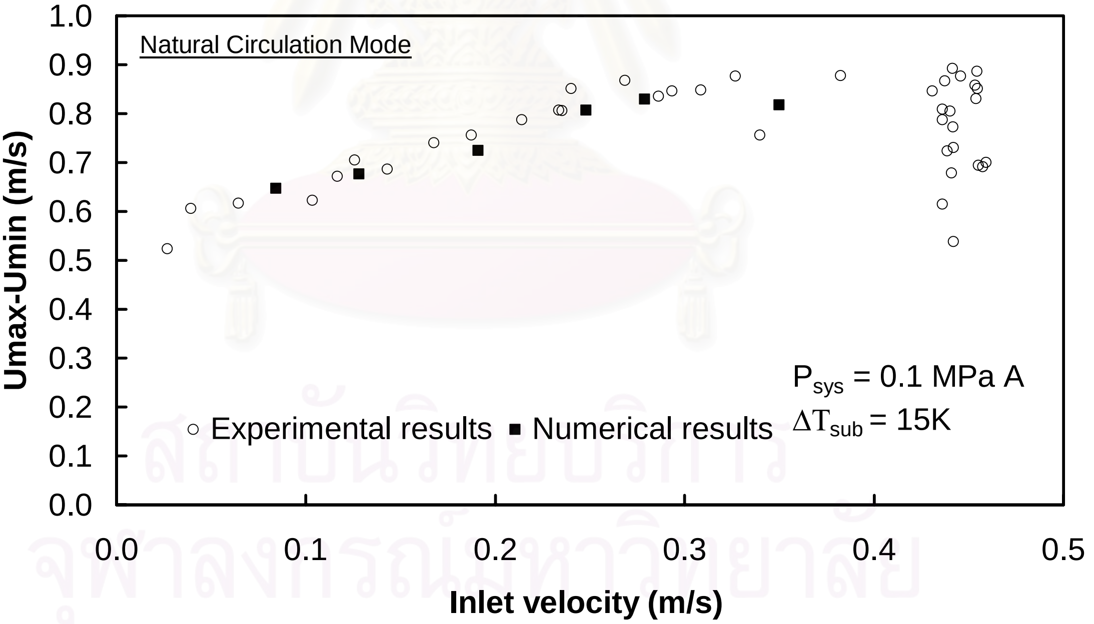

Fig.5.53 Comparison of numerical and experimental results of the amplitude of the velocity and inlet velocity at pressure 0.1 MPaA and subcooling 15 K

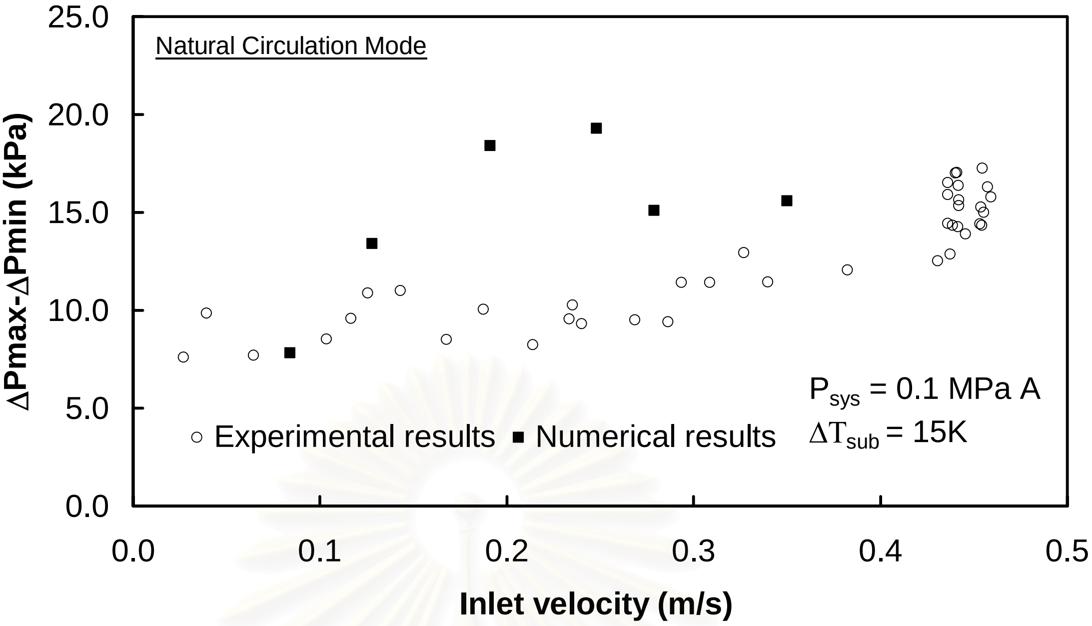

Fig.5.54 Comparison of numerical and experimental results of the amplitude of the pressure drop and inlet velocity at pressure 0.1 MPaA and subcooling 15 K

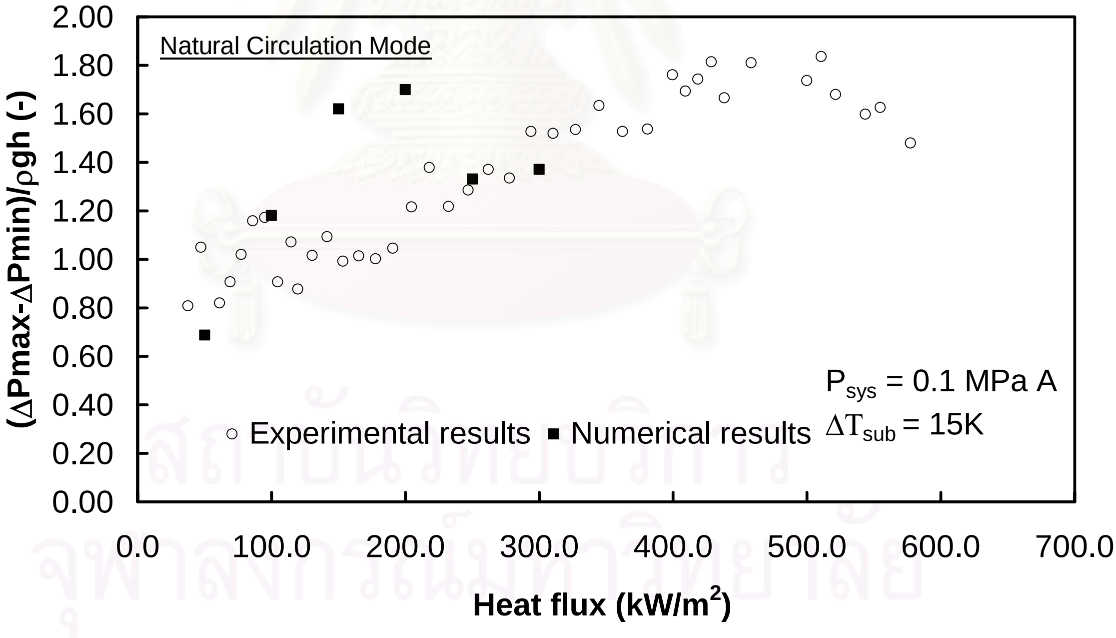

Fig.5.55 Comparison of numerical and experimental results of the amplitude of the dimensionless of the pressure drop and the head and heat flux at pressure 0.1 MPaA and subcooling 15 K

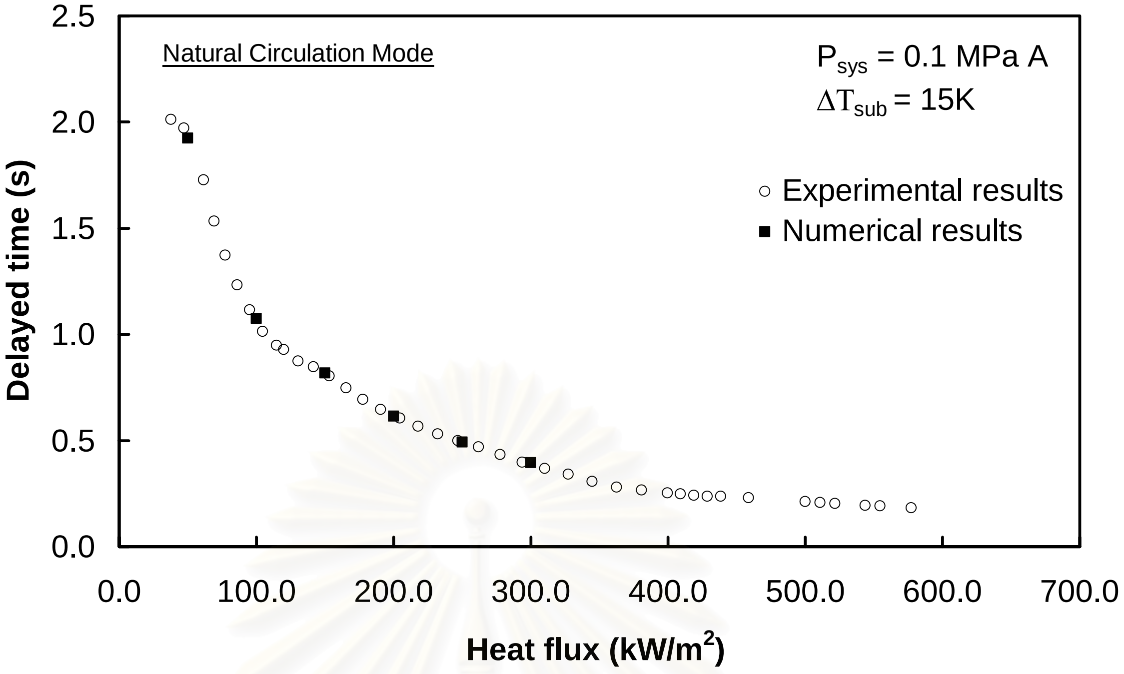

Fig.5.56 Comparison of numerical and experimental results of the delayed time and heat flux at pressure 0.1 MPaA and subcooling 15 K

In Fig. 5.51 to 5.56 the feature of the flow oscillation at pressure 0.1 MPaA and subcooling 15 K are shown. For the amplitude of the velocity the two-fluid model can give the good agreement with the experimental results. However, the average total inlet velocity and the average channel velocity of the two-fluid model are lower than those of the experimental results. The amplitude of the pressure drop and the dimensionless of the pressure drop are in good agreement with the experimental results except in the range of the inlet velocity between 0.1 and 0.2 m/s for the amplitude of the pressure drop and the heat flux of 150 and 250 kW/m^2 for the dimensionless of the pressure and the head. Fig. 5.56 shows the very good agreement of the delayed time of the two-fluid model and the experiment. In conclusion the two-fluid model can give the good results in comparison with the experimental results. However to be able to accomplish to run the two-fluid model it requires the good initial and boundary conditions. Moreover some coefficients in the heat transfer coefficients will be modified to receive more accurate results from the two-fluid model.

5.8 Effect of the channel diameter

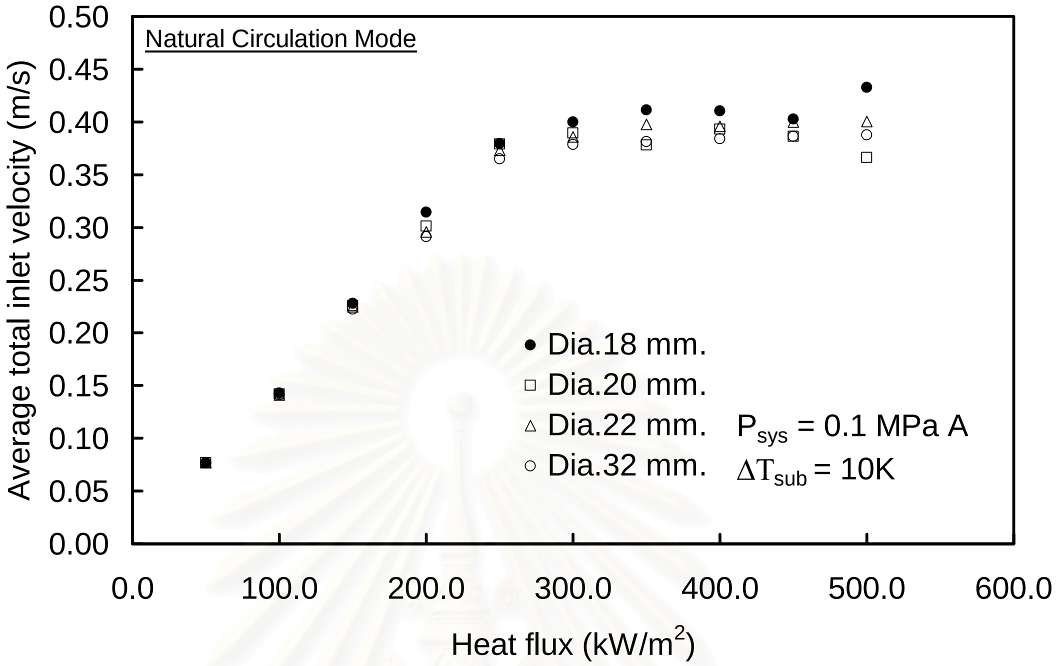

Fig.5.57 Effect of channel diameter on the average total inlet velocity and heat flux at pressure 0.1 MPaA and subcooling 10 K

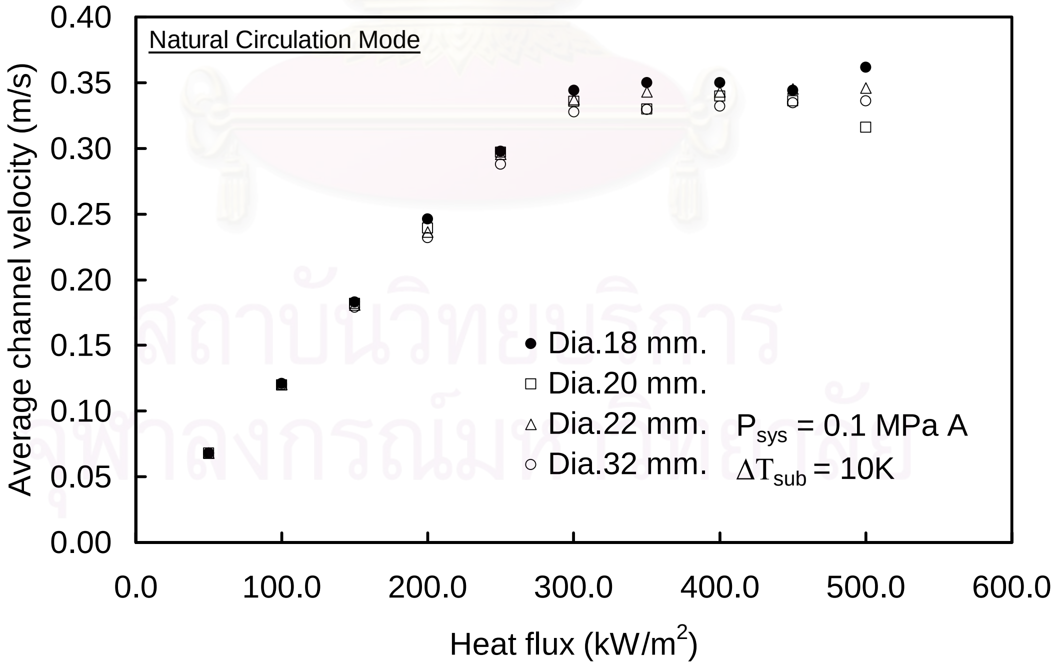

Fig.5.58 Effect of channel diameter on the average channel velocity and heat flux at pressure 0.1 MPaA and subcooling 10 K

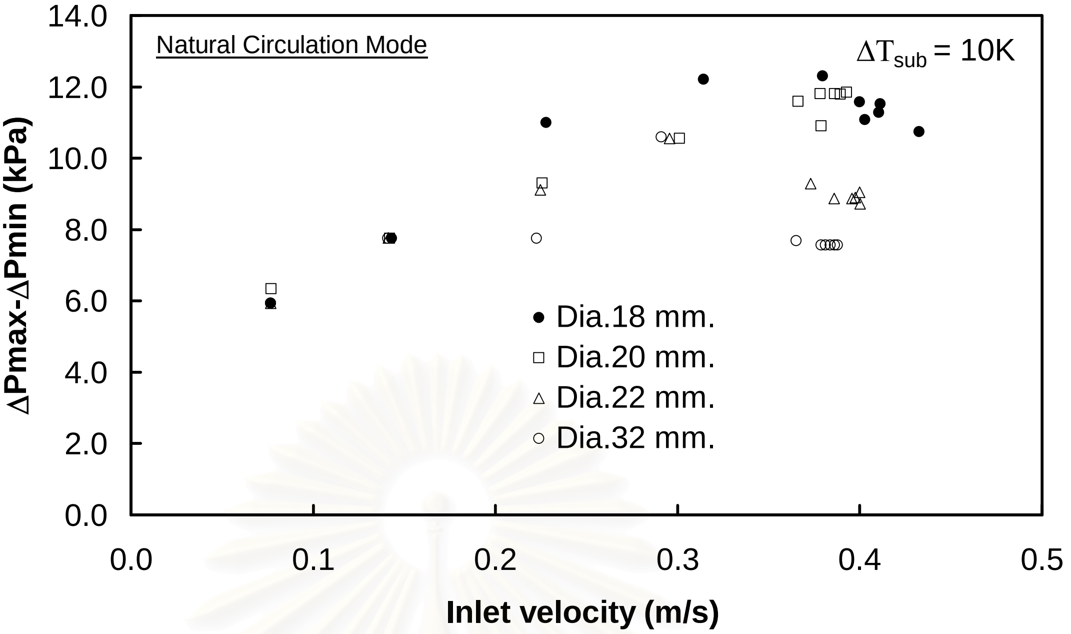

Fig.5.59 Effect of channel diameter on the amplitufe of the pressure drop and inlet velocity at pressure 0.1 MPaA and subcooling 10 K

Due to the difficulty to change the channel diameter in the experiment the two-fluid model is used to investigate the effect of channel velocity on the average total inlet velocity, the average channel velocity and the amplitude of the pressure drop at pressure 0.1 MPaA and subcooling 10 K. The two-fluid model was verified by the experimental results in the previous section. Consequenly, it is expected that the two-fluid model can be used to predict the effect of channel diameter on the feasture of the flow oscillation in some extents. The channel diameter of the test section was changed from 18, 20, 22, and 32 mm., respectively at the pressure 0.1 MPaA and subcooling 10 K. The diameter of the heater inside the test section is kept constant at 10 mm. for all sizes of the channel diameter. As shown in Fig. 5.57-5.58 it is clearly seen that the channel diameter doesn’t has much effect on the average total inlet velocity, the average channel velocity and the amplitude of the pressure drop at the heat flux less than 300 kW/m^2. However, at the heat flux greater than 300 kW/m^2 the average total inlet velocity and the average channel velocity become faster in the small diameter test section. The results from the numerical model indicates that at the inlet velocity greather than 0.22 m/s the amplitude of the pressure drop in the small diameter test section significantly greater than that in the large diameter test section as shown in Fig. 5.59. From Fig. 5.57-5.59 it can be interpreted that at the larger diameter test section and the inlet velocity greater than 0.22 m/s the flow characteristic may change from natural oscillation to density wave oscillation. The effect of channel diameter will be investigated experimentally in the future.

สถาบันวิทยบริการ
จุฬาลงกรณ์มหาวิทยาลัย

Chapter VI
Conclusion and Suggestion

6.1 Conclusion

1. The two-fluid model was developed to investigate the effect of the channel diameter, the system pressure, and the subcooled condition on the stability of the system in natural circulation. The semi-implicit scheme was employed to replace the derivatives of the differential equations into the algebraic equations. The Newton Block Gauss Seidel (NBGS) method was utilized to provide the numerical solutions
2. The instability of the two-phase flow natural circulation due to the effect of heat flux, pressure, and subcolling in the proposed channel configuration was investigated in a 1 meter long chimney above the test section. The heat flux was increased from 50 to 550 kW/m^2. The pressure was varied from 0.1, 0.2, 0.4, 0.5, and 0.7 MPaA and the subcooling was varied from 5, 10, and 15 K.
3. The numerical and experimeatal results showed that the increase in the system pressure and the subcooling at low heat flux decreased the average total inlet amplitude of the pressure drop, the dimensionless of the pressure drop and the head. Therefore the increase in the system pressure and the subcooling stabilize the system because of the reduction of void fraction, the increase in non-boiling length and the lower heat transfer coefficients. It is not clearly seen the effect of the system pressure and the subcooling on the period and the delayed time of the flow oscillation.
4. In this experiment at the heat flux higher than 300 kW/m^2 the average total inlet velocity, the average channel velocity increase with the increasing subcooling due to the high condensation at the high subcooling, which increases the flow reversal. Therefore the amplitude of the velocity, the amplitude of the pressure drop and the dimensionless of the pressure drop increase with the increasing subcooling at the outlet plenum.
5. The effect of the heat flux, the system pressure and the subcooled condition on the flow characteristics was investigated by the two-fluid model at pressure 0.1 MPaA and subcooling 5, 10, and 15 K. The numerical results were in good agreement

with the experimental results. However, the parametric test shall be performec in the future in order to apply this model for general cases.

6. The effect of the channel diameter was investigated by using the two-fluid model. The channel diameter was varied from 18, 20, 22, and 32 mm. The prediction of the effect of the channel diameter on the flow oscillation from the two-fluid model indicated that the change in the channel diameter affected the flow instability pattern at the heat flux higher than 300 kW/m2. As the frictional pressure drop was dominant at the high heat flux, the flow instability map changed from natural circulation to density wave oscillation.
7. The new discovery received from the experiment showed that the geysering occurred at the system pressure higher than 0.35 MPaA and at the velocity higher than 0.2 m/s due to the effect of channel geometry. The slug bubble has the high velocity in the test section due to the annular shape between the test section and the heater. Because of the circular shape of the riser when the slug bubble enters into the riser, the shape of the slug bubble changes and the velocity of the slug bubble decreases. At the point where the pressure head increases it is easier for the slug bubble to collapse before entering at the upper plenum. This makes the geysering occurred at the higher pressure.

6.2 Suggestion and Comment

Suggestion and comment are as follows:

1. There are some errors during the experiment due to the difficulty in controlling the subcooling condition. Therefore it is needed to develop the automatic control system for controlling the subcooling condition.
2. The capacity of the preheater at the upper tank should be increased to be able to control the accurate subcooling condition.
3. The effect of riser geometry shall be studied in the future.
4. The void fraction measurement system should be installed to investigate the effect of those parameters on void fraction.
5. The visualization system should be developed for the round tube to investigate the phenomenon during the transient condition.

6. The two-fluid model should be modified to be able to predict the phenomenon for general cases.
7. To use the two-fluid for general cases the parametric test shall be performed in the future

สถาบันวิทยบริการ
จุฬาลงกรณ์มหาวิทยาลัย

References

Achard, J.-L, Drew, D.A., and Lahey, R.T., Jr. The analysis of nonlinear density-wave oscillations in boiling channels. J. Fluid Mech. Vol.155 (1985): 213-232.

Araseki, H., and Ishiguro, G. Thermal Hydraulic Analysis by Skew Upwind Finite Element Method. J. Nucl. Sci. Technol. Vol.24 No.5 (1987): 343-354.

Araseki, H., Suemura, T., and Ishiguro, Application of Galerkin Finite Element Method to Subchannel Analysis, (II) Unsteady-State Two-Phase Flow. J. Nucl. Sci. Technol. Vol.22 No.5 (1985): 371-378.

Aritomi, M., Aoki, S., and Inoue, A. Instabilities in Parallel Channel of Forced Convection Boiling Upflow System, (I) Mathematical Models. J. Nucl. Sci. Technol. Vol.14 No.2 (1977a): 22-30.

Aritomi, M., Aoki, S., and Inoue, A. Instabilities in Parallel Channel of Forced Convection Boiling Upflow System, (II) Experimental Results. J. Nucl. Sci. Technol.. Vol.14 No.2 (1977b): 88-96.

Aritomi, M., Aoki, S., and Inoue, A. Instabilities in Parallel Channel of Forced Convection Boiling Upflow System, (III) System with Different Flow Conditions between Two Channels. J. Nucl. Sci. Technol. Vol.16 No.5 (1979): 343-355.

Aritomi, M., Aoki, S., and Inoue, A. Thermo-hydraulic Instabilities in Parallel Channel System Part 1. A non-linear and a linear analytical model. J. Nucl. Eng. Des. Vol.95 (1986a): 105-116.

Aritomi, M., Aoki, S., and Inoue, A. Thermo-hydraulic Instabilities in Parallel Channel System Part 2. Experimental results. J. Nucl. Eng. Des. Vol.95 (1986b): 117-127.

Aritomi, M., Chiang, C.H., Nakahashi, T., Wataru, M., and Mori, M. Fundamental Study on Thermo-Hydraulics during Start-up in Natural Circulation Boiling Water Reactors, (I) Thermo-Hydraulic Instabilities. J. Nucl. Sci. Technol. Vol.29 No.7 (1992): 631-641.

Aritomi, M., Chiang, C.H., and Mori, M. Geysering in parallel boiling channels. J. Nucl. Eng. Des. Vol.141 (1993): 111-121.

Belblidia, L.A., Weaver, L.E., and Carlson, R.W. Nodal analysis of density-wave oscillations in boiling water nuclear reactor. Ann. Nucl. Energy Vol.10 No.10 (1983): 505-534.

Bergdahl, B.G., Reisch, F., Oguma, R., Lorenzen, J., and Akerhielm, F. BWR stability investigation at Forsmark I. Ann. Nucl. Energy Vol.16 No.10 (1989): 509-520.

Boure, J.A., Bergles, A.E., and Tong, L.S. Review of Two-Phase Flow Instability. J. Nucl. Eng. Des. Vol.25 (1973): 165-192.

Chatoorgoon, V. SPORTS- A Simple Non-linear Thermalhydraulic Stability Code. J. Nucl. Eng. Des. Vol.93 (1986): 51-67.

Cheng, H., Hillis, J.H., and Azzorpardi, B.J. A study of the bubble-to-slug transition in vertical gas-liquid flow in columns of different diameter. Int. J. Multiphase Flow Vol.24 No.3 (1998): 431-452.

Chiang, J.H. Thermo-Hydraulics during Start-up in Natural Circulation Boiling Water Reactor. Ph.D. Dissertation, Research Laboratory for Nuclear Reactors, Tokyo Institute of Technology, 1994.

Clausse, A., Lahey, R.T., Jr., and Podowski, M. An analysis of stability and oscillation modes in boiling multichannel loops using parameter perturbation methods. Int. J. Heat Mass Transfer Vol.32 No.11 (1989): 2055-2064.

Corradini, M.L.General Introduction and Concepts. Multiphase Flow and Heat Transfer for Industrial Application, Switzerland, May 17-19, 1993.

Drew, D., Chen, L., Lahey, R.T., Jr., and Becker, M. The analysis of virtual mass effects in two-phase flow. Int. J. Multiphase Flow Vol.5 (1979): 233-242.

Duncan, J.D. SBWR, A Simplified Boiling Water Reactor. J. Nucl. Eng. Des. Vol.109 (1988): 73-77.

Fukada, K., and Kobori, T. Classification of two-phase flow stability by density-wave oscillation model. J. Nucl. Sci. Technol. Vol.16 (1979): 95-108.

Fukada, K., and Hasegawa, S. Analysis on Two-Phase Flow Instability in Parallel Mutichannels. J. Nucl. Sci. Technol. Vol.16 No.3 (1979): 190-199.

Furutera, M. Validity of homogeneous flow model for instability analysis. J. Nucl. Eng. Des. Vol.95 (1986): 65-77.

Guenther, C., and Syamlal, M. The effect of numerical diffusion on simulation of isolated bubbles in a gas-solid fluidized bed. Power Technology Vol.116 (2001): 142-154.

Guido, G., Converti, J., and Clausse, A. Density-wave oscillations in parallel channels-an analytical approach. J. Nucl. Eng. Des. Vol.125 (1991): 121-136.

Gurgenci, H., Veziroglu, T.N., and Kakac, S. Simplified nonlinear descriptions of two-phase flow instabilities in vertical boiling channel. Int. J. Heat Mass Transfer Vol.26 No.5 (1983): 671-679.

Hashimoto, K. Linear modal analysis of out-of-phase instability in boiling water reactor cores. Ann. Nucl. Energy Vol.20 No.12 (1993): 789-797.

Hetsroni, G. Handbook of Multiphase Systems. McGraw-Hill Book. New York: Hemisphere publishing, 1982.

Hsu, Y.Y., and Graham, R.W. Transport Processes in Boiling and Two-Phase Systems. American Nuclear Society, 1986.

Hibiki, T., and Ishii, M. Effect of inlet geometry on hot-leg U-bend two-phase natural circulation in a loop with a large diameter pipe. J. Nucl. Eng. Des. Vol.203 (2001): 209-228.

Hirt, C.W. Heuristic Stability Theory for Finite-Difference Equations. J. Comp. Phys. Vol. 2 (1968): 339-355.

Huh, K.Y., Golay, M.W., and Manno, V.P. A Method for Reduction of Numerical Diffusion in the Donor Cell Treatment of Convection. J. Comp. Phys. Vol. 63 No. 1 (1986): 201-221.

Ishii, M., and Mishima, K. Two-fluid model and hydrodynamic constitutive relations. J. Nucl. Eng. Des. Vol.82 (1984): 107-126.

Jiang, S.Y., Yao, M.S., Bo, J.H., and Wu, S.R. Experimental simulation study on start-up of the 5 MW nuclear heating reactor. J. Nucl. Eng. Des. Vol.158 (1995): 111-123.

Jiang, S.Y., Wu, X.X., and Zhang, Y.J. Experimental Study of Two-Phase Oscillation in Natural Circulation. J. Nucl. Sci. Eng. Vol.135 (2000): 177-189.

Kazami, M.S., and No, H.C. On the formulation of the virtual mass term in Two-fluid models. J. Nucl. Eng. Des. Vol.95 (1986): 163-170.

Kataoka, Y., Suzuki, H. Murase, M., Sumida, I., Horiuchi, T., and Miki, M. Conceptual design and thermal-hydraulic characteristics of natural circulation boiling water reactors. J. Nucl. Technol. Vol.82 (1988): 1473-156.

Kim, J.H., Kim, T.W., Lee, S.M., and Park, G.C. Study on the natural circulation characteristics of the integral type reactor for vertical and inclined conditions. J. Nucl. Eng. Des. Vol.207 (2001): 21-31.

Kim, J.H., and Lee, S.Y. Experimental Observation of flow instability in a semi-closed two-phase natural circulation loop. J. Nucl. Eng. Des. Vol.196 (2000): 359-367.

Kleiss, E.B.G., and Van Dam, H. A simplified model for the dynamics of a BWR. Ann. Nucl. Energy Vol.12 No.5 (1985): 233-245.

Kocamusatafaogullari, G. Flow Patterns Predictions. Multiphase Flow and Heat Transfer for Industrial Application, Switzerland, May 17-19, 1993.

Lahey, R.T., Jr. Advances in the analytical modeling of linear and nonlinear densitywave instability modes. J. Nucl. Eng. Des. Vol.95 (1986): 5-34.

Lahey, R.T., Jr., and Drew, D.A. The Analysis of Two-Phase Flow and Heat Transfer Using a Multidimensional, Four Field, Two-Fluid Model. Proceedings of NUTETH-9, USA, October 3-8, 1999.

Lahey, R.T., Jr., and Moody, F.J. The thermal-hydraulic of a boiling water nuclear reactor. 2nd ed. American Nuclear Society, 1993.

Lahey, R.T., Jr., and Podowski, M. An analysis of stability and oscillation modes in boiling multichannel loops using parameter perturbation methods. Int. J. Heat Mass Transfer Vol.32 No.11 (1989): 2055-2064.

Lee, S.C., and Bankoff, S.G. Prediction of the onset of flow instability in transient subcooled flow boiling. J. Nucl. Eng. Des. Vol.139 (1993): 149-159.

Lee, S.Y., and Lee, D.W. Linear analysis of flow instabilities in an open two-phase natural circulation loop. J. Nucl. Eng. Des. Vol.128 (1991): 317-330.

Lee, S.Y., and Ishii, M. Characteristics of two-phase natural circulation in Freeon-113 boiling loop. J. Nucl. Eng. Des. Vol.121 (1990): 69-81.

Lies, D.R., and Reed, Wm.H.A Semi-Implicit Method for Two-Phase Fluid Dynamics. J. Comp. Phys. Vol. 26 (1978): 390-407.

Lin, Y.N., and Pan, C. Non-linear analysis for a natural circulation boiling channel. J. Nucl. Eng. Des. Vol.152 (1994): 349-360.

Lyczkowski, R.W., Gidaspow, D., and Solbrig, C.W. Characteristics and Stability Analysis of Transient One-Dimensional Two-Phase Flow Equations and Their Finite Difference Approximations. J. Nucl. Sci. Eng. Vol.66 (1978): 378-396.

Macian-Juan, R., and Mahaffy, J.H. Numerical diffusion and the tracking of solute fields in system code Part I. One-dimensional flows. J. Nucl. Eng. Des. Vol.179 (1998): 297-319.

Mahaffy, J.H. A Stability-Enhancing Two-Step Method for Fluid Flow Calculations. J. Comp. Phys. Vol. 46 (1982): 329-341.

Mahaffy, J.H. Numerics of codes: stability, diffusion, and convergence. J. Nucl. Eng. Des. Vol.145 (1993): 131-145.

March-Leuba, J., and Blakeman, E.D.A Mechanism for Out-of-phase Power Instabilities in Boiling Water Reactors. J. Nucl. Sci. Eng. Vol.107 (1991): 173-179.

Minato, A., and Kawabe, R. Numerical Analysis Method for Two-Dimensional Two-Fluid Model Using Control Volume Formulation. J. Nucl. Sci. Technol. Vol.25 No. 12 (1988): 901-913.

Minato, A., Takamori, K., and Ishida, N. An Extended Two-Fluid Model for Interface Behavior in Gas-Liquid Two-Phase Flow. Proceedings of ICONE8, USA, April 2-6, 2000.

Muncharoen, C., Aritomi, M., Sumitra, T., and Takemoto, T. The Effect of Numerical Diffusion on Oscillatory Flow in Two-Phase Boiling Channel. Proceedings of ICONE10, USA, April 14-18, 2002a.

Muncharoen, C., Aritomi, M., Sumitra, T., and Takemoto, T. The Effect of Numerical Diffusion on Oscillatory Flow in Two-Phase Boiling Channel. ANS/ASME Student Program, USA, April 12-14, 2002b.

Muncharoen, C., Aritomi, M., Sumitra, T., and Takemoto, T. The Effect of Flow Loop Conditions on Stabilities of Two-Phase Natural Circulation Caused By Boiling-Experimental and Numerical Results. J. Nucl. Sci. Technol. (Submitted, 2002c)

Muncharoen, C., Nilsuwankosit, S., and Sumitra, T. The Effect of Flow Loop Conditions on Stabilities of Two-Phase Natural Circulation Caused by Boiling-(I) Modeling development. Proceeding of the 8th Conference on Nuclear Science and Technology, Bangkok, June 21-22, 2001.

Muncharoen, C., Sumitra, T., and Takemoto, T. Comparison of Two-Fluid and Drift-Flux Models of Two-Phase Flow in a Natural Circulation Boiling Channel. Internatinal Conference on Computational Mathematics and Modeling, Bangkok, May 22-24, 2002d.

Nigamatulin, B.I., Melikhov, O.I., Blinkov, V.N., and Gakal, P.G. The numerical analysis of boiling flow instabilities in parallel heated channels. J. Nucl. Eng. Des. Vol.139 (1993): 235-243

Ohnuki, A., and Akimoto, H. Experimental study on transition of flow pattern and phase distribution in upward air-water two-phase flow along a large vertical pipe. Int. J. Multiphase Flow Vol.26 (2000): 367-386.

Okawa, T., and Kataoka, I. Characteristics and Stability of a Two-Fluid Model for Bubbly Two-Phase Flow. Proceedings of ICONE8, USA, April2-6, 2000.

Park, G.C., Podowski, M.Z., Becker, M., Lahey, R.T., Jr., and Peng, S.J. The development of a closed-form analytical model for the stability analysis of nuclear-coupled density-wave oscillations in boiling water nuclear reactors. J. Nucl. Eng. Des. Vol.92 (1986): 253-281.

Peng, S.J., Podowski, M.Z., Lahey, R.T., Jr., and Becker, M. NUFREQ-NP: A Computer Code for the Stability Analysis of Boiling Water Nuclear Reactors. J. Nucl. Sci. Eng. Vol.88 (1984): 404-411.

Ramshaw, J.D., and Trapp, J.A. Characteristics, Stability, and Short-Wavelength Phenomena in Two-Phase Flow Equation Systems. J. Nucl. Sci. Eng. Vol.66 (1978): 93-102.

Ransom, V.H., and Hicks, D.L. Hyperbolic Two-Pressure Models on Two-Phase Flow. J. Comp. Phys. Vol. 53 (1984): 124-151.

Ransom, V.H., et al. RELAP5/MOD3.2 Code Manual, Volume 1:Code Structure, System Models, and Solution Methods. NUREG/CR5535-V1, 1995.

Rizwan-Uddin, and Dornign, J.J. Some nonlinear dynamics of a heated channel. J. Nucl. Eng. Des. Vol.93 (1986): 1-14.

Saha, P., and Zuber, N. An analytical study of the thermally induced two-phase flow instabilities including the effect of thermal non-equilibrium. Int. J. Heat Mass Transfer Vol.21 (1978): 415-426.

Shieh, A.S.-L., Krishnamurthy, R., and Ransom, V.H. Stability, Accuracy, and Convergence of the Numerical Methods in RELAP5/MOD3 J. Nucl. Sci. Eng. Vol.116 (1994): 227-244.

Shoukri, M., Stankovic, B., Hassan, I., and Dimmick, J. Effect of Pipe Diameter on Flow Pattern Transitions and Void Fraction of Air-water Flow in Vertical Pipes. Proceedings of ICONE8, USA, April2-6, 2000.

Song, J.H., and Hong, S.W. A Characteristic Analysis for the One-Dimensional Two-Fluid Model”, Proceedings of ICONE8, USA, April2-6, 2000.

Song, J.H., and Ishii, M. The one-dimensional two-fluid model with momentum flux parameters. J. Nucl. Eng. Des. Vol.205 (2001): 145-158.

สถาบันวิทยบริการ
จุฬาลงกรณ์มหาวิทยาลัย

Stewart, H.B. Calculation of Transient Boiling Flow in Channels. J. Comp. Phys. Vol. 30 (1979): 61-75.

Stewart, H.B. Stability of Two-Phase Flow Calculation Using Two-fluid Models. J. Comp. Phys. Vol. 33 (1979): 259-270.

Stewart, H.B. Fractional Step Methods for Thermohydraulic Calculation. J. Comp. Phys. Vol. 40 No. 1 (1981): 77-90.

Stewart, H.B., and Wendroff, B. Two-Phase Flow: Models and Methods. J. Comp. Phys. Vol. 56 (1984): 363-409.

Subki, M.H., Aritomi, M., Watanabe, N., and Muncharoen, C. Experimental Study on Thermal-Hydraulics During Start-Up in The Natural Boiling Water Reactor Concept. Proceedings of ICONE10, USA, April14-18, 2002.

Sumida, I., and Kawai, T. Theory of hydraulic stability of boiling channels. J. Nucl. Sci. Technol. Vol.15 No. 5 (1978): 323-337.

Takitani, K., and Takemura, T. Density Wave Instability in Once-Through Boiling Water Flow System, (I) Experiment. J. Nucl. Sci. Technol. Vol.15 No.5 (1978): 355-364.

Tonimoto, K., Ishii, M., and S.Y. Lee Examination of transient characteristics of two-phase natural circulation with a Freon-113 boiling /condensing loop. J. Nucl. Eng. Des. Vol.183 (1998): 77-95.

Trapp, J.A., A Nearly-Implicit Hydrodynamic Numerical Scheme for Two-Phase Flows. J. Comp. Phys. Vol. 66 No. 1 (1986): 66-82.

Uehiro, M., Rao, Y.F., and Fukuda, K. Linear Stability Analysis on Instabilities of In-phase and Out-of-phase in Boiling Water Reactors. J. Nucl. Sci. Technol. Vol.33 No.8 (1996): 628-635.

Van Bragt, D.D.B., and Van Der Hagen, T.H.J.J. Stability of natural circulation boiling water reactors: part I-description stability model and theoretical analysis in terms of dimensionless groups. J. Nucl. Technol. Vol.121 (1998): 40-51.

Van Der Hagen, T.H.J.J., Stekelenburg, A.J.C., and Van Bragt, D.D.B. Reactor experiments on type-I and type-II BWR stability. J. Nucl. Eng. Des. Vol.200 (2000): 177-185.

Van Leer, B. Stabilization of difference schemes for the equations of inviscid compressible flow by artificial diffusion. J. Comp. Phys. Vol. 3 No. 4 (1969): 473-485.

Wang, F.S., Hu, L.W., and Pan, C. Thermal and Stability Analysis of a Two-Phase Natural Circulation Loop. J. Nucl. Sci. Eng. Vol.117 (1994): 33-46.

Wang, G., and Hochreiter, L.E. Natural Circulation Behavior Analysis of The Penn State Low Pressure Integral Test Facility. Proceedings of ICONE8, USA, April 2-6, 2000.

Watanabe, T., and Kukita, Y. The effect of the virtual mass term on the stability of the two-fluid model against perturbations. J. Nucl. Eng. Des. Vol.135 (1992): 327-340.

Wulff, W. Computer simulation of two-phase flow in nuclear reactors. J. Nucl. Eng. Des. Vol.141 (1993): 303-313.

Yadigaroglu, G. Instabilities in two-phase flow. Short Courses in Modeling and Computation of Multiphase Flows, Switzerland, March 16-20, 1998.

Yoneda, K., Okawa, T., Yasuo, A., and Zhou, S. Flow Structure of Developing Steam-water Two-phase Flow in a Large-diameter Pipe. Proceedings of ICONE8, USA, April2-6, 2000.

Zhou, J., and Podoski, M.Z. Modeling and analysis of hydrodynamic instabilities in two-phase flow using two-fluid model. J. Nucl. Eng. Des. Vol.204 (2001): 129-142.

สถาบันวิทยบริการ
จุฬาลงกรณ์มหาวิทยาลัย

Appendix

สถาบันวิทยบริการ
จุฬาลงกรณ์มหาวิทยาลัย

A.1 Differential Pressure Sensor Calibration

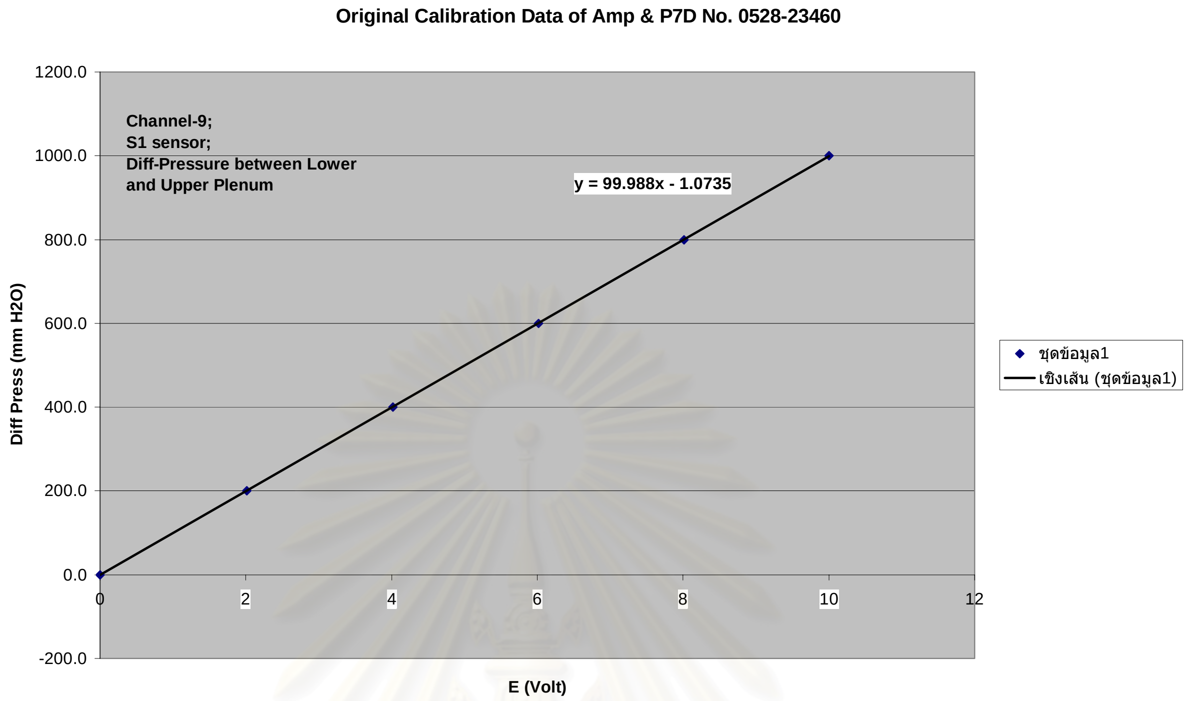

Fig. A1.1 Calibration curve of differential pressure sensor between lower and upper plenum

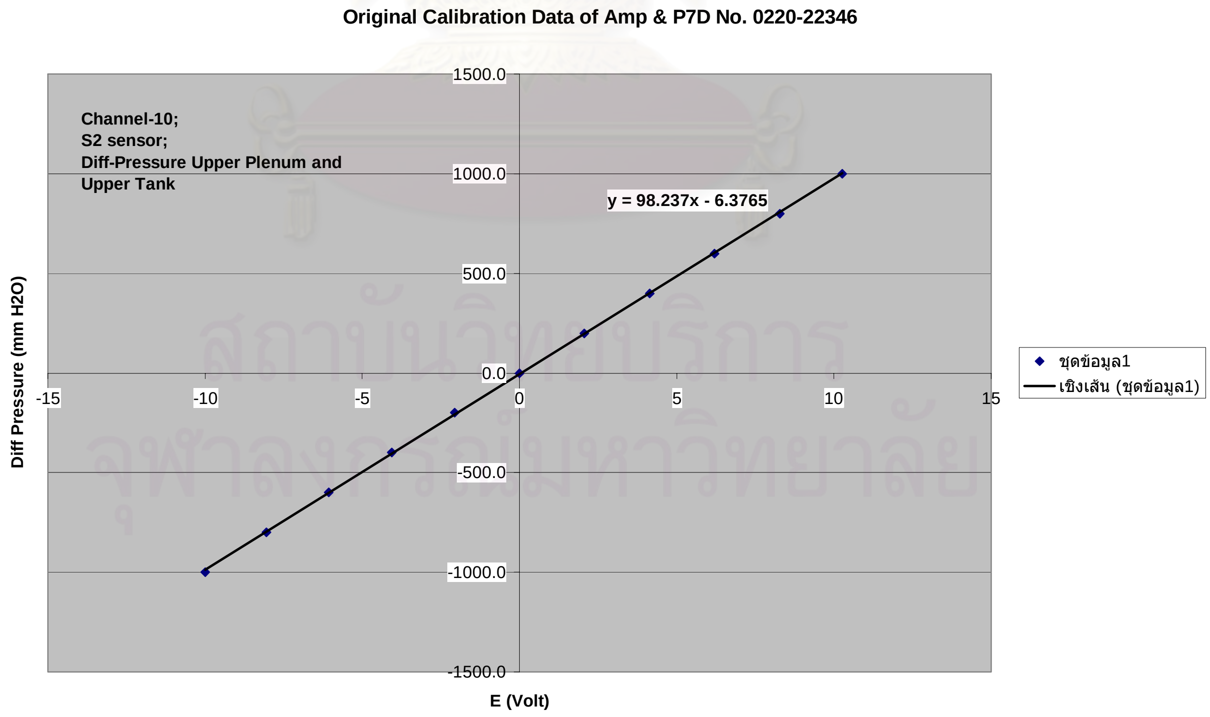

Fig. A1.2 Calibration curve of differential pressure sensor between upper plenum and upper tank

สถาบันวิทยบริการ
จุฬาลงกรณ์มหาวิทยาลัย

A.2 Main Power Heater Calibration

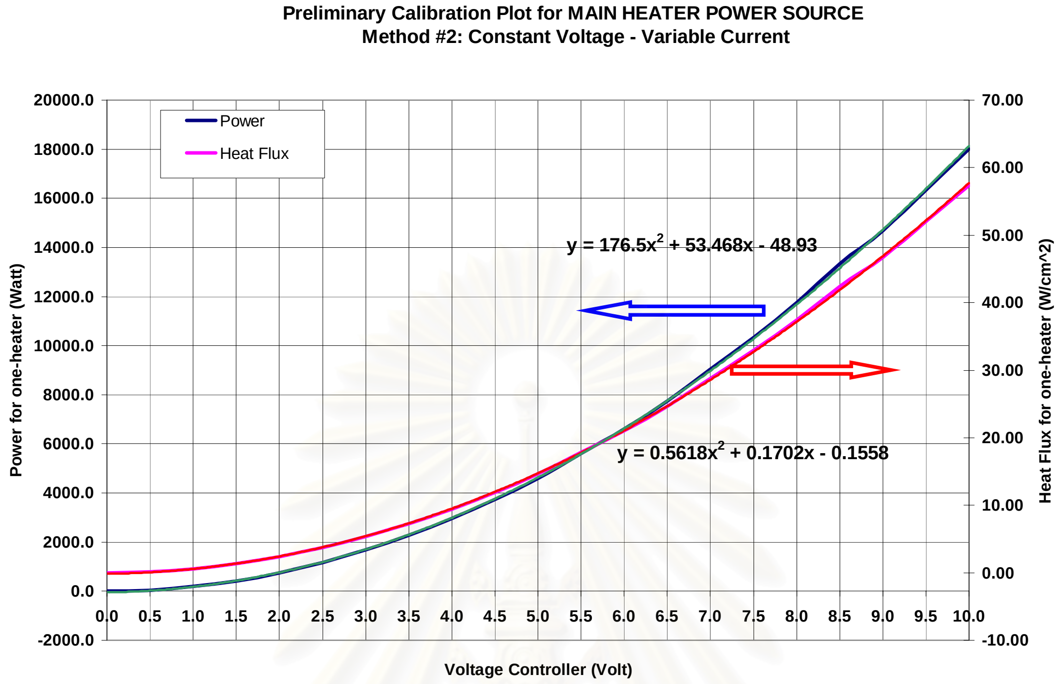

Fig. A2 Calibration curve of main power heater

สถาบันวิทยบริการ
จุฬาลงกรณ์มหาวิทยาลัย

A.3 Inlet Orifices Calibration

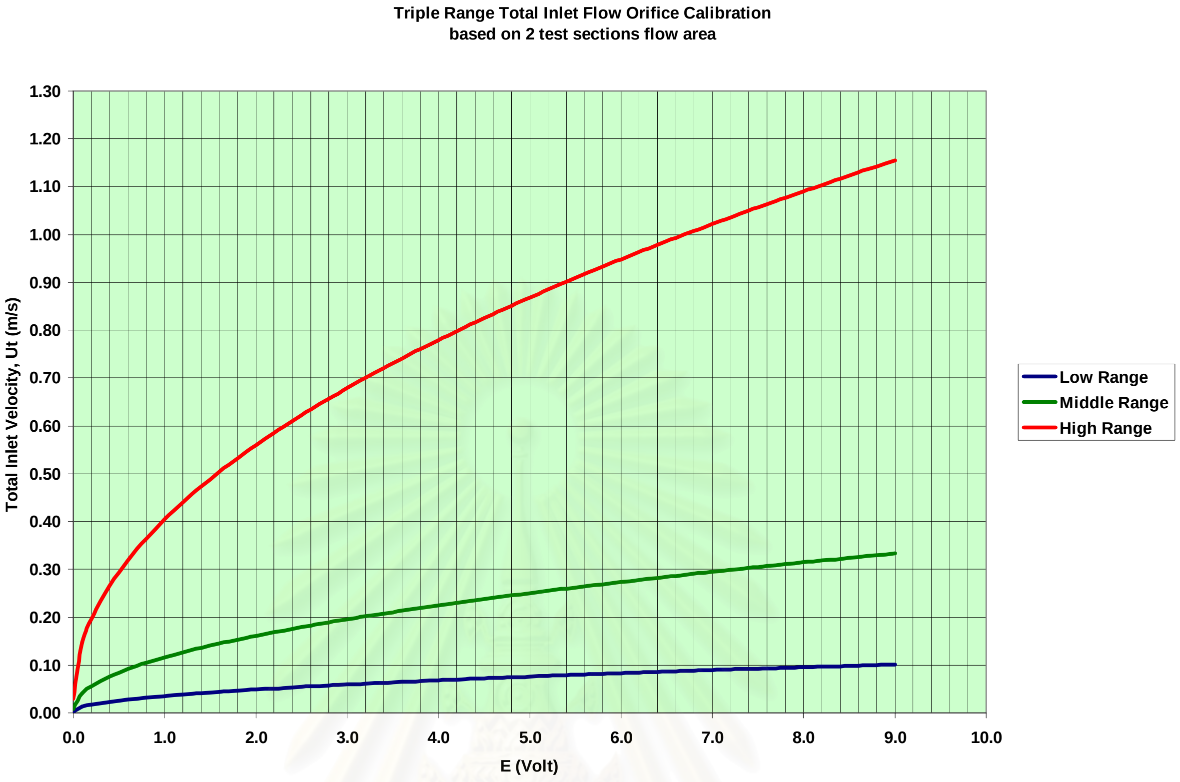

Fig. A3 Calibration curve of low, middle, and high range inlet orifices

สถาบันวิทยบริการ
จุฬาลงกรณ์มหาวิทยาลัย

A.4 Test Section Orifices Calibration

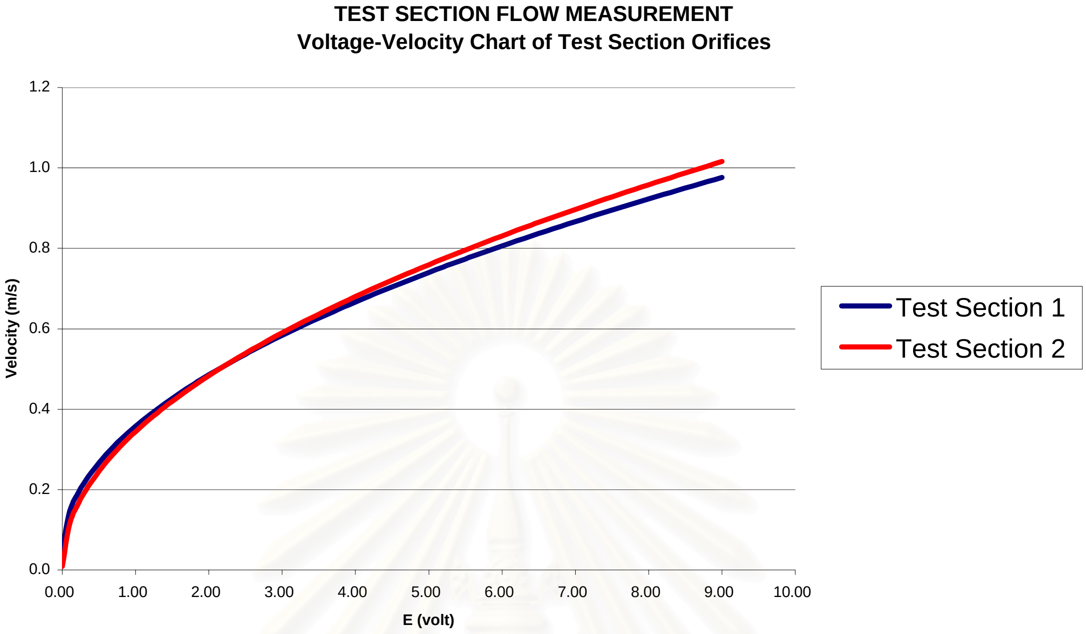

Fig. A4 Calibration curve of test section orifices

สถาบันวิทยบริการ
จุฬาลงกรณ์มหาวิทยาลัย

Biography

Mr. Chaiwat Muncharoen was born in April 19, 1970 at Lampang province. He got Bachelor degree from department of mechanical engineering, faculty of engineering, Chulalongkorn univeristy in 1993. After graduated he worked for Pipeline company in the position of Project Engineer for 2 years. At the same time he joined department of nuclear technoloty, faculty of engineering, Chulalongkorn univeristy in 1995, he worked for SNB consultant company in the position of Mechanical design engineer. He got the fellowship from AECL under Thai-Canadian Human Resource Development program to undertake his thesis in Canada for 8 months. He presented his paper in the 7th National Nuclear Science and Technology conference in 1998. Finished his master degree in 1998 he continued his doctoral degree in department of nuclear technology and received the scholarships from the Thailand Research Fund under Royal Golen Jubilee Ph.D. program (RGJ). Under RGJ program he went to Tokyo Institute of Technology to conduct the experiment in Research Laboratory for Nuclear Reactors for 10 months. Before going to Japan he submited one paper to the 8th National Nuclear Science and Technology conference in 2001. He received the scholarships from Japan Association of Mechanical Engineers (JSME) to present his papers at ANS/ASME 2002 Student Program in Pittsburgh, USA and The 10th International Conference On Nuclear Engineering in Washington D.C., USA. In May 2002, he presented another paper at Internatinal Conference On Computational and Modeling. The two papers have been submitted to Journal of Nuclear Science and Technology in Japan and Research and Development Journal of the Engineering Institute of Thailand.

สถาบันวิทยบริการ
จุฬาลงกรณ์มหาวิทยาลัย